Cascade Air-to-water Heat Pump With and Without Thermal Energy Storage: A Study for UK Domestic Retrofit

Khoa Xuan Le
MSc

Belfast School of Architecture and the Built Environment
Faculty of Computing, Engineering and the Built Environment
University of Ulster

A thesis submitted for the degree of
Doctor of Philosophy

June 2020

Abstract

Cascade air-to-water heat pumps have better overall efficiency than single-stage air-to-water heat pumps when operating at low ambient temperatures for high temperature water supply. Cascade heat pumps therefore have good potential for retrofitting UK domestic buildings because they can directly replace existing conventional boilers without significant modifications to the heat distribution systems, compared to single-stage heat pumps. However, little information about retrofit applications of cascade heat pumps in residential buildings is available in the literature, especially for the UK's context.

In this research, the techno-economic assessment of a variable capacity cascade air-to-water heat pump retrofitted into UK residential buildings was conducted by means of experimentally validated TRNSYS simulations. The cascade heat pump coupled with thermal energy storage operating in different scenarios was further studied. Laboratory and field trial results were obtained to develop and calibrate/validate the developed models. Additionally, different load shifting strategies for the integrated system of the cascade heat pump and thermal energy storage were simulated. These simulations were investigated to find the best load shifting algorithm which could help to achieve enhanced system energy efficiency with minimised running costs and reduced wind energy curtailment, while avoiding peak demand periods and guaranteeing thermal comforts for end-users.

Acknowledgements

I would like to take this opportunity to thank Professor Neil J. Hewitt and Dr. Ming Jun Huang, who are my supervisors, for giving a great chance to conduct research within Centre for Sustainable Technologies, along with providing valuable advices and supports throughout the journey of my PhD.

I would love to express my greatest thanks to my mother who has grown me up with amazing supports and endless sacrifices. I also thank my big family and friends who are always by my side, especially brother Nhut Duong and Hai Nguyen who spent precious time supporting me when I got troubles in the last three years. Finally, the greatest loves would be deserved to the angel, Angelie Lam-Anh Le-Pham.

I greatly thank my colleagues, Dr. Nikhilkumar Shah and Dr. Christopher Wilson, for helping me have valuable comments and measurement data which I could use to develop and validate the TRNSYS models.

I gratefully acknowledge the support funding from Vice-Chancellor's Research Scholarships (VCRS) of Ulster University and Research Councils UK (RCUK) under i-STUTE project.

Note on Access to Content

"I hereby declare that with effect from the date on which the thesis is deposited in the Library of the University of Ulster, I permit:

1. The Librarian of the University to allow the thesis to be copied in whole or in part without reference to me on the understanding that such authority applies to the provision of single copies made for study purposes or for inclusion within the stock of another library.

2. The thesis to be made available through the Ulster Insitutional Repository and/or EThOS under the terms of the Ulster eThesis Deposit Agreement which I have signed.

IT IS A CONDITION OF USE OF THIS THESIS THAT ANYONE WHO CONSULTS IT MUST RECOGNISE THAT THE COPYRIGHT RESTS WITH THE AUTHOR AND THAT NO QUOTATION FROM THE THESIS AND NO INFORMATION DERIVED FROM IT MAY BE PUBLISHED UNLESS THE SOURCE IS PROPERLY ACKNOWLEDGED".

List of Publications

Some of the main results in this thesis have been published in the high quality journal (Applied Energy) and peer-reviewed conferences:

Journal papers:

1. **Khoa Xuan Le**, Ming Jun Huang, Nikhilkumar Shah, Christopher Wilson, Paul MacArtain, Raymond Byrne, Neil J. Hewitt. "Techno-economic assessment of cascade air-to-water heat pump retrofitted into residential buildings using experimentally validated simulations", Applied Energy, vol. 250 (2019), pp. 633-652.

2. **Khoa Xuan Le**, Ming Jun Huang, Christopher Wilson, Nikhilkumar Shah, Neil J. Hewitt. "Tariff-based load shifting for domestic cascade heat pump with enhanced system energy efficiency and reduced wind power curtailment", Applied Energy, vol 257 (2020), pp. 113976.

Conference papers:

1. **Khoa Xuan Le**, Ming Jun Huang, Neil J. Hewitt. "Demand-side management study for cascade air-water heat pump coupled with thermal energy storage in the UK domestic sector", SusTEM2019, May 14-16, 2019, Hangzhou, China.

2. **Khoa Xuan Le**, Ming Jun Huang, Neil J. Hewitt. "Domestic High Temperature Air Source Heat Pump: Performance Analysis Using TRNSYS Simulations", 5th International High Performance Buildings Conference at Purdue University, July 9-12, 2018, Indiana, USA.

3. **Khoa Xuan Le**, Ming Jun Huang, Nikhilkumar Shah, Christopher Wilson, Paul Mac Artain, Raymond Byrne, Neil J. Hewitt. "High Temperature

Air Source Heat Pump Coupled with Thermal Energy Storage: Comparative Performances and Retrofit Analysis", 10th International Conference on Applied Energy (ICAE2018), 22-25 August 2018, Hong Kong, China.

4. **Khoa Xuan Le**, Ming Jun Huang, Nikhilkumar Shah, Christopher Wilson, Paul Mac Artain, Raymond Byrne, Neil J. Hewitt. "High Temperature Air Source Heat Pump Coupled with Thermal Energy Storage: An Analysis of Demand-Side Management Designed for Flattening the Grid Demand", 17th International Conference on Sustainable Technologies (SET 2018), August 21-23, 2018, Wuhan, China.

5. **Khoa Xuan Le**, Nikhilkumar Shah, Ming Jun Huang, Neil J. Hewitt. "High Temperature Air-Water Heat Pump and Energy Storage: Validation of TRNSYS Models", Proceedings of the World Congress on Engineering and Computer Science 25-27, 2017, San Francisco, USA.

Contents

List of Figures

List of Tables

List of Symbols and Abbreviations

Symbols

ρ	Density of water [kg/m^3]
C_p	Water specific heat capacity [kJ/kg.K]
T	Temperature [°C]
RH	Ambient relative humidity [%]
$\dot{m}$	Volumetric flow rate [l/s]
OWT	Outlet water temperature [°C]
COP	Coefficient of performance of heat pump [-]
COP_{sys}	Coefficient of performance of heat pump system which accounts for heat loss of the whole system [-]
E	Energy [kWh]
Q	Thermal heat output [kW]
W	Eletric input power [kW]
PLR	Part load ratio [-]
EIR	Electric input ratio [-]
PLF	Part load factor [-]
$\triangle t_{def}$	Period between defrost cycles or frosting time [minute]
a, b, c, d, f, g, h	Empirical coefficients obtained from polynomial regression [-]
DeltaT	Difference between outlet and inlet water temperature at the heat sink of the heat pump [°C]

t_{def}	Time of a defrost cycle [minute]
f	Cost function/normalized value [-]
$CV(RMSE)$	Coefficient of variations of root mean square errors [-]
$RMSE$	Root mean square errors [-]
Y_{sim}	Simulated value [-]
$Y_{measure}$	Measured value [-]
n	number of observations [-]
$\overline{Y}_{measure}$	Arithmetic mean of measured value regarding n observations [-]
$\overline{C}OP$	Arithmetic mean of COP regarding n observations [-]
$\overline{Q}$	Arithmetic mean of thermal output regarding n observations [kW]

Subscripts

a	Ambient
w	Water
out	Outlet
in	Inlet
hp	Heat pump
$house$	House
$store$	Thermal energy storage
$setpoint$	Set point of model
$full$	Full load
pm	Performance map
ref	Reference
c	Cooling
def	Defrost
fr	Frosting

e	Electric use
q	Heat
$require$	Require
$load$	Load side
$interpolation$	Interpolation
$daily$	Daily
sim	Simulation
$measure$	Measure

Abbreviations

DB	Ambient dry bulb temperature
WB	Ambient wet bulb temperature
AWHP	Air-to-water heat pump
HT-AWHP	High temperature air-to-water heat pump
EVI	Enhanced Vapour Injection
CAWHP	Cascade air-to-water heat pump
TES	Thermal energy storage
DSM	Demand-side management
DHW	Domestic hot water
GSHP	Ground source heat pump
EQ	Electric-Thermal
ASHRAE	American Society of Heating, Refrigerating and Air Conditioning Engineers
HVAC	Heating, Ventilation and Air Conditioning
HDD	Heating degree day

Chapter 1

Introduction, Literature Review and Motivations of This Research

1.1 Introduction

1.1.1 Air-to-water heat pumps as a means for decarbonising UK domestic heating

In the European Union, buildings accounted for about 40% of the energy consumption and 36% of CO_2 emissions [9]. In the UK, the domestic sector was responsible for the second highest final energy consumption since 1990 (Figure 1.1). In 2017 particular, this sector accounted for 28% of total final energy consumption [1] and 17% of all carbon dioxide emissions [10]. Space and hot water heating demands comprised approximately 83% of heat emissions at this sector (Figure 1.2) [2], and about 88% of these demands were provided by fossil-fuel boilers [11]. With the commitment to reducing greenhouse gas emissions by at least 100% by 2050 compared to 1990 levels [12], many researchers and policy makers in the UK have focused on decarbonising space and hot water heating

at the domestic level by using renewable-based alternatives, such as greening gas or heat pumps.

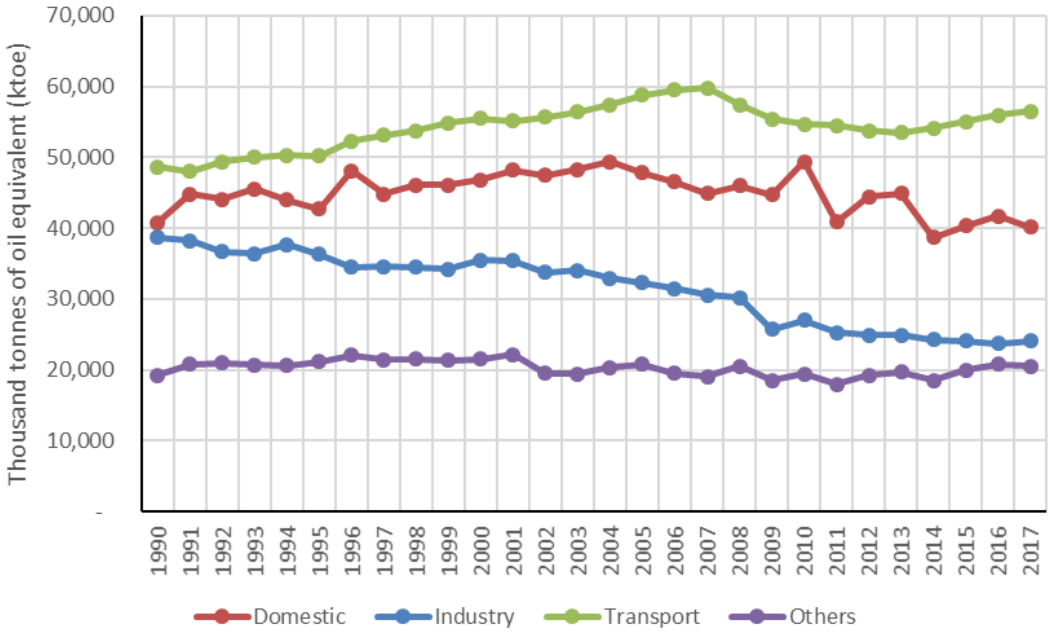

FIGURE 1.1: Final energy consumption by sector in the UK [1].

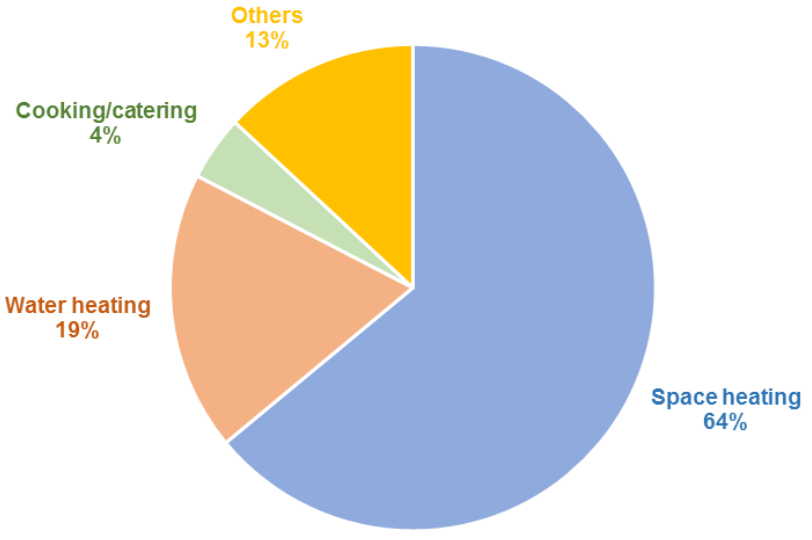

FIGURE 1.2: Emissions from heat at the UK domestic level in 2017 [2].

Greening gas (utilising biomethane or hydrogen) is attractive for decarbonising domestic heating; however, this technology seems to cost much money and lack

of convinced results. Alternatively, decarbonising heating through heat pumps using electricity seems to be more feasible in practice.

Heat pumps have been used as a retrofit solution due to its high efficiency as well as capability to directly replace existing fossil-fuel boilers. Furthermore, an increasing proportion of electricity generation from renewable sources, such as solar, wind, etc., means heat pumps have increased potential to reduce carbon footprint in the UK. This is because the carbon intensity on the grid has been decreased considerably [13]. For example, in the first six months of 2018, there was a reduction of 19% in the electricity carbon emissions factor compared to the previous year [14]. Since ground source heat pumps (GSHPs) have significantly higher initial costs than conventional heating systems (mainly due to the capital costs of the heat pump unit and the ground work) [15], air-to-water heat pumps (AWHPs) appear attractive for building retrofit.

1.1.2 Cascade air-to-water heat pumps as a retrofit solution

UK residential buildings heavily rely on fossil-fuelled boilers to satisfy space and hot water demands. Conventional boilers have been well established with high temperature distribution systems (over 60 °C), such as traditional wet radiators, hot water tanks, pipes, etc. However, heat pumps' efficiency inevitably reduces when working at high temperature lift, so replacing existing boilers with heat pumps should be carefully considered.

According to BS-EN 14511:2013 [16], AWHPs can be categorised based on outlet water temperature ranges, which are described as: (1) low temperature (35 °C); (2) medium temperature (45 °C); (3) high temperature (55 °C); and (4) very high temperature (above 65 °C). AWHPs in which the flow temperatures reach up to 55 °C are normally single-stage heat pumps, and they are re-defined as standard AWHPs in this thesis. AWHPs that can produce outlet water temperatures over

65 °C are named high temperature AWHPs (HT-AWHPs). HT-AWHPs in the UK market include heat pumps with optimised design for specific refrigerants, cascade systems, Enhanced Vapour Injection (EVI) and sorption [17].

As for the retrofit aspect in the UK, using standard AWHPs (or single-stage AWHPs) to replace existing conventional boilers is unlikely to be viable. This is due to high installation costs as a result of considerable adjustments to the heat distribution systems to increase heat pumps' efficiency. Therefore, standard AWHPs are more suitable for installing in new buildings rather than for retrofit purposes. HT-AWHPs, cascade air-to-water heat pumps (CAWHPs) to be more specific, may be a potential solution for retrofitting the UK built environment since they are designed to work more efficiently at high temperature water supply compared with standard AWHPs (single-stage AWHPs). CAWHPs can provide high flow water temperatures that are the same as the outlets of boilers, thereby being able to replace existing boilers without the requirement of significant modifications to the heat distribution systems. As a result, it can help to reduce installation costs and disruptions when retrofitting.

1.1.3 Market analysis of cascade air-to-water heat pumps for retrofit in the UK

There were about 27.4 million and 800000 domestic dwellings in Great Britain [18] and Northern Ireland [19], respectively. Approximately 85% of these dwellings are using gas boilers to satisfy space heating and hot water demands, while the rest 15% is utilising solid fuel, oil or electricity to supply heat demands as they are in off-gas-grid areas in which there were approximately from 4.1 million to 4.6 million residential buildings [20].

Standard AWHPs are unlikely to be a feasible solution for retrofit as of high installation costs due to the required replacement of high distribution systems

such as radiators, pipes, hot water tank, etc. Alternately, gas boilers and HT-AWHPs, particularly cascade heat pumps, are more potential because the modification of high distribution systems can be avoided.

Due to the current competitive gas prices in the UK, replacing conventional boilers with gas-fired ones in domestic buildings is more preferable than high temperature heat pumps where gas networks are available. Therefore, CAWHPs are more suitable for retrofitting into dwellings in off-gas-grid places. According to the research of Department for Business, Energy and Industrial Strategy [20], the authors estimate that the potential market for this kind of heat pumps is from 25% to 50% of off-gas-grid buildings (approximately 1 - 2.3 millions dwellings).

The product costs of CAWHPs are high, ranging from about £5900 to £7900 with respect to product capacity ranges of 11 kW and 16 kW [21] [22]. The installation costs were from £3000 to £4000 [17] . As a result, the capital costs for retrofit with this kind of heat pumps turn out to be £8900 - £11900, which is high in the UK market.

1.1.4 Cascade air-to-water heat pump: State-of-the-art of the technology

CAWHPs differ from single-stage AWHPs in the capability of providing high flow water temperature (over 65 °C) with better overall efficiency at low ambient temperatures. In terms of system design, the main difference between CAWHPs and single-stage AWHPs is that the former has two refrigerant cycles connected by an intermediate heat exchanger or a middle water loop, whilst the latter has only one refrigerant stage. According to the recent reviews of Chua et al. [23] and Zhang et al. [3], cascade heat pump systems were first invented by Ma et al. [24] in 2001. These cascade heat pumps had a middle water loop

to exchange the heat between two refrigerant cycles, as shown in Figure 1.3a. Later on, many fellow researchers developed cascade heat pump systems further using intermediate shell-tube or plat-shell heat exchangers (Figure 1.3b) instead of middle water loops. Nowadays, cascade heat pumps featured with intermediate heat exchangers are becoming popular.

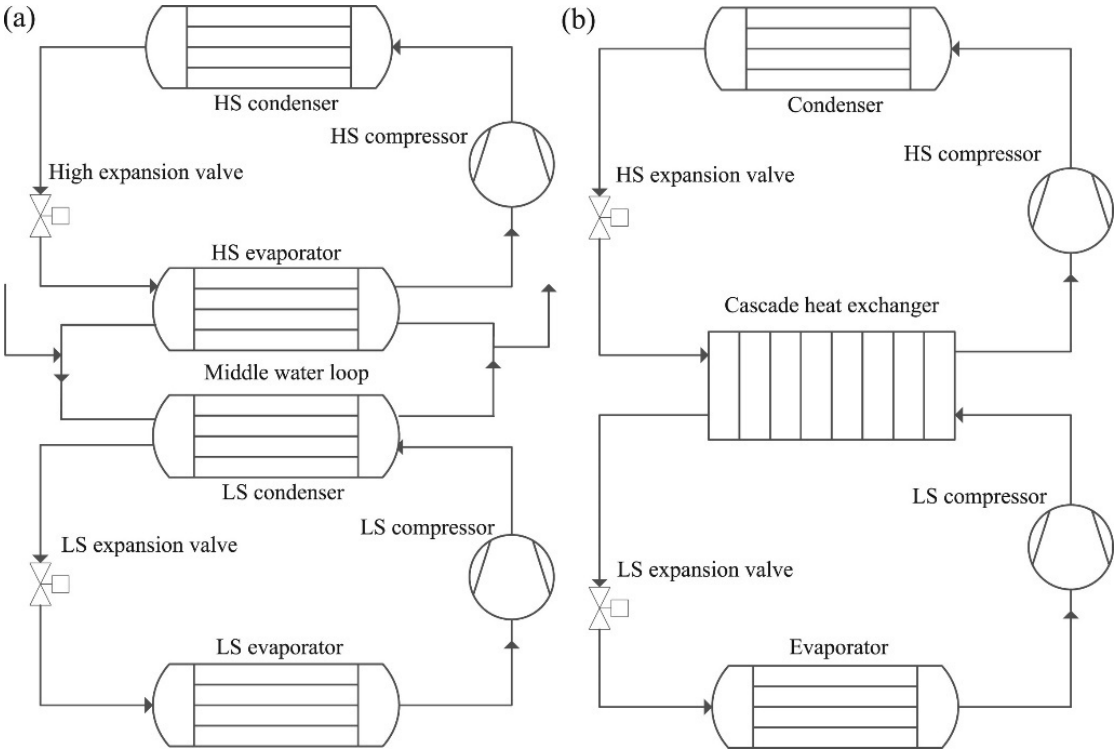

FIGURE 1.3: Schematic of a cascade air-to-water heat pump with: (a) middle water loop; (b) intermediate heat exchanger [3].

A CAWHP comprises two separate single-stage refrigeration cycles, including the lower refrigeration cycle maintaining a lower evaporating temperature and providing a refrigeration effect, and the higher refrigeration cycle working at a higher evaporating temperature [25], as depicted in Figure 1.3. These two refrigeration cycles using different refrigerants are joined by a water loop or an intermediate heat exchanger to transfer heat from the condenser in the lower refrigeration cycle to the evaporator in the higher refrigeration cycle.

In Figure 1.3b, the refrigerant R-410a is utilised in the low cycle, while the refrigerant R-134a is used in the high cycle. The refrigerant R-410a is capable of

evaporating at low ambient temperatures and condensing at a comparatively low pressure and a temperature of approximately 45 °C [17]. Then, the heat from the condenser of the low cycle is transferred to the evaporator of the high cycle via the intermediate heat exchanger, which causes the refrigerant R-134a to evaporate. After that, this refrigerant is condensed at low pressures to transfer heat to the water side, which can bring the outlet water temperatures up to 80 °C. Based on this state-of-the-art of the technology, CAWHPs can address the problems of high compressor ratios and high discharge temperatures occurring in single-stage AWHPs when attempting to lift outlet water temperatures to high levels.

1.1.5 Heat pumps coupled with thermal energy storage as a demand-side management tool

A rising proportion of renewable electricity generation from renewable sources (e.g. solar, wind, etc.) in combination with the widespread uptake of heat pumps has been considered as a solution for reducing carbon footprint at the domestic level [4]. Nevertheless, a significantly increasing number of heat pumps retrofitted into residential buildings may pose some challenges to the electricity supply network. For example, the low voltage distribution network will bear a potential burden of heavy load if a widespread uptake of heat pumps happens. This is highly likely to result in voltage dips and cable overload [26]. Therefore, attentions should be paid carefully if there is high penetration of heat pumps retrofitted. Furthermore, renewable energy generation (especially wind energy) has increased in the UK, but there are high figures of wind curtailment because of the mismatch between electricity supply and demand [27].

Thermal energy storage (TES) coupled with heat pumps for load shifting has significant merits for demand-side management that may play a considerable

role in future energy systems with increased proportions of non-dispatchable renewable energy [28]. This system can be used as a means for shifting load from peak-demand to low-demand periods or from high to low electricity rates, which can help to balance the grid and reduce electricity bills for end-users when taking advantage of electricity tariffs [29]. Additionally, such a system can help increase consumption of intermittent renewable energy by means of shifting the operation of heat pumps for storing energy to periods when high figures of renewable energy are unused. For example, the high figures of wind curtailment occurring at night (off-peak periods) can be mitigated if the thermal demands are shifted to this period thanks to the flexibility of TES coupled with heat pumps. Moreover, TES combined with heat pumps is potential to increase buildings' energy efficiency [30].

In short, the coupling system of heat pumps and TES for load shifting is a promising technology for mitigating the burden on the national utility and improving proportions of renewable energy to be integrated onto the grid when an increasing number of heat pumps, cascade air-to-water heat pumps in particular, are retrofitted.

1.2 Literature Review

1.2.1 Literature review on single-stage air-to-water heat pumps as a retrofit technology

There are many studies conducting the performance of AWHPs when retrofitted into existing housing stock in different nations, but most of them considered single-stage AWHPs reproducing low or medium flow temperatures (below 60 °C). Madonna and Bazzocchi [31] used in-situ validated simulations to evaluate the annual performance of reversible AWHPs in small residential dwellings in

Italy. The supply temperatures were limited to 45 °C. Asaee et al. [32] assessed the techno-economic feasibility of retrofit AWHPs for the Canadian housing stock. The space and domestic hot water (DHW) heating was provided from two stages. The first stage was supplied by the AWHPs to provide the outlet water temperature of 50 °C, and then the 50 °C water flow was heated in the second stage to a maximum of 55 °C by auxiliary boilers. The study found that the reductions of 36% of energy consumption and 23% of green-house gas emissions could be achieved if all eligible houses were retrofitted by the single-stage AWHPs. In Germany, the field test results of 21 single-stage AWHPs and 22 brine-to-water GSHPs were gathered to evaluate the heat pumps' retrofit performance [33]. The tested heat pump systems comprised the heat pump units providing hot water floor heating and/or radiators with the flow temperatures of 40 °C and 55 °C, respectively. In the UK, Kelly and Cockroft [13] evaluated the running costs and carbon emissions of single-stage AWHPs when retrofitted into domestic dwellings in Scotland. The retrofit AWHPs fed hot water radiators with the nominal flow temperature of 55 °C, whereas DHW was supplied separately by electric heating coils. The authors concluded that the retrofit AWHPs could obtain 12% carbon savings compared to condensing gas boiler systems, but there was a cost penalty of 10% to operate the heat pumps. Cabrol and Rowley [34] conducted a comparative analysis of the UK domestic buildings with the integrated system of underfloor heating and single-stage AWHPs. Both the Energy Saving Trust (EST) and Department of Energy and Climate Change (DECC) [20] investigated two main field trials for single-stage AWHPs and GSHPs in the UK, and both field trials considered outlet water temperatures between 30 °C and 55 °C.

However, using single-stage AWHPs as a retrofit alternative is unlikely to be a feasible solution in practice. This is because 35% of the EU's buildings [9] and 27.5 million UK's residential houses [35] are ageing, heavily relying on conventional boilers with high temperature (over 60 °C) heating distribution systems

(wet radiator systems) to supply space and hot water heating demands. Indeed, the existing high temperature wet radiators were designed to work efficiently with the flow temperature of 75 °C as suggested by BS-EN 442-2:2014 [36]. In order to provide this high outlet water temperature, the condensing temperature in single-stage AWHPs should be kept at a high level, which leads to high compression ratios and high compressor discharge temperatures as stated by Jung et al. [37]. Besides, at low ambient temperatures, the efficiency and heat capacity of an air source heat pump water heating decrease when attempting to lift its outlet water temperatures above 60 °C [25]. Therefore, replacing existing boilers with single-stage heat pumps in the housing stock of the EU, particularly the UK, is more difficult because it requires the adjustment of the heat distribution systems, which results in high installation costs and disruptions when retrofitting. Furthermore, recent field trials [20] and previous studies [13] [34] investigated the techno-economic performance of retrofit single-stage AWHPs in the UK with the compromise of using oversized or underfloor radiators; however, the authors did not consider the installation costs.

1.2.2 Literature review on cascade air-to-water heat pumps for domestic space and hot water heating

A CAWHP comprises two separate single-stage refrigeration cycles, including the lower refrigeration cycle maintaining a lower evaporating temperature and providing a refrigeration effect, and the higher refrigeration cycle working at a higher evaporating temperature [23]. These two refrigeration cycles are joined by an intermediate heat exchanger to transfer heat from the condenser in the lower refrigeration cycle to the evaporator in the higher refrigeration cycle. Therefore, CAWHPs can address the problems of high compressor ratios and high discharge temperatures occurring in single-stage AWHPs when attempting to lift the outlet water temperatures to high levels [37]. According to the

study of Bertsch and Groll [38], a cascade compression system could also obtain better performance at low external air temperatures. As a result, CAWHPs may be a potential solution for retrofit application in the UK since they can directly replace existing boilers without the requirement of considerable modifications to the heat distribution systems, thereby reducing installation costs and disruptions compared to single-stage AWHPs.

The number of studies on CAWHPs for space and hot water heating has increased recently, according to the extensive reviews of Chua et al. [23]; Willem et al. [39]; and Zhang et al. [3]. For example, Jung et al. [37] carried out experiments to compare the performance between a cascade multi-functional AWHP and a single-stage multi-functional AWHP providing space and hot water heating. The performance of the cascade heat pump was measured by adjusting the refrigerant charge amount, electronic expansion valve opening, water flow rate, and water inlet temperature. Park et al. [40] conducted a thermodynamic analysis with the aims to optimise the intermediate temperature of a cascade refrigeration system. Later on, these authors investigated another study on the transient behaviour of the system of a cascade heat pump coupled with a water storage tank [41]. Optimising the intermediate temperature of a CAWHP system using R134a and R410A refrigerants was also studied by Kim et al. [42]. Kim et al. [43] further carried out how the refrigerant charge amount affected the cascade heat pump cycles. Ma et al. [44] investigated how other working fluids (BY-3 in the low-stage refrigerant cycle and R245fa in the high-stage refrigerant cycle) influenced cascade AWHPs. Wu et al. [25] experimentally evaluated the transient behaviour and dynamic performance of a cascade AWHP system operating with and without phase change material storage tank. This study also compared the performance between single-stage mode and cascade mode. Wang et al. [45] developed a cascade AWHP system in which the heat of the two-stage cycles was exchanged by a circulating water loop. This heat pump system was then tested in a field trial located in the northwest suburb

of Beijing, China, with the aim to enhance the working condition and heating performance under cold climates.

Whilst there are many studies on CAWHPs investigating the specific feature of equipment performance as mentioned above, little information about CAWHPs for the real retrofit applications in residential buildings, especially attempting to quantify energy and carbon savings, is available in literature. Summary of the research about CAWHPs can be seen in Table 1.1. Recently, the UK Department for Business, Energy and Industrial Strategy [17] released a technical report aiming to investigate the retrofit potential of domestic high temperature air source heat pumps for space and hot water heating. This research was carried out by gathering short-term field trial results in different sites across the UK. Another study by Shah et al. [46] conducted field trials of a cascade AWHP integrated with a TES tank to highlight its retrofit performance in the UK, but again the field trials were carried out in short periods. However, short-term field trials alone could not accurately evaluate the potential costs and carbon savings of these heat pumps because AWHPs' performance is sensitive to seasonal and boundary conditions.

TABLE 1.1: Summary of research about CAWHPs for domestic space and hot water heating in the literature.

Reference	Type of article	Objective	Method	Category
Chua et al. [23]	Literature review	-	-	-
Willem et al. [39]	Literature review	-	-	-
Jung et al. [37]	Research	Compare the performance between a cascade multi-functional AWHP and a single-stage multi-functional AWHP.	Experiment	Equipment performance
Park et al. [40]	Research	Optimise the intermediate temperature of a cascade refrigeration system.	Modelling	Equipment performance
Park et al. [41]	Research	Transient behaviour of the system of a cascade heat pump coupled with TES.	Modelling	Equipment performance
Kim et al. [42]	Research	Optimise intermediate temperature of a CAWHP system.	Experiment & Modelling	Equipment performance
Kim et al. [43]	Research	Impacts of refrigerant charge amount on cascade heat pump cycles.	Experiment & Modelling	Equipment performance
Ma et al. [44]	Research	Impacts of BY-3 in low-stage refrigerant cycle and R245fa in high-stage refrigerant cycle on CAWHPs.	Experiment & Modelling	Equipment performance
Wu et al. [25]	Research	Transient behaviour and dynamic performance of a CAWHP with and without PCM storage tank.	Experiment	Equipment performance
Wang et al. [45]	Research	Develop a CAWHP system with a circulating water loop.	Experiment	Equipment performance
DECC [17]	Technical Report	Investigate retrofit potential of domestic high temperature air source heat pumps for space and hot water heating.	Evidence gathering	Equipment performance & Integrated performance with building
Shah et al. [46]	Research	Field trials of a CAWHP with TES.	Experiment	Integrated performance with building

1.2.3 Literature review on modelling and simulations of cascade air-to-water heat pump

There are many publications about modelling and simulations of CAWHPS that were validated against laboratory and in-situ results; however, most of modelling work was carried out for equipment performance. For example, Park et al. [40] developed a mathematical model, which was validated against laboratory results, to investigate the thermodynamic analysis of a cascade refrigeration system with R134a and R410A to find the optimal intermediate temperature. The author and co-workers later developed another experimentally validated steady-state cascade heat pump model coupled with a water storage tank model to assess the transient behaviour of the system [41]. Soltani et al. [47] modelled and compared three AWHP systems, including single-stage, single refrigerant cascade and two-refrigerant cascade, to ascertain the suitability of cascade heat pumps for hydronic residential systems. Kim et al. [42] carried out a numerical and experimental study of a cascade AWHP adopting R134a and R410A refrigerant to optimize intermediate temperature of the system. These authors also conducted another study about the effect of the refrigerant charge amount on single and cascade cycle heat pump systems by means of numerical and experimental approaches [43].

1.2.4 Literature review on the coupling system of cascade air-to-water heat pumps with thermal energy storage

Although there are many merits that the combined system of heat pumps and TES can bring to, few studies in the literature conducted the integrated performance with buildings of CAWHPs and TES. For example, Wu et al. [25] carried out a study of cascade heat pump water heater with phase change material storage. However, this work just limited at laboratory experiments to study the

transient and dynamic performance of the heat pump rather than integrated operations with buildings. Park et al. [41] developed and validated the models of a cascade heat pump water heater and a water storage tank to investigate the system performance, but this study also limited at equipment level rather than integrated level with buildings. Shah et al. [46] carried out a performance evaluation of a CAWHP with TES in different system configurations in a residential dwelling. Nevertheless, the varied system configurations were experimentally conducted under different weather conditions, so the findings just limited at highlighting the performance at each system operation rather than an extensive comparison.

1.2.5 Literature review on load shifting for heat pumps coupled with thermal energy storage in residential buildings

TES supporting heat pumps for load shifting can play a significant role in avoiding the overload problems of the grid and renewable energy curtailment [28]. As a result, load shifting has become an attractive research topic. According to the extensive literature reviews of Fischer and Madani [48] and Pean et al.[49], there are two main control approaches to shift electrical heating or cooling demands: non-predictive control and model predictive control. While the latter has been found to outperform the former at achieving control goals (e.g. minimising running costs, maximising thermal comfort, etc.), the high costs of needing expertise in design and computational resources of a predictive model are such problems to be considered [48]. In contrast, non-predictive control can be simply designed without requiring many computational resources, but it still shows good performance and robustness. Non predictive control can be categorised as: rule-based control and fixed scheduling. Rule-based control can be simply defined as if-then algorithms. Fixed scheduling is a demand-side management (DSM) control approach in which the operation of heat pumps is

blocked to the predefined hours to avoid peak power demand or high electricity rates. The predefined hours can be identified based on the already available information of a national electricity grid or the availability of static time-of-use tariffs. Fixed scheduling is simple and implemented easily, and it can obtain a substantial performance with better results than more advanced rule-based controls at some points [48]. Therefore, fixed scheduling is selected as a means of a DSM strategy for load shifting in this study.

There is much research on load shifting of heat pumps coupled with TES using predefined schedules. Kelly et al. [4] used a detailed simulation model in ESP-r software to carry out a system of an AWHP integrated with a buffering TES tank. The times to move the heat pump to off-peak periods followed a UK available time-of-use tariff. They found that 1 m^3 of hot water buffering or 0.5 m^3 of phase change material-enhanced hot water buffering was enough to shift the heat pump's operation fully to off-peak hours, without negatively influencing the provision of space heating and DHW for the final customers. Arteconi et al. [50] investigated a load shifting strategy for heat pumps coupled with buffering TES operating with radiators or underfloor heating distribution systems. The heat pumps were forced to switch off during peak hours defined by a time-of-use tariff in the UK to level off the grid power demand curve. However, these studies just focused on the system designs (e.g. optimal tank sizes, different system configurations) for the schedule load shifting strategies, whereas they did not truly conduct the optimal system operation efficiency to further obtain the control goals (e.g. minimised running costs, maximised thermal comfort). While the efficiency of an AWHP can be enhanced if it was shifted to hours where ambient temperatures were highest, this effect was not considered.

Whilst many studies investigated the enhancement of overall system efficiency of schedule load shifting heat pumps coupled with TES to acquire optimal control goals, most of them focused on one aspect of heating (either space heating

or hot water heating). For example, Guo et al. [51] experimentally conducted an optimised operation strategy of a heat pump water heating system to minimise the operating costs. The optimal start-up time was between 12.00 h and 14.00 h where the ambient temperatures were high, and the electricity prices were low. Ibrahim et al. [52] examined the optimised system efficiency of a heat pump water heating system for Lebanon, with the operation of the heat pump was constrained to the low electricity rates and high ambient temperatures to minimise the running costs. Coninck et al. [53] conducted the system of a heat pump coupled with TES for space heating. The operation of the heat pump was moved to daytime to improve the overall efficiency to reduce energy consumption while still avoiding the high-demand hours of the grid.

1.3 Motivations of This Research

Based on the systematic literature review above, it evidences that there are some research gaps needing to further investigate:

- While much research developed the models of CAWHPs validated against laboratory and in-situ data, most of the modelling work was carried out for equipment performance rather than integrated performance with buildings.
- There is no study conducting the full-scale retrofit performance of CAWHPs using experimentally validated dynamic building simulation models, especially quantifying operating costs and carbon emissions savings when compared with the performance of fossil-fuelled boilers in the UK.
- Few studies investigated the integrated performance with buildings of the coupling system of CAWHPs and TES.

- There is lack of information about how and when heat pumps and TES should operate interactively in shifting and meeting both space and hot water heating demands, with improved system operation efficiency to obtain better control goals. Furthermore, most of the final goals of the cited publications about schedule load shifting were minimised running costs or reduced energy consumption rather than other goals, such as increased renewable energy use.
- No work on CAWHPs coupled with TES applied schedule load shifting for both space and hot water heating at the domestic level to obtain both enhanced system energy efficiency and increased renewable energy utilisation.

1.4 Objectives of This Research

The objectives of this research are as follows:

- A CAWHP model integrated with a dynamic building simulation model, validated against experimental results, was developed. This objective could contribute to the lack of literature about integrated performance with buildings of experimentally validated CAWHP models.
- Since there is no study on assessment of retrofit ability of CAWHPs by means of experimentally validated models, this research gap was addressed in this thesis. In particular, the techno-economic performance of CAWHP systems (without TES) when retrofitted into UK residential buildings, especially endeavoring to quantify carbon and energy savings compared with oil and gas fired boilers, was investigated.
- The system performance of retrofit CAWHPs coupled with TES in different configurations in a residential dwelling was evaluated. This objective

aimed to address the lack of information about this such system operations in the literature.

- There is no work on schedule load shiftings for CAWHPs coupled with TES to satisfy both space heating and hot water demands with lower operating costs and higher renewable energy use. Therefore, in this research, different schedule operation strategies for a CAWHP with TES were designed to shift both space heating and hot water demands from peak to off-peak periods, with increased system energy efficiency to obtain minimised running costs and reduced wind energy curtailment.

1.5 Overview of This Thesis

The rest of this thesis is summarised as follows:

- **Chapter 2** presents the experimental set-up of a CAWHP coupled with a TES tank providing heat to the house to satisfy both space heating and hot water demands. Details of the selected CAWHP and the custom design TES tank are also presented clearly, along with a test house which was a hard-to-heat mid-terraced building. The CAWHP was first tested under laboratory conditions. Then, the field trials of the coupling system of the CAWHP and the TES tank were carried out in different scenarios, including direct mode, storage mode, and combined mode. Finally, the data collected from the measurements were checked to make sure they were reliable to be used for modelling and calibration/validation purposes.

- **Chapter 3** deals with the model development and calibration/validation. TRNSYS 17 software was utilised to model and simulate the selected CAWHP and the TES tank in line with the hard-to-heat mid-terraced dwelling. The predicted performance of the CAWHP was calibrated and validated

against the collected data from laboratory and field trial tests. The performance of the TES in TRNSYS model was calibrated and validated for three operation modes: standby mode, charging mode and discharging mode. The predicted building heat demands were also calibrated and compared with the measured building heat demands.

- **Chapter 4** describes the techno-economic performance of the CAWHP system (without TES) when retrofitted into UK residential buildings, especially endeavouring to quantify carbon and energy savings compared with oil and gas fired boilers. The retrofit CAWHP system was conducted with different property types and ages, various locations across the UK, and varied control strategies (fixed flow water temperature and weather compensation).

- **Chapter 5** explains how the CAWHP coupled with the TES tank performed in different system configurations in a residential dwelling. In particular, three operation modes, including direct heating, buffering system, and combined mode, were carried out to compare their energy performance along with running costs.

- **Chapter 6** presents a load shifting study for the domestic CAWHP integrated with the TES. Different fixed scheduling strategies based on a time-of-use tariff were designed to shift the operation of the cascade heat pump to off-peak periods. The main objective of this investigation was to find the best schedule to operate the cascade heat pumps efficiently with minimised running costs and reduced wind energy curtailment, while shifting wholly the electrical heating loads to off-peak periods. What the sizing and temperature set points of the TES tank were best suitable to perform the designed load shifting strategies was also investigated. Finally, a retrofit assessment was carried out to evaluate how the designed load

shifting strategy could help the CAWHP save operating costs and carbon emissions when compared with the performance of gas and oil boilers.

- **Chapter 7** summarises the main findings of this research and suggests some works that could be conducted in the future.

Chapter 2

Experiment

2.1 Introduction

A CAWHP integrated with a TES tank was used to deliver heat to a hard-to-heat mid-terraced building at the Jordanstown Campus, Ulster University. In this chapter, the set-up of laboratory and field trial measurements along with the details of data consistencies are presented. In particular, the laboratory set-up for measuring the selected CAWHP in line with three series of the field trials for the whole couple system, carried out by Shah et al. [46], are primarily described. Then, the data consistencies of the measured cascade heat pump, the building heat demand, and the TES tank are investigated. Hence, the rest of this chapter is organised as follows:

- Section 2.2 describes in detail the experimental set-up which includes the laboratory and field trial experiments.
- Section 2.3 analyses the measurement errors.
- Section 2.4 summarises the chapter.

2.2 Experimental Set-up

2.2.1 Laboratory experiment

The selected CAWHP was previously tested in the laboratory, with the outdoor unit mounted inside a climatic chamber (Figure 2.1). Within the chamber, the air temperatures and humidity were maintained at specific levels, while the indoor unit was located outside the chamber. The indoor unit was connected with a dedicated water circuit, including a heat exchanger, a storage tank, a three-way valve, an actuator and a PID controller, to keep the inlet and outlet water temperature of the cascade heat pump constant during the tests.

FIGURE 2.1: Climatic chamber utilised for testing the CAWHP in the lab.

The cascade heat pump was tested following the conditions suggested by the European Standard EN14511 – Part 3 [54]. The testing conditions are reported in Table 2.1. The inlet and outlet water temperatures, water flow rates, and electric consumption of the cascade heat pump were measured using the instruments mentioned in Table 2.2. It is worth noting that the electric utilisation of the cascade heat pump outdoor and indoor units was measured directly by

two energy meters, which accounted for the total consumption of the two compressors, controllers, valves, fans, and a circulating pump inside the indoor unit.

TABLE 2.1: Testing conditions of the CAWHP in the lab.

T_a (°C)	$T_{w,out}$ (°C)	$T_{w,in}$ (°C)	RH (%)	$\dot{m}$ (l/s)
2	55	45	76	0.34
7	55	45	76	0.33
12	55	45	76	0.36
2	65	55	76	0.32
7	65	55	76	0.37
12	65	55	76	0.37
2	75	65	76	0.36
7	75	65	76	0.39
12	75	65	76	0.42

TABLE 2.2: Used sensors and uncertainty ranges.

Instrument	Type and model	Uncertainties
Fluid temperature	Inline and Surface PT 100, Eltek GD24	± 0.3°C
Flow meter	Electromagnetic, Eltek GC 62	± 1.5%
Electric consumption meter	Landis and Gr P350	± 1.5%

2.2.2 Field trial experiment

Two mid-terraced "hard-to-heat" dwellings designed under 1900s specifications were built at Jordanstown campus of University of Ulster to carry out UK retrofit technologies, as shown in Figure 2.2. The house to the left in Figure 2.2 is named House 64, and the one to the right is called House 63. The adjacent spaces of each house, named control rooms, were for equipment setting and climate control. These control rooms were maintained at 21 °C by separate air

conditioners. This research concentrated on House 64 that has been occupied by three inhabitants, including one teenager boy and two adults.

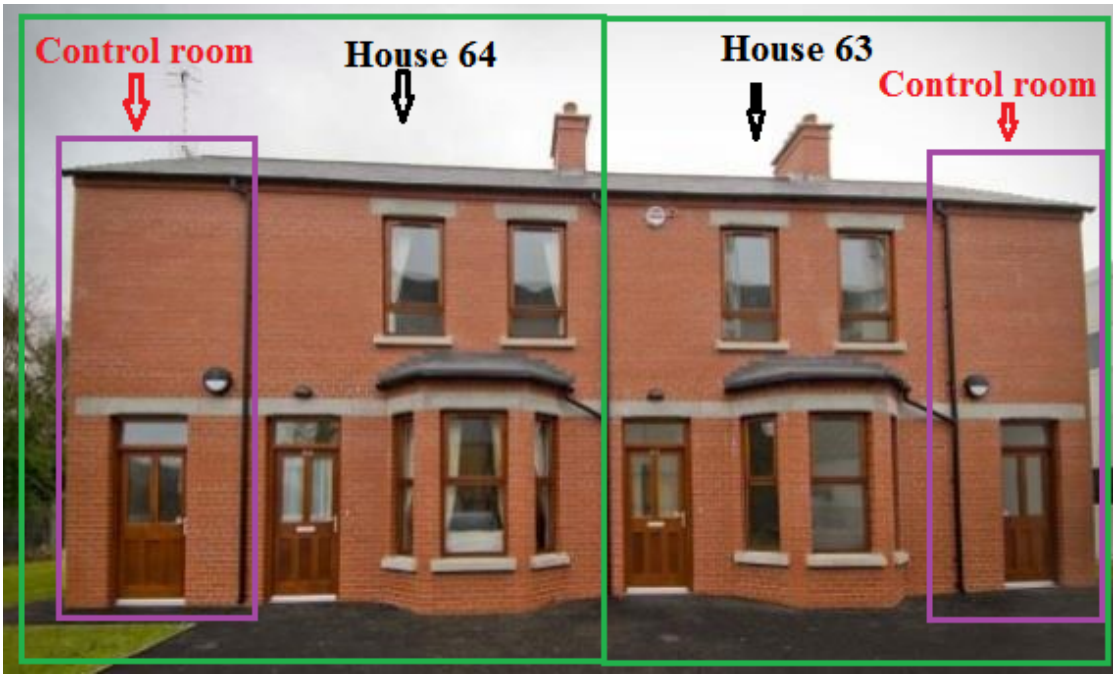

FIGURE 2.2: Two mid-terraced hard-to-heat dwellings (the house to the left is called House 64, and the one to the right is named House 63).

House 64, focused on this study, was retrofitted with a variable capacity CAWHP coupled with a TES tank to provide space heating and domestic hot water (DHW), with the schematic being depicted in Figure 2.3. Before the variable capacity CAWHP was retrofitted, the dwelling was equipped with a gas boiler providing heat directly to the building for DHW and space heating via conventional wet radiators through insulated pipes under the flooring. The nominal flow of the heating system was 75 °C. In this work, the heat distribution system was remained, whereas the boiler was replaced by the CAWHP.

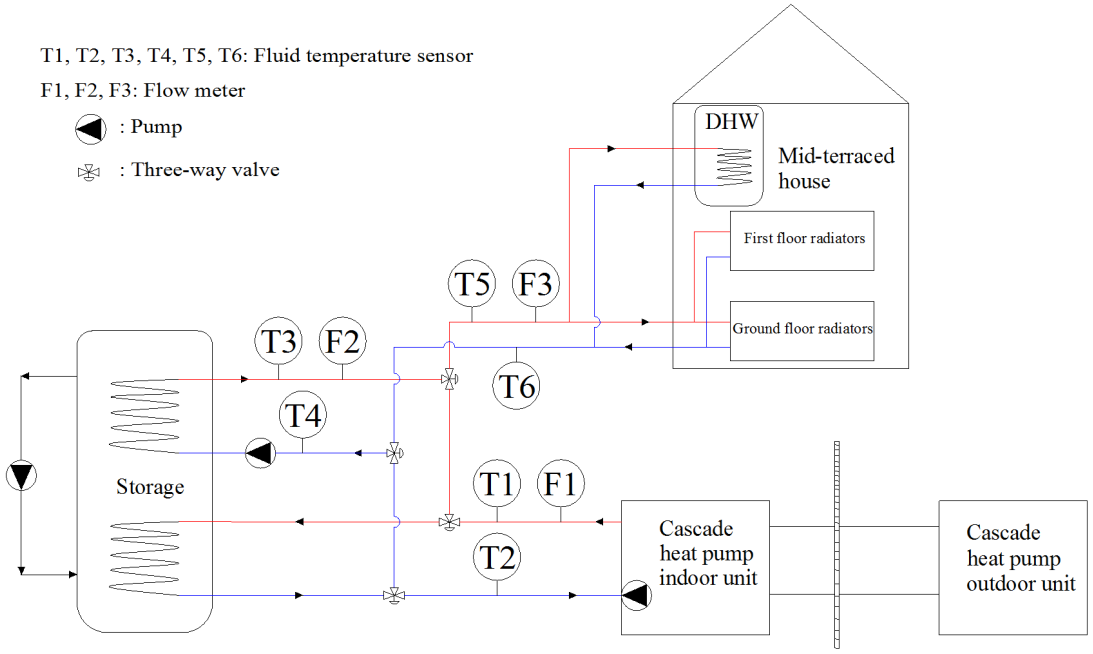

FIGURE 2.3: Schematic of the retrofit CAWHP system investigated in this research.

The investigated building (House 64) had two floors, including ground floor and first floor. Living room, dining room, storing room, and kitchen were placed at the ground floor, whilst the first floor was the areas of three bedrooms and a bathroom. Both floors had an area of 55 m^2 in accordance with the height of 2.7 m. As the storing room did not need heating, the heated volume of the ground floor was calculated to be 120 m^3, whilst 150 m^3 was accounted for the heated volume of the first floor. The capacity of the DHW tank was 162 litres with the inner heat exchanger coil area of 0.88 mm^2. The heat storage capacity of the DHW was 3.78 kWh (45 °C/65 °C) with maximum standing heat loss of 2.74 kWh/24 hrs.

The selected CAWHP had two separate compressors using different refrigerant fluids, including R-410A for the outdoor unit and R-134a for the indoor unit. The outdoor unit extracted heat from the ambient and transferred to the indoor

unit by means of the intermediate heat exchangers. Thanks to this technology, the indoor unit can lift the outlet water temperature up to 80 °C without an additional heater, making it suitable for directly replacing existing boilers without the need for modifying the distribution system. According to the manufacturer's published data, the cascade heat pump had a nominal COP of 2.5 with the nominal heating capacity of 11 kW at 7 °C (44.6 °F) DB / 6 °C (42.8 °F) WB of the outdoor unit and 80 °C (176 °F) outlet water temperature of the indoor unit [55]. The selected CAWHP was a variable capacity unit, meaning that its thermal output can be modulated depending on the required thermal load. Additionally, a pump circulating hot water from the condenser heat exchanger to the house was installed inside the indoor unit, which was designed by the manufacturer.

The TES tank was a custom made sensible vertical cylinder, as illustrated in Figure 2.4. The storage was made by copper material with 600-liter capacity, 2m height and 0.6m diameter. The tank was insulated with 75mm thick foam. The charging heat exchanger coil connecting to the heat pump was placed at the bottom part, whereas the discharging coil supplying heat to the house was at the upper part of the tank. There were seven temperature thermocouples located at an equal distance (0.33 m) for control and monitoring purposes. In this research, stratification effects occurring naturally within the sensible TES were eliminated by using a de-stat pump installed on the storage to mix thermally fully inside the tank.

The external walls of the house comprised of 215 mm fair faced clay bricks and 15 mm inner plaster insulation, in which the total U value was 1.64 W/m^2K. The garret ceiling consisted of 19 mm ply flooring and 150 mm quilt insulation and 15 mm plaster board, and the pitched roof was constructed of resin slate tiles lying on timber battens with the support of DuPont Tyvek vapor barriers, all of which resulted in U value of 1.42 W/m^2K. The floors (U value of 0.67

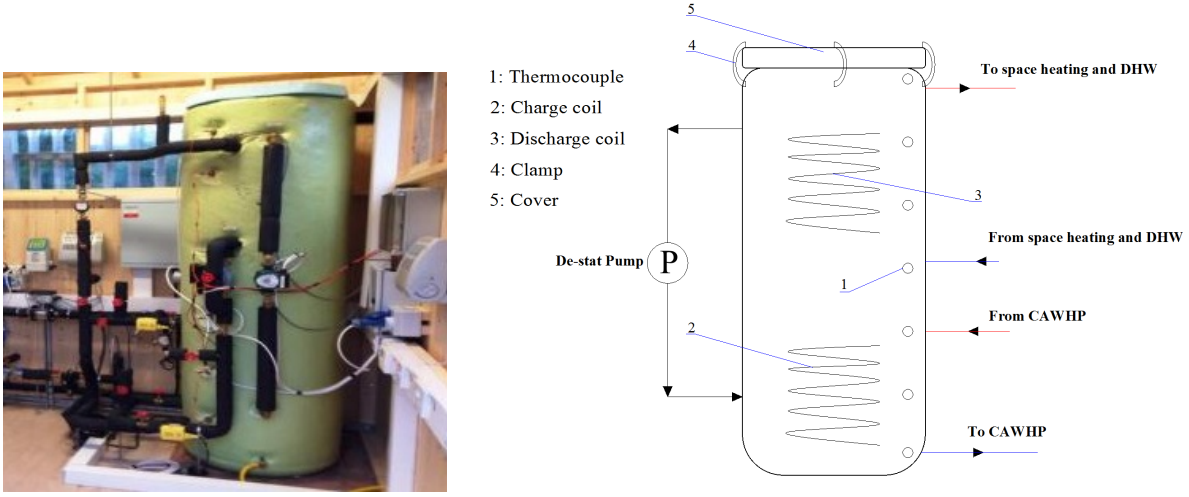

(A) In the shed (B) Its schematic

FIGURE 2.4: The measured TES tank.

W/m^{2}K) comprised of timber covering by carpets, with the vented space below the flooring. Timber double-glazed windows (U value of 4.8 W/m^{2}K) and doors (U value of 0.422 W/m^{2}K) were assembled on the external walls.

The heating system was controlled by a scheduled programmer combined with a thermostat placed in the dining room. The occupants were able to choose the set point for the room temperature and the operation time whenever they preferred. They could also freely open windows and doors as well as occupy the house. The collected field trial data were subdivided into three sessions which are described as follows:

- The first session, named **Direct Mode**, from 26/11/2014 to 10/02/2015: The cascade heat pump delivered heat directly to the house. The outlet water temperature of the CAWHP was set to 75 °C that was the same as the outlet water temperature of the replaced boiler. This session is shown in Figure 2.5a.

- The second session, named **Indirect Mode**, from 21/02/2015 to 28/03/2015: The CAWHP provided heat to the TES tank, and that heat was then transferred to the house. The cascade heat pump was switched on to reheat the

tank if the average tank temperature was below 65 °C, and it was off when the tank reached 70°C. This session can be known as a buffering system, as illustrated in Figure 2.5b.

- The third session, named **Combined Mode**, from 16/04/2015 to 07/06/2015: The cascade heat pump was switched on at 1.00am (at night) to store energy in the storage, bringing the water tank temperature to 75 °C. When the house required the first heating demand of the day, the stored energy was delivered to the house until its temperature dropped to 55 °C. After that, the heat pump took over to provide heat to the house in rest of the day. This operation can be assigned as demand-side management in which the heat pump was shifted to off-peak hours (at night) with cheap electricity prices (Economy 7 tariff [1]) to store the energy which was later used in the peak demand of the day (in the early morning). This session can be assigned as the shifted load operation, as depicted in Figure 2.5c.

[1]The electricity tariff in which the night rates are cheaper than the date rates.

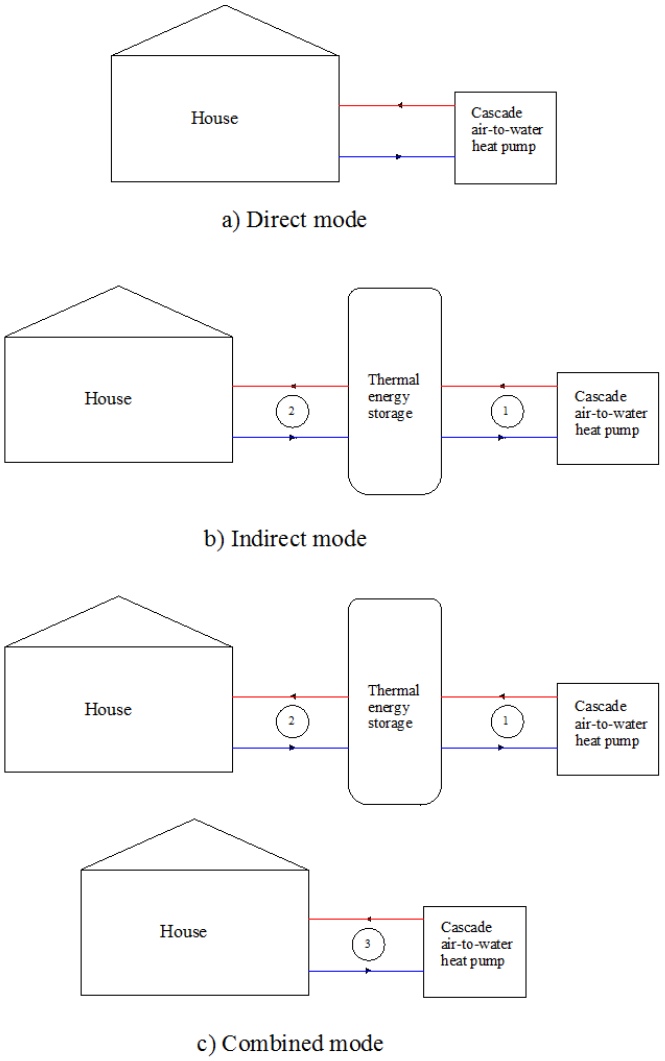

FIGURE 2.5: Operations between the cascade heat pump and the storage and the house investigated in the field trials.

The monitoring campaigns focused on the characterization of the performance of the CAWHP coupled with the TES tank in the mid-terraced hard-to-heat dwelling. As a result, the following parameters were measured:

- Heat output of the cascade heat pump, heat input/output of the storage tank and heat input to the house were calculated using water flow rates, water inlet and outlet temperatures recorded from the sensors illustrated in Figure 2.3.

- Electricity consumption of the cascade heat pump outdoor and indoor units was measured directly by two energy meters. It is worth noting that the measured electricity accounted for the total consumption of the two compressors, controllers, valves, fans and a circulating pump inside the indoor unit.

- Temperatures at the thermocouples placed on the TES were recorded. The locations of the thermocouples are depicted in Figure 2.4.

A wireless radio data logger and 15 transmitters with built-in sensors (Table 2.2) were employed to monitor the system. Data was logged in 1-minute intervals by means of a desktop computer-based data acquisition. Uncertainties of the sensors used in the measurements are reported in Table 2.2. With the ignorance of the data acquisition system's error, uncertainty analysis of the field trial measurements on the basis of sensors' errors was carried out using the method suggested by Holman [56]. Therefore, the relative uncertainties of COP and heat outputs were found ± 5.59% and ± 5.17%, respectively.

2.3 Analysis of Data Consistency

As the field trials were carried out for the different periods, the consistencies of the monitored data were checked to assess their reliability before being used for modelling and validation that are explained in the next chapter. The following subsections discuss in detail the data analysis of the measured cascade heat pump, the building thermal input/building heat demand, and the TES tank.

2.3.1 Data elaboration

Based on the measured parameters related to the heat pump, the storage, and the house, as illustrated in Figure 2.3, it is possible to acquire thermal energy output power of the heat pump ($Q_{q,hp}$), the storage ($Q_{q,store}$), and the house ($Q_{q,house}$) along with the heating coefficient of performance (COP) of the whole heat pump unit, as expressed as follows:

$$Q_{q,hp} = \rho \times C_p \times \dot{m}_{hp} \times (T_{out,hp} - T_{in,hp}) \tag{2.1}$$

$$Q_{q,store} = \rho \times C_p \times \dot{m}_{store} \times (T_{out,store} - T_{in,store}) \tag{2.2}$$

$$Q_{q,house} = \rho \times C_p \times \dot{m}_{house} \times (T_{out,house} - T_{in,house}) \tag{2.3}$$

$$COP = \frac{Q_{q,hp}}{W} \tag{2.4}$$

Where $T_{out,hp}$, $T_{in,hp}$, $T_{out,store}$, $T_{in,store}$, $T_{in,house}$, and $T_{out,house}$ are respectively water temperature sensors T1, T2, T3, T4, T5, and T6, as illustrated in Figure 2.3. $\dot{m}_{hp}$, $\dot{m}_{store}$, and $\dot{m}_{house}$ are respectively flow rate sensors F1, F2, and F3, as shown in Figure 2.3. It is noted that electric consumption of the heat pump was measured including the consumption of both compressors and auxiliaries of the whole unit, so COP in Equation 2.4 accounts for efficiency of the whole heat pump unit.

2.3.2 Data consistency of the cascade air-to-water heat pump

Heat capacity and electric consumption of the CAWHP were screened to check their measurement consistency before being used for developing and validating the heat pump model. An EQ (Electric-Thermal output) graph showing the relationship between daily heat output and daily electric consumption is plotted in Figure 2.6 in order to check the measurement errors, as proposed in the work of the Energy Saving Trust's heat pump field trials [20]. It can be seen that the relationship trends in each monitoring period are likely to form the regression lines that can be used as the references for observation of the abnormal points. Two outliers lying on y-axis can be explained by missing the heat output data, while four points close to the x-axis and far from the respective references are caused by missing data or sensor errors of the electric consumption. The rest of the visualised data is consistent so that they can be used for modelling and simulation.

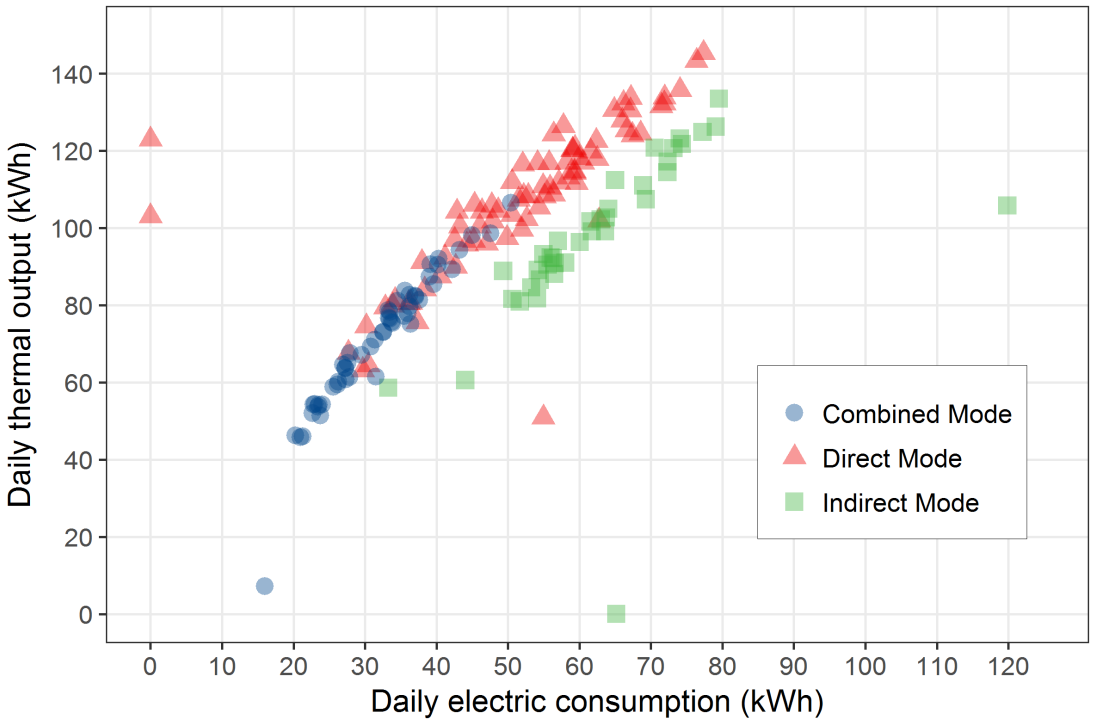

FIGURE 2.6: Daily electric utilisation versus daily thermal output of the cascade heat pump during three monitoring sessions.

2.3.3 Data consistency of the building heat demand

In order to check the data consistency of the building heat demand, the graph showing daily thermal output to the house (including space heating and DHW) versus daily mean air temperatures is illustrated in Figure 2.7. Three sparks, that are much higher than the density points respective to the y-axis, and two negative daily thermal output points can be explained by the sensors' errors. These abnormal data can be seen clearly in Figure 2.8. Also, in Figure 2.7, there are three points lying on the x-axis, which can be explained by the sensors' errors or the house occupants shutting of the heating system in those days. The rest of the data seems to form a regression line so that they can be used as a reference for the house heat demand (Figure 2.7).

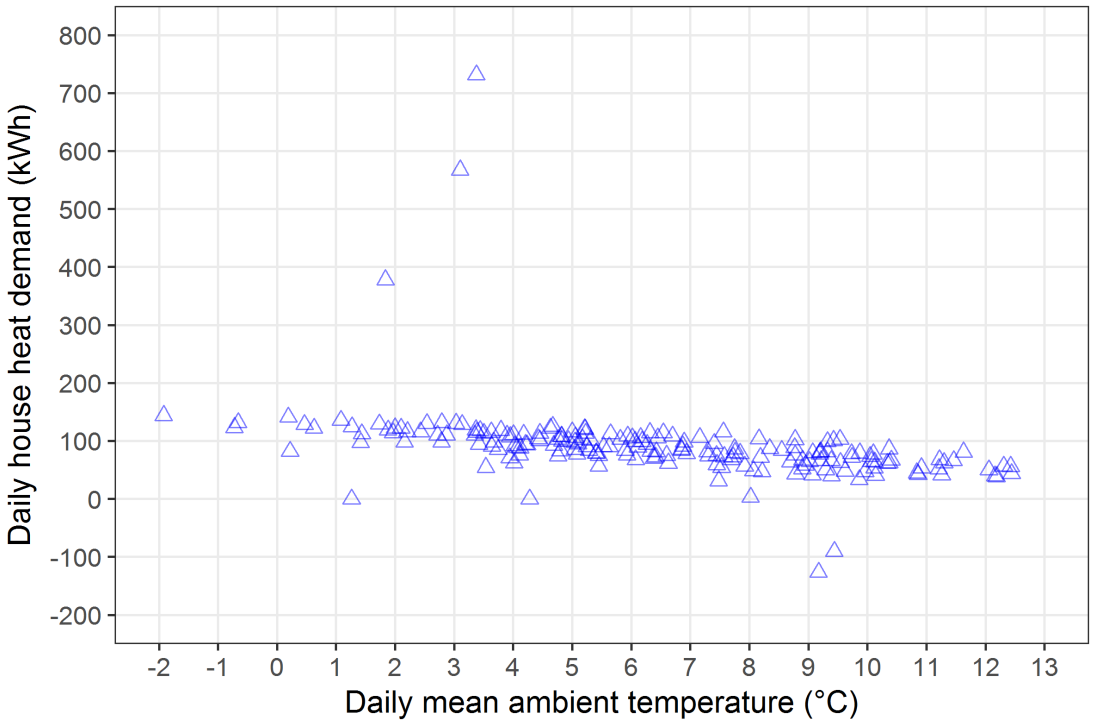

FIGURE 2.7: Collected data of daily building heat demand/building thermal input versus external air temperatures in three periods.

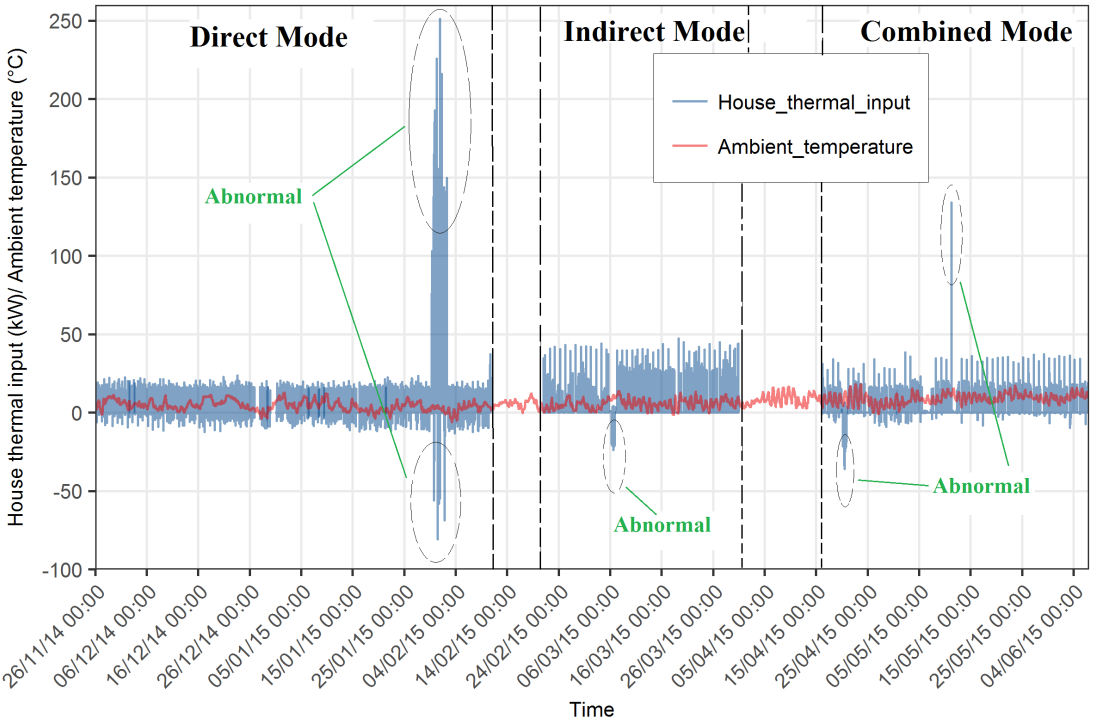

FIGURE 2.8: Collected data of daily building heat demand/building thermal input and ambient temperatures over three periods.

2.3.4 Data consistency of the thermal energy storage

To analyse data consistency of the measured TES tank, the temperatures at seven thermocouples along the vertical direction of the tank during the indirect mode and the combined mode are visualised, as shown respectively in Figures 2.9 and 2.10.

With regards to the indirect mode (the 2^{nd} monitoring campaign), the majority of the data of the temperatures at seven thermocouples seem to be reliable (Figure 2.9), except the thermocouple 6 on 6^{th} March 2015.

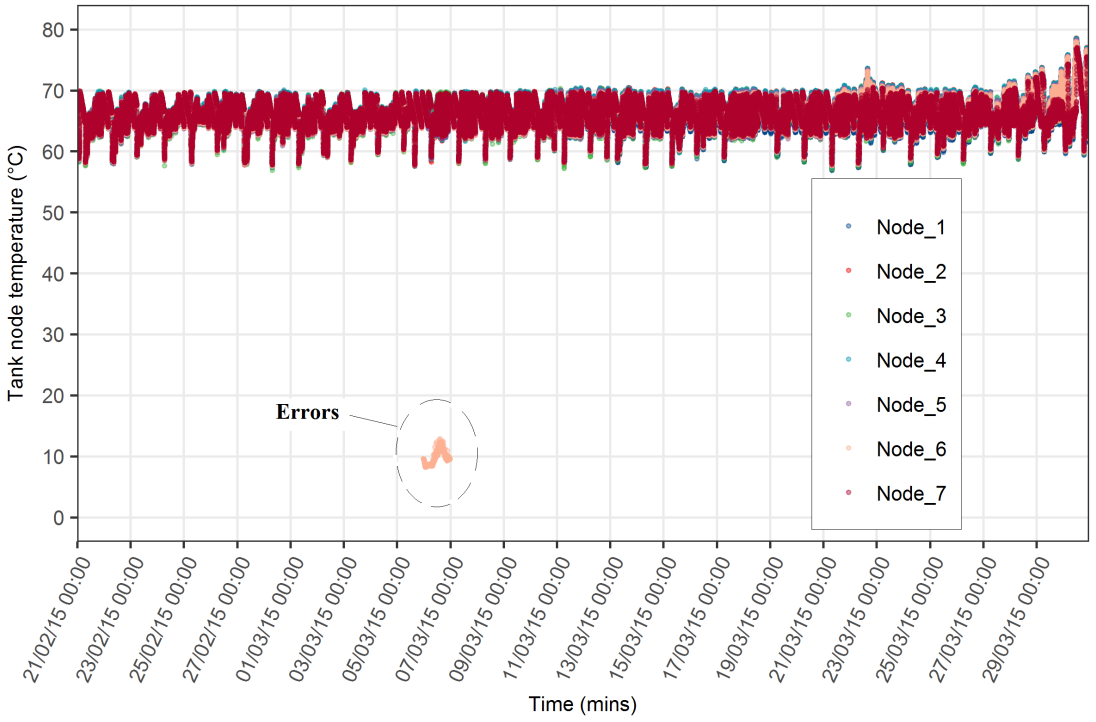

FIGURE 2.9: Temperatures at seven thermocouples along the TES tank in the indirect mode (the 2^{nd} monitoring session).

Considering the combined mode (3^{rd} monitoring campaign), looking at Figure 2.10, there are some errors or missing data in the periods from 16^{th} April to 11^{st} May 2015 and from 19^{th} May to 22^{sd} May 2015. In order to figure out these errors, Figure 2.11 shows the scatter matrix of the temperatures at seven thermocouples (seven nodes). It can be seen from the graph that there are some errors of the thermocouple 4 and thermocouple 7 (node 4 and node 7 in Figure 2.11). The data of the thermocouple 2, thermocouple 3, and thermocouple 5 seem to be reliable, while there are some errors of the thermocouple 6 occurring on 19^{th} April 2015 (Figure 2.10).

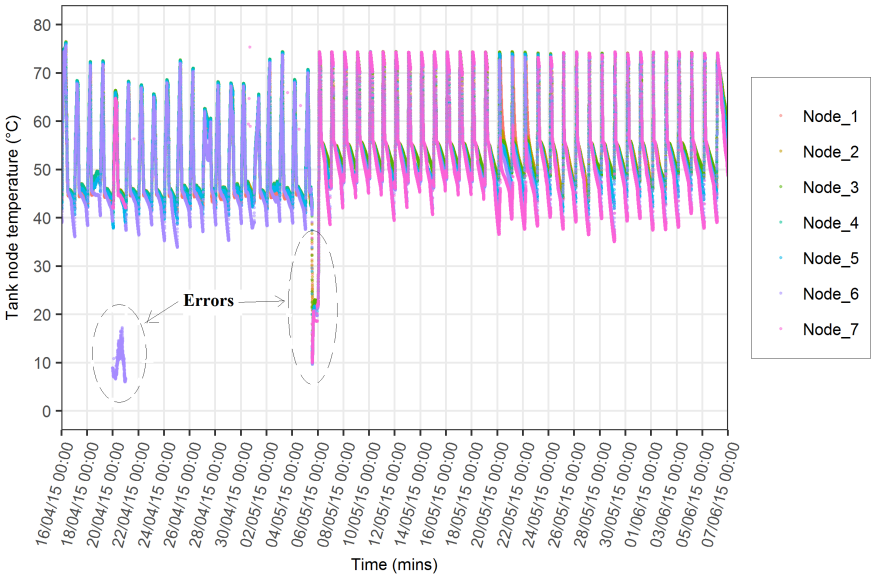

FIGURE 2.10: Temperatures at seven thermocouples (seven nodes) along the TES in the combined mode (the 3^{rd} monitoring session).

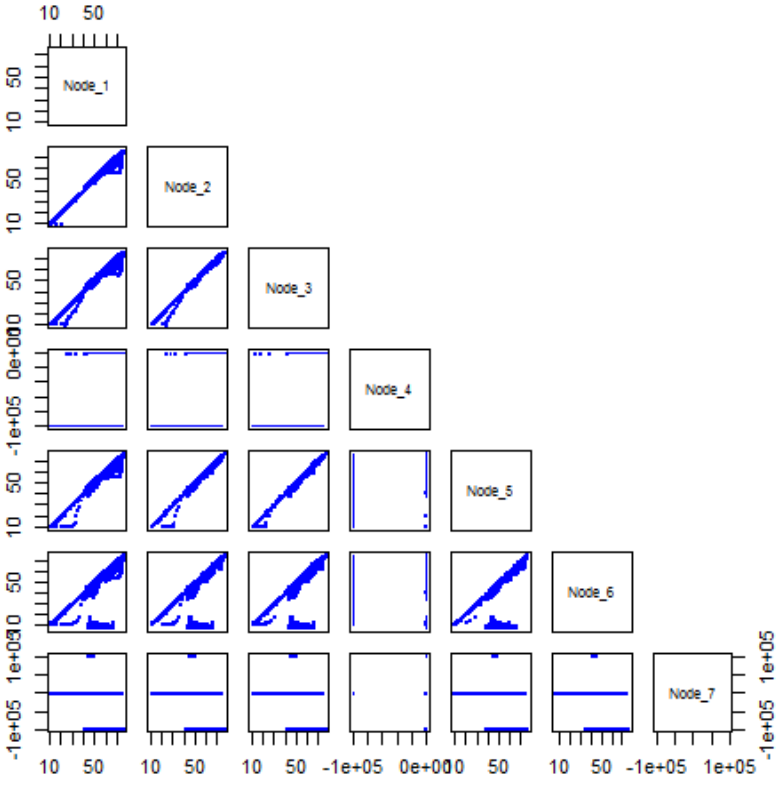

FIGURE 2.11: Scatter matrix of temperatures at seven thermocouples (seven nodes) during the combined mode (the 3^{rd} monitoring campaign).

2.4 Summary

In this chapter, the laboratory and the field trial measurements are described. In particular, how the laboratory and the field trials were set up along with how the data were measured are presented. Furthermore, the measurement consistencies of the CAWHP, the building heat demand and the TES tank are analysed to check their reliability before those data could be used for modelling and simulation purposes that are mentioned in the next chapter.

Chapter 3

Modelling and Validation

3.1 Introduction

This chapter presents the developed models and calibration/validation of the variable capacity CAWHP, the TES tank, the mid-terraced hard-to-heat dwelling, and a whole couple building simulation in TRNSYS environment. In particular, the inverter CAWHP was modelled using performance map approach. Then, it was calibrated and validated in two steps including component itself and integration with the whole building model. The calibration and validation of the heat pump model were carried out using the measured data acquired from both laboratory and field trial tests. The other models of the thermal store, the building, and its whole couple simulation model were also developed, calibrated/validated accordingly to the field data, using either component itself or integration with the whole building model. The rest of this chapter explains in detail these processes and is organised as follows:

- Section 3.2: The reason why TRNSYS environment was used to model and simulate the investigated system in this study is explained.

- Section 3.3: TRNSYS modelling is demonstrated, including the developed models of the variable speed compressor CAWHP, the TES tank, the hard-to-heat building, the DHW tank, and the whole couple building simulation.
- Section 3.4: Calibration and validation of the developed models are discussed.
- Section 3.5: Summary of this chapter is drawn.

3.2 Selection of Modelling Tools

TRNSYS simulation software version 17 [57] was utilised as a principal tool to model and simulate the investigated system of this research. TRNSYS, advanced by University of Wisconsin, is a transient system simulation tool in which individual components called "types" are linked to each other to model the energy performances of the HVAC systems and the buildings of which their behaviors are highly complicated. In addition, this tool can enable the links between itself and other simulation environments, such as Google SketchUp [58], GenOpt [59], Engineering Equation Solver (EES) [60], MATLAB and SIMULINK [61], etc. One of the examples of these useful links is the connection between TRNSYS and GenOpt environment that can help to solve optimisation problems, such as building calibration, system parameter optimisations, etc., at the same time steps. Another example is that TRNSYS can plug in with Google SketchUp to create building geometry and thermal characteristics of building envelops from scratch. Due to its strengths and advantages, TRNSYS has been widely known and used for numerous studies, and this tool was also chosen for modelling and simulation purposes of this research.

3.3 Modelling

3.3.1 Cascade air-to-water heat pump model

To model the inverter CAWHP, TRNSYS Type 1217 (non-standard TESS library component [62]) was used to predict the performance of the selected cascade heat pump. This model can be categorised as a "black box" relying on a performance map requiring the information acquired from field observations or manufacturer/laboratory data based on the users' need. This kind of heat pump model needs less information compared to physical models requiring a high level of system parameters which are often unapproachable due to commercial constraint or are uncertain [63]. Complexity also increases if modelling cascade units that employ two separate compressors. For example, Stefano et al. [64] modelled a cascade air source heat pump system in TRNSYS by means of connecting two single-stage heat pumps via a heat exchanger. The single-state heat pump was a semi-physical model developed by Heinz and Haller [65] considering thermal dynamic refrigerant cycle and thermal refrigerant properties of the heat pump. This cascade model thus required details of each compressor unit. However, it is impossible in the author's case to obtain that information because of commercial sensitivity and measurement costs. Furthermore, model errors can increase as more parameters involve in the model, making it more difficult for calibration and validation. This research aims to assess seasonal performances of the cascade heat pump rather than evaluating the component design level. Therefore, it is suitable in the author's circumstance to use Type 1217 which relies on a characterised performance map to model the selected CAWHP.

Regarding Type 1217, parameters stated in the performance map were heat capacity and electric input power as functions of ambient temperatures, desired outlet water temperatures, and more importantly, part load ratios at which the

heat pump operated to maintain the user-specified outlet water temperatures regardless of alterations in inlet water temperatures or external air conditions. Once the performance map was known, a series of calculations were performed. First, after heating control signal input to the heat pump model was on, the heat required to bring the inlet water temperature up to the user-defined outlet water temperature at the condenser side was calculated using Equation 3.1.

$$Q_{require} = C_p \times \dot{m} \times (T_{w,setpoint} - T_{w,in}) \tag{3.1}$$

Then, the model determined the actual energy delivered to water by means of comparing the calculated required heat and the present heating capacity which was returned by the data interpolation routine, as expressed in Equation 3.2.

$$Q_{load} = Minimum(Q_{interpolation}, Q_{require}) \tag{3.2}$$

After that, outlet water temperature was calculated using the following Equation 3.3.

$$T_{w,out} = T_{w,in} + \frac{Q_{load}}{\dot{m} \times C_p} \tag{3.3}$$

Finally, COP of the heat pump is expressed in Equation 3.4.

$$COP = \frac{Q_{load}}{W_e} \tag{3.4}$$

The performance map, containing full load and part load curves, is the heart of the heat pump model Type 1217, and thus obtaining performance curves is a considerate task. The performance data provided by the manufacturer and the laboratory results contained nominal values obtained from standard tests,

which were different with the data from field operations in the manner that the operation ranges were limited. Also, no data about the part load operation was available from the manufacturer. Therefore, the data collected from the field trial monitoring were used for performance map creation. This characterised performance map can allow the model to be performed like the real operation; however, note that the model accounted for steady states only.

To build the performance map and the defrost model, the recorded raw data regarding the cascade heat pump from three monitoring sessions, mentioned in Chapter 2, were processed using R (programming language) software [66] along with the suggested procedure of Underwood et al. [63] as follows:

- The time-series data in each monitoring session were gathered into one file and null value rows, indicating when the heat pump was switched off, were discarded from the file.
- The processed data was then divided into two separate files. The first data file was used for creating the performance map of the heat pump model, with all data rows describing defrost cycles being removed (defrost events were observed by abnormal low and negative thermal output during steady state periods at low outdoor air temperatures and high relative humidity). These defrost data were retained in the second file to investigate the defrost model.

The following subsections discuss in detail how the performance map (including full load and part load curves) and the defrost model were created based on the two data files.

3.3.1.1 Full load curves

To build the full load curves of the variable capacity CAWHP model, the monitoring results of the first data file regarding thermal output and electric input power as the functions of external air temperatures were analysed. Figure 3.1 shows the monitoring data of the cascade heat pump producing outlet water temperature of 75 ± 1 °C, which is the set temperature carried out in the field trials. It is worth noting that the electric input power of the compressors, fans, controllers and a circulating pump was totally accounted for in the performance curves due to the field measurement set-up explained in Chapter 2. The data points are coded with color gradient referring to DeltaT that is the difference between outlet and inlet water temperatures at the heat sink. It can also be seen in the figures that the higher DeltaT, the higher thermal output and electric input power, all of which represent the higher load operation of the cascade heat pump.

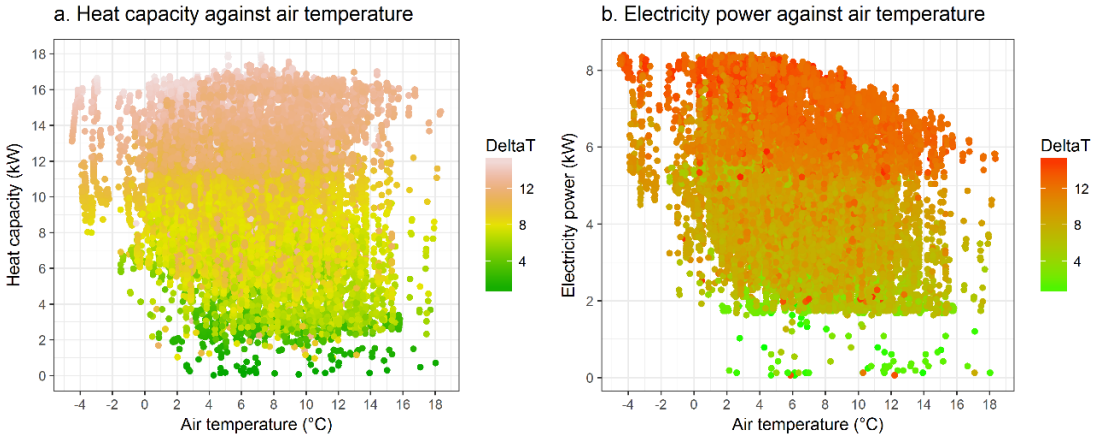

FIGURE 3.1: Measured data of heat and electric power versus ambient temperatures with water flow temperature of 75 ± 1 °C (DeltaT is the difference between outlet and inlet water temperatures at the condenser side of the cascade heat pump).

Since there were not enough data for sampling with the smaller intervals of DeltaT (e.g. 13 - 14 °C, or 14 - 15 °C), all data points with DeltaT above 12 °C were screened to analyse the full load curves, as illustrated in Figure 3.2. The

trends of median values of the box plots in both graphs (Figures 3.2a and 3.2b) are likely to form regression lines. Consequently, after removing the outliers observed in the whisky box plots (these random spikes related to transient states when the heat pump was switched on or off), the regression lines of the median values were then assumed as the full load curves of the heat pump model for the outlet water temperature of 75 °C.

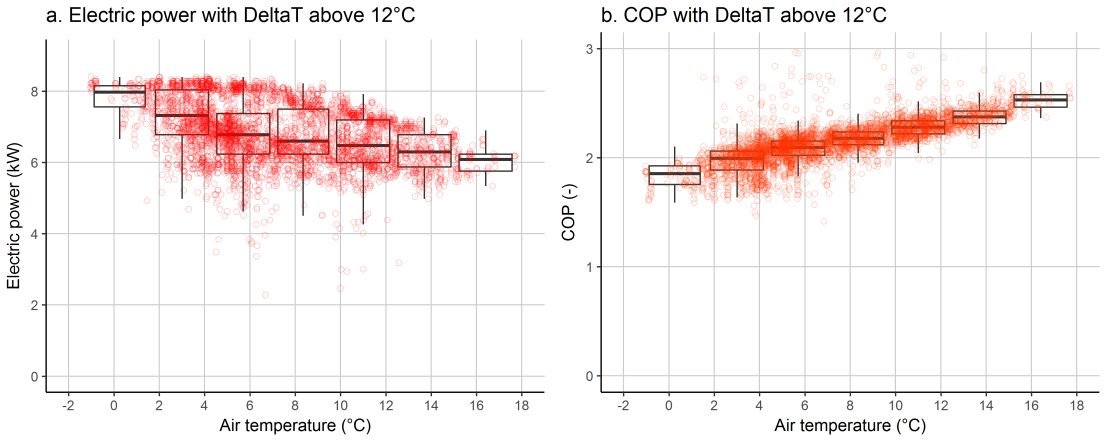

FIGURE 3.2: Measured data of electric power and COP versus ambient temperatures with DeltaT above 12 °C and water flow temperature of 75 ± 1 °C.

Investigating the same approach for the rest data with other outlet water temperatures, a characterized performance map for full load operation was obtained for the heat pump model. The empirical correlations of the obtained full load curves are defined in the following Equation 3.5 and Equation 3.6 where the heat capacity (Q_{full}) and compressor electric power (W_{full}) at full load operation are the functions of external air temperatures (T_a) and desired outlet water temperatures ($T_{w,out}$). These equations were received from polynomial regression.

$$\begin{aligned} Q_{full} = &-451 + 21 \times T_{w,out} - 1.14 \times T_a - 0.03 \times T_{w,out}^2 - 0.009 \times T_a^2 \\ &+ 0.001 \times T_{w,out}^3 + 0.03 \times T_{w,out} \times T_a - 0.0002 \times T_{w,out}^2 \times T_a \end{aligned} \tag{3.5}$$

$$\begin{aligned} W_{full} = &-1.01 + 0.7 \times T_{w,out} + 0.24 \times T_a - 0.01 \times T_{w,out}^2 \\ &+ 0.000051 \times T_{w,out}^3 - 0.0105 \times T_{w,out} \times T_a + 0.000075 \times T_{w,out}^2 \times T_a \end{aligned} \tag{3.6}$$

3.3.1.2 Part load curves

The retrofit CAWHP can ramp up or down its thermal output to maintain the desired water outlet temperatures. As part load operation highly influences the heat pump efficiency, the model needs to take this effect into consideration.

Figure 3.3 illustrates the measured part load data of the heat pump to maintain the outlet water temperature of 75 °C at different external air temperatures, with part load ratio (PLR), electric input ratio (EIR) and part load factor (PLF) being expressed in the following Equations 3.7, 3.8, and 3.9, respectively. The data shown in the figures are grouped with external air temperature intervals of 1 °C ranging from 7 °C to 13 °C. The data outside of this range are not plotted to make the graph easier to look.

$$PLR = \frac{Q}{Q_{full}} \tag{3.7}$$

$$EIR = \frac{W}{W_{full}} \tag{3.8}$$

$$PLF = \frac{COP}{COP_{full}} \tag{3.9}$$

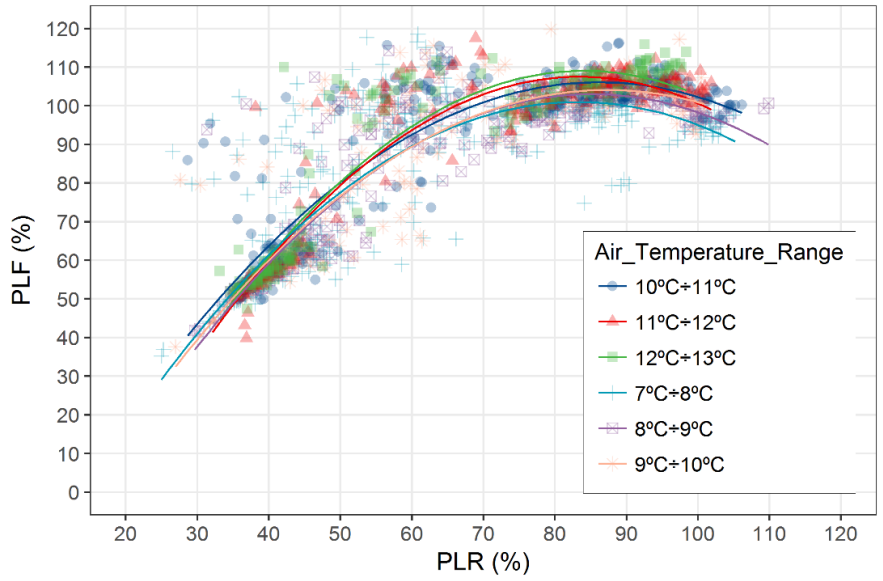

(A)

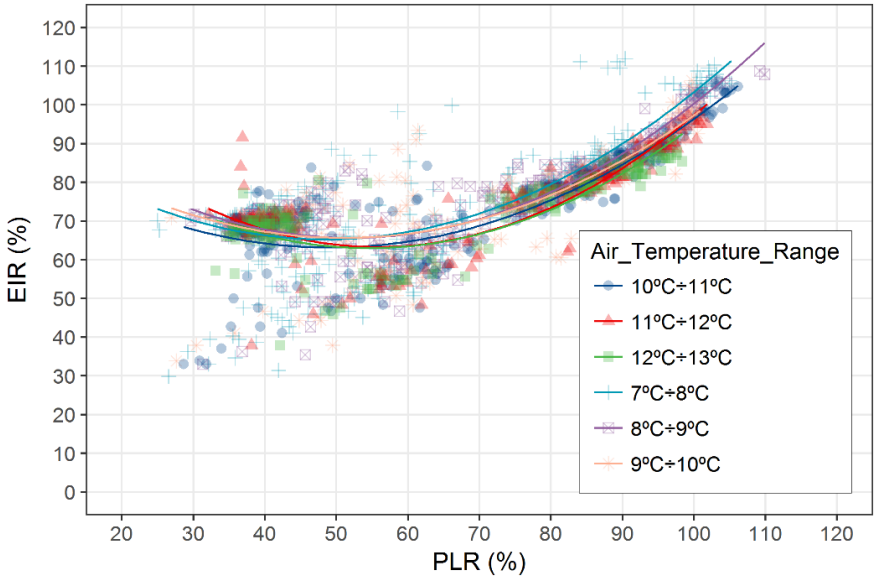

(B)

FIGURE 3.3: Part load curves of the heat pump to maintain outlet water temperature of 75 °C with different external air temperatures acquired from the field trial results: (a) PLF versus PLR with different air temperature ranges; (b) EIR versus PLR with different air temperature ranges.

In Figure 3.3, the regression curves are not much different, while the air temperatures vary. Therefore, the curves respective to the external air temperature of 8 - 9 °C were assumed as the identical part load operation of the heat pump

model, as shown in Figure 3.4. It is worth noting that the part load curves found in this study are similar to the results of Bettanini et al. [67] and Fischer et al. [68]. However, the highest efficiency of the CAWHP in this study can be achieved if operating at about 85% of the maximum heat load, which differs from the studies of those authors in which the highest efficiency of the heat pumps can be acquired when operating from 40% to 60% of the full load capacity. This discrepancy may be due to the different types of the heat pumps used. In other words, the heat pump carried out in this research is cascade unit, while the heat pumps conducted in those studies are single-stage ones.

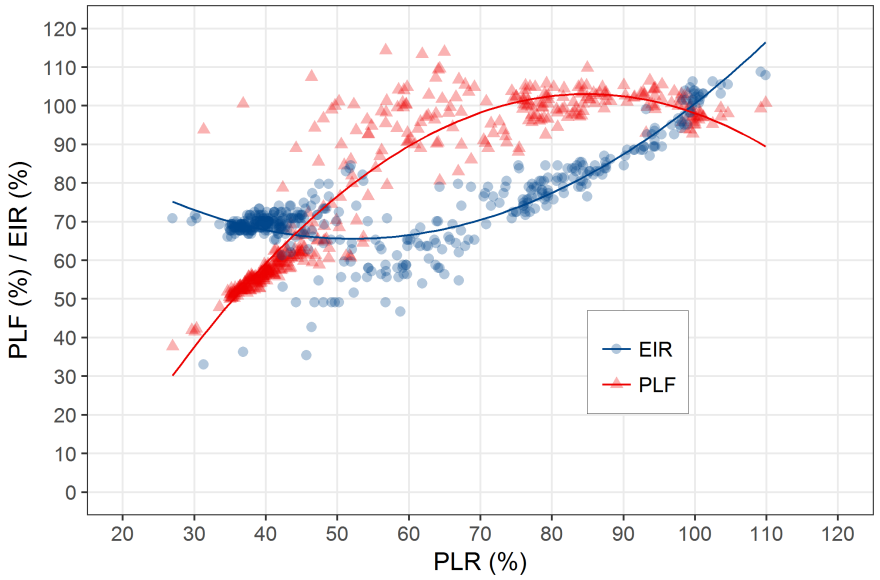

FIGURE 3.4: Part load curves of the cascade heat pump at the ambient temperature of 8 - 9 °C.

3.3.1.3 Normalised performance map

To let the TRNSYS Type 1217 heat pump model understand the declared performance map, the full load and part load curves mentioned above were normalised, as required by the TRNSYS developer. The normalised values were calculated using the following Equations 3.10 and 3.11. The heat capacity and electric input power values at the external air temperature of 7 °C in accordance

with the outlet water temperature of 75 °C were chosen as reference values, being 14.95 kW and 6.48 kW, respectively. These values were set up in the initial model and calibrated later as mentioned in the following Section 3.4.1.

$$f_q = \frac{Q_{pm}}{Q_{ref}} \tag{3.10}$$

$$f_e = \frac{W_{pm}}{W_{ref}} \tag{3.11}$$

3.3.1.4 Defrost cycles

The initial heat pump model was carried out utilising the collected performance data that excluded periods of defrost operation (the first data file). Therefore, a model accounted for defrost operation was developed and integrated outside the heat pump model.

Literally, when frost is formed on the surface of the evaporator heat exchanger, the heat pump's performance is reduced, and the compressor may be damaged because frost accumulation on the evaporator coil acts as a thermal insulator in addition to reducing air flow passage [31]. To address this problem, air source heat pumps need to activate defrost cycles periodically to melt the ice on the outdoor coils. Reverse cycle, reversing refrigerant fluid, is a popular defrost method, and it was also adopted in the selected CAWHP in this research.

Modelling defrost operation regarding reverse cycle is commonly challenging [69]. Particularly, how often an air source heat pump activates defrost and how long a defrost cycle lasts are often difficult to predict. This is because the rate of frost growth on the evaporator coils are affected by three main factors which cannot be determined sufficiently: (1) outdoor air conditions; (2) characteristics

of air source heat pumps (e.g. outdoor heat exchanger geometry [70], outdoor fan speed [71]); and (3) operating conditions (e.g. thermal load).

Consequently, the proposed defrost model in this research was simplified using empirical correlations obtained from the monitoring results. The recorded data showed that if the external air temperature was below 7 °C and relative humidity was above 65% for a long period, the heat pump terminated heating to activate defrost operation, which is similar to other works of Underwood et al. [63] and Madonna and Bazzocchi [31]. The time between defrost cycles or frosting time (minutes) was determined based on the external air temperature and relative humidity, as expressed in the following Equation 3.12.

$$\triangle t_{def} = a_{fr} + b_{fr} \times T_a + c_{fr} \times RH + d_{fr} \times T_a^2 + f_{fr} \times RH^2 + g_{fr} \times T_a^3 + h_{fr} \times RH^3 \tag{3.12}$$

in which $\triangle t_{def}$ is the time between defrost cycles or frosting time (min). T_a and RH are ambient air temperature (°C) and relative humidity (%), respectively. a_{fr}, b_{fr}, c_{fr}, d_{fr}, f_{fr}, g_{fr}, h_{fr} are empirical coefficients determined from polynomial regression surface. The values and units of these coefficients are reported in Table 3.1.

TABLE 3.1: Empirical coefficients of frosting function.

Empirical coefficient	Unit	Value
a_{fr}	min	39
b_{fr}	min/°C	-1.06
c_{fr}	min/%	0.33
d_{fr}	min/°C^2	0.13
f_{fr}	min/$\%^2$	-0.0093
g_{fr}	min/°C^3	-0.018
h_{fr}	min/$\%^3$	-0.00006

Duration of a defrost cycle was calculated using Equation 3.13. The typical period of a defrost cycle was from one minute to ten minutes according to the monitoring results.

$$t_{def} = a_{def} + b_{def} \times T_a + c_{def} \times \triangle t_{def} + d_{def} \times T_a^2 + f_{def} \times \triangle t_{def}^2 + g_{def} \times T_a^3 + h_{def} \times \triangle t_{def}^3 \tag{3.13}$$

where t_{def} is the period of a defrost cycle (min). $\triangle t_{def}$ is frosting time (min), and T_a is external air temperature (°C). a_{def}, b_{def}, c_{def}, d_{def}, f_{def}, g_{def}, h_{def} are empirical coefficients obtained from polynomial regression surface. These values are presented in Table 3.2.

TABLE 3.2: Empirical coefficients of defrost function.

Empirical coefficient	Unit	Value
a_{def}	min	56.2
b_{def}	$\text{min}/°C$	-0.34
c_{def}	-	-3.56
d_{def}	$\text{min}/°C^2$	-0.047
f_{def}	1/min	0.079
g_{def}	$\text{min}/°C^3$	0.0096
h_{def}	$1/min^2$	-0.00057

The proposed cooling energy of a defrost cycle ($E_{c,def}$) (Equation 3.14), which is the energy extracted from indoor to outdoor unit to melt the ice accumulation on the evaporator surface, and the proposed electric consumption ($E_{e,def}$) (Equation 3.15) during a defrost cycle are defined as follows.

$$E_{c,def} = \frac{t_{def} \times Q_{def,mean}}{60} \tag{3.14}$$

$$E_{e,def} = \frac{t_{def} \times W_{def,mean}}{60} \tag{3.15}$$

where average cooling capacity during defrost cycles ($Q_{def,mean}$) was obtained from the monitoring results, equalling 1.92 kW. Mean electric input power during defrost cycles ($W_{def,mean}$) was found 0.97 kW from the collected data. These average values were set up in the initial defrost model and calibrated later (explained in below Section 3.4.1).

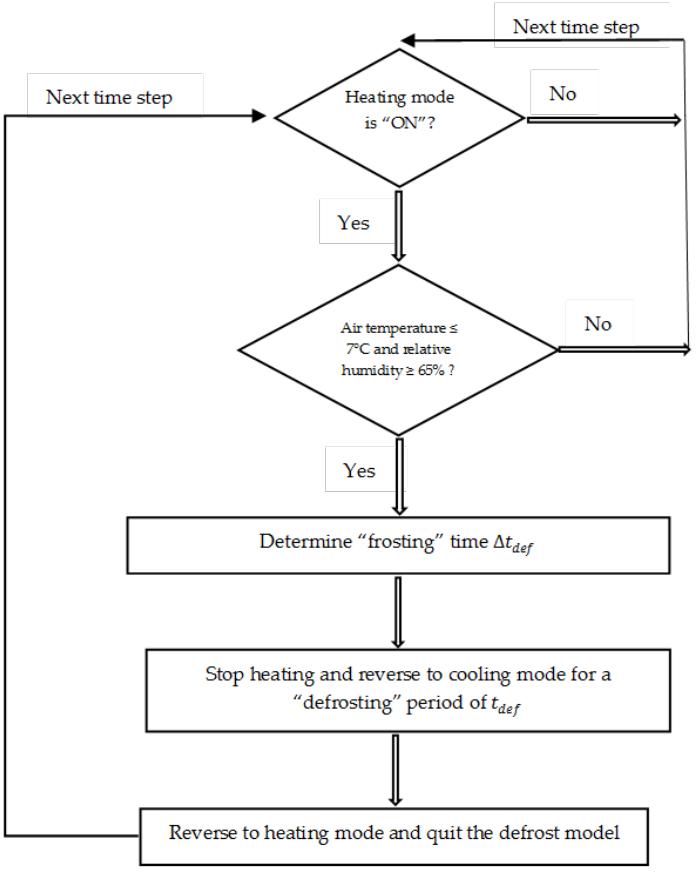

FIGURE 3.5: Flow chart of the defrost model in TRNSYS.

Figure 3.5 shows the flow diagram of the proposed simple defrost model implemented in TRNSYS. The dynamic defrost cycle model was managed by using a

simple frosting time ($\triangle t_{def}$) and defrosting time (t_{def}) on a modified timer trigger developed by Olivier et al. [72]. Particularly, when the heating signal of the heat pump was on and frost conditions were met, the timer waited for a certain period (frosting time $\triangle t_{def}$) before activating the defrost signal which forces the heat pump into cooling mode for the specified defrosting time.

3.3.2 Thermal energy storage model

TRNSYS Type 534 (TESS library [62]) was used to model the TES. The tank dimensions and characteristics were set up similarly to the field trial TES which is described in Chapter 2. Particularly, there were seven thermocouples along the vertical line of the cylinder so that seven level nodes with equal distances were set up in the tank model. Two coiled tube heat exchangers were identified with the heat exchanger for charging the tank occupied in three nodes placed at the tank's bottom, while the another for discharging was in the other four nodes.

There was a de-stat pump forcing water convection inside the tank to prevent stratification effect so that a pump model (Type 3d) was also incorporated into the storage tank model.

3.3.3 Building model

The building geometry was first drawn in Sketchup software [58], illustrated in Figure 3.6, based on the layout of the real house (Figure 3.7) and was then imported into TRNSYS Type 56, with known building dimensions and envelop characteristics explained in Chapter 2. The infiltration rate of the house was initially set to one air change per hour following the standard proposed by CIBSE

[73]. The boundary profiles obtained from the collected data containing adjacent room temperatures of the adjacent house (House 63 to the right in Figure 2.2) was assigned as inputs that affected the internal heat gains of the building model. Since occupancy patterns, lights and other electric appliances were not monitored, characteristic internal heat gains regarding weekdays and weekends for the building model were developed based on surveys and interviews.

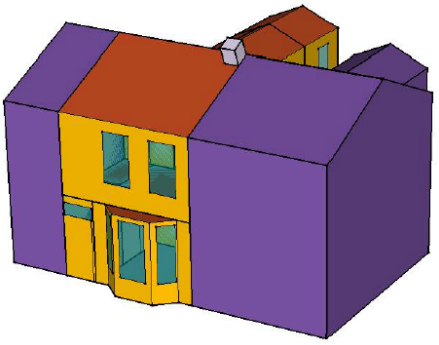

FIGURE 3.6: House model drawn in SketchUp software.

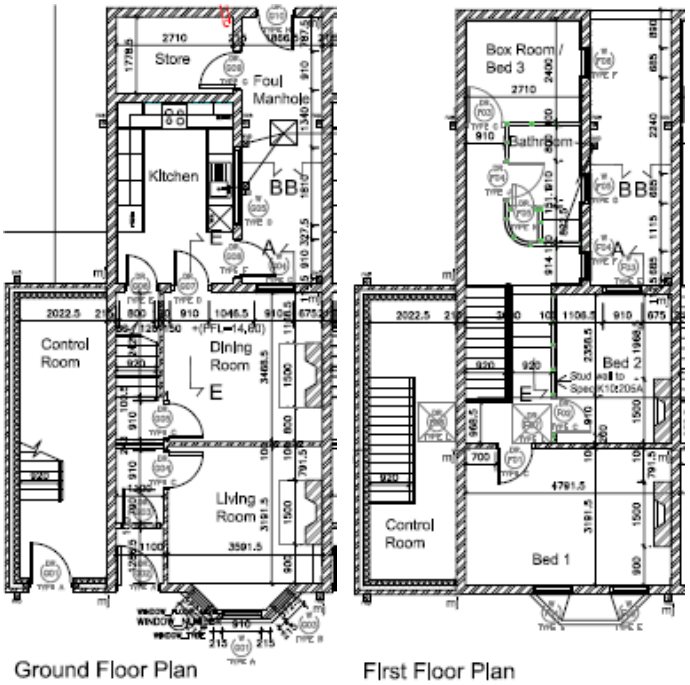

(A) (B)

FIGURE 3.7: Layout of the investigated house (House 64 in Figure 2.2): (a) Ground floor; (b) first floor.

3.3.4 Domestic hot water model

The DHW tank was modelled using Type 534 [57], containing one immersed heat exchanger as well as thermal characteristics that were the same as the one in the field trial. DHW was charged by the heating system if the top tank temperature was below 50 °C, and it was off when the top tank temperature reached 60 °C. Hot water drawing patterns in the model were the same as the ones in the monitored data, as shown in Figure 3.8, which allows the hot water consumption of the DHW model operate like the practical hot water use.

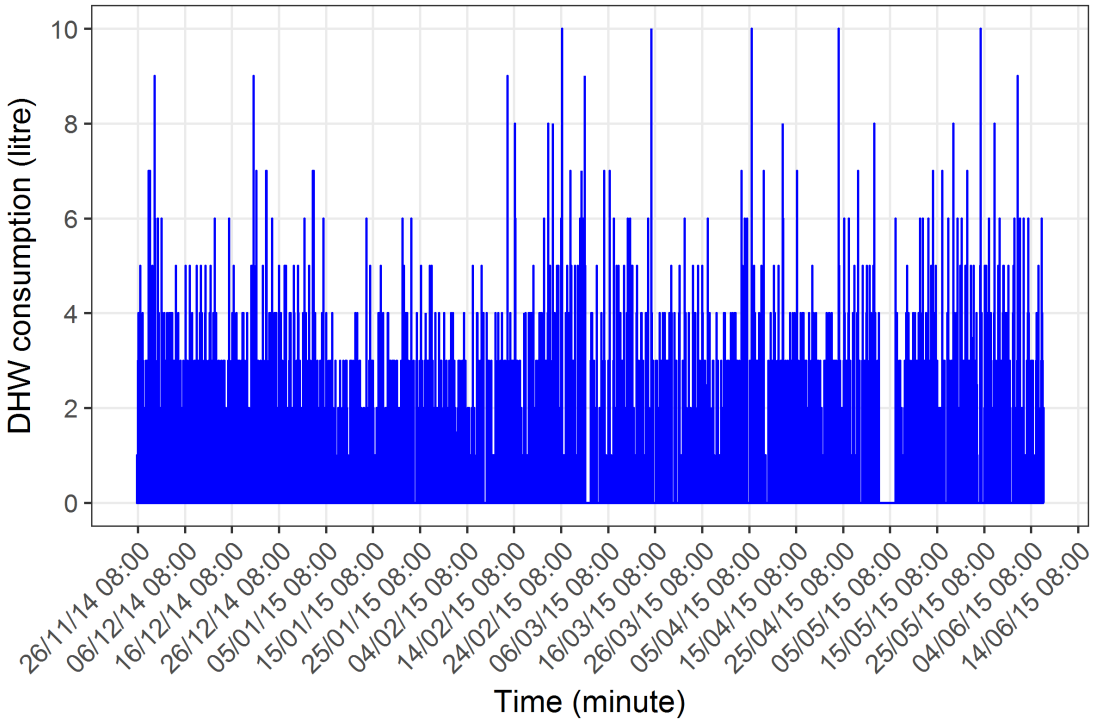

FIGURE 3.8: Example of one-minute measured profile of hot water drawing patterns from 26^{th} November 2014 to 7^{th} June 2015.

3.3.5 Whole building simulation model

The cascade heat pump model, the TES model, the building model and the DHW model above were integrated with other TRNSYS component models to compose a whole system, as depicted in Figure 3.9. The heat distribution

system was modelled thoroughly, including radiators (Type 1231), valves (Type 11 and Type 647), piping (Type 31), temperature sensors (Type 911) that were available in TRNSYS standard [57] and TESS component libraries [62]. Type 15 was utilised to model the weather data, and the irradiation macro model is illustrated in Figure 3.10. The DHW macro model is shown in Figure 3.11 which contains the storage tank Type 534 and hot water drawing pattern input, all of which are mentioned section Figure 3.3.4. The defrost control is depicted in Figure 3.12 in which defrost cycles were modelled using TRNSYS Types as explained in section 3.3.1.4.

The heating system operated from 7.00am to 11.00pm every day observed from the monitoring data, and thus the heat pump model was also controlled on/off during that time. The temperatures within the dining room were maintained between 19.5 °C and 21.5 °C. The flow temperatures from the heat pump to the radiators were fixed to 75 °C which are the same as the field trial ones.

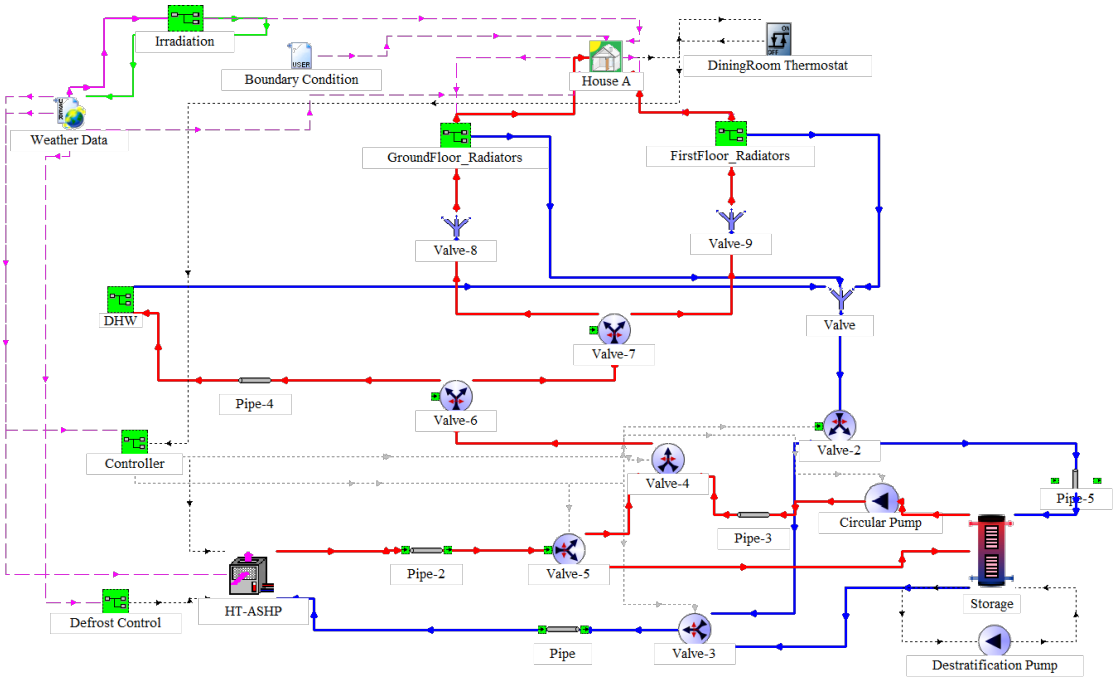

FIGURE 3.9: Overview of the whole integrated building model in TRNSYS Studio.

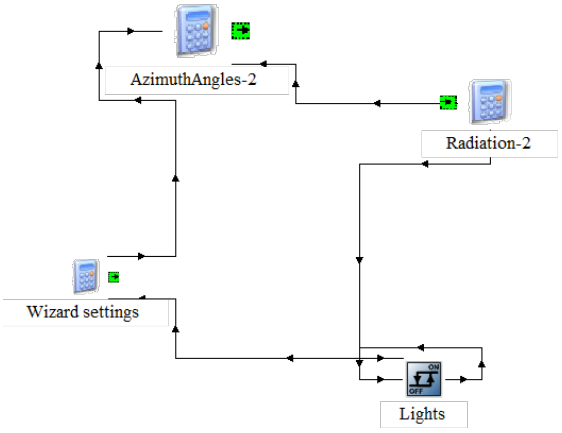

FIGURE 3.10: Model of irradiation in TRNSYS Studio

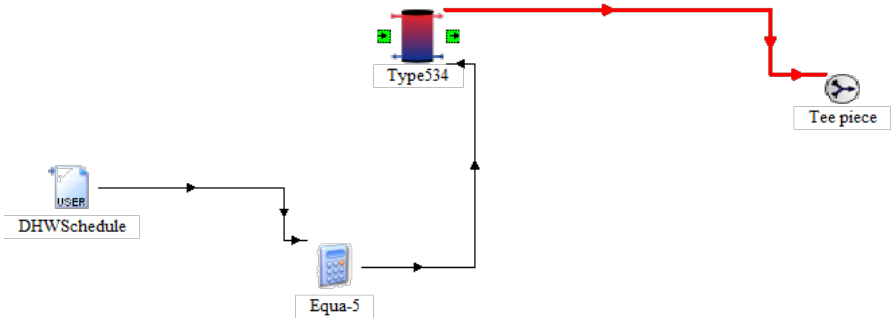

FIGURE 3.11: Model of DHW in TRNSYS Studio

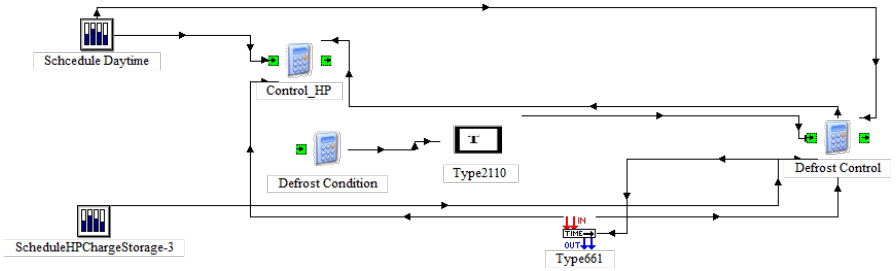

FIGURE 3.12: Model of heat pump defrost cycles in TRNSYS Studio

3.4 Calibration and Validation

After developing the models, calibration and validation were carried out to ascertain that the developed models were reliable for further extracted simulations. Calibration is the process in which some parameters are changed to minimise the errors between the model and the experimental results. Validation

is another process in which the parameters' values obtained from calibration are used to verify the errors between the model and experimental results for different periods rather than the periods used for calibration.

The following subsections describe in detail the calibration and validation of the developed heat pump model, the TES model and the whole coupled building simulation model.

3.4.1 Calibration and validation of the cascade heat pump model

There were two main steps to calibrate and validate the performance map-based cascade heat pump model Type 1271:

- First, the developed heat pump model was calibrated and validated at ***component level***. This means that the performance map-based heat pump model Type 1271 was calibrated and validated itself without coupling with the whole building simulation model shown in Figure 3.9.
- Second, the heat pump model was then integrated into the whole simulation model (Figure 3.9) to calibrate and validate, named ***integrated level***. This step aimed at finding the right values of the performance map-based heat pump model's parameters, proving that the model was reliable for running further simulations when it was linked with the whole building model.

It is noted that the calibration of the heat pump model was the process in which some parameters were altered automatically using GenOpt software [59] to minimise the cost function which accounts for the differences of COP and outlet water temperatures between the model's results and the measured data, as described in detail in the following sections. The validation was the step in which

the calibrated parameters were kept constant to predict the model's results for a different time period, and then the predicted results were compared with the measured data.

3.4.1.1 Component level

Methods: The scheme of the heat pump model for calibration and validation at component level in TRNSYS Studio is depicted in Figure 3.13. The data reader Type 9a [57] containing the experimental results of mass flow rates and inlet water temperatures were obtained as the inputs for the heat pump model, which makes the inlet conditions of the heat pump model similar to the inlets of the measured cascade heat pump. The predicted results of the outlet water temperatures and the heat pump COPs were compared with the measured data. TRNSYS Type 15 was utilised to model the weather data obtained from the on-site weather station or from the laboratory testing conditions. The simulations were initiated with one-minute intervals to capture the high accurate operation of the heat pump model.

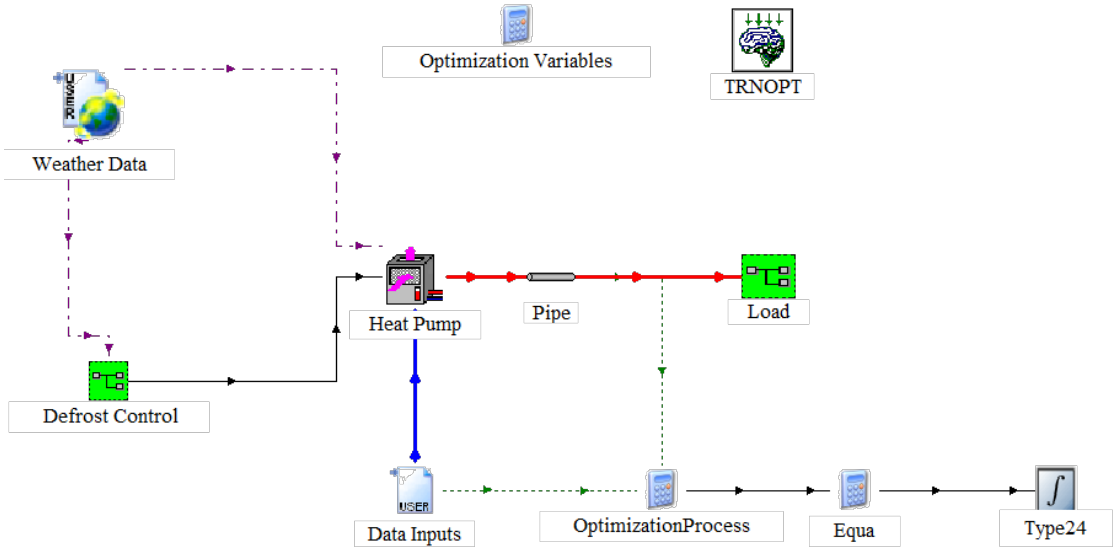

FIGURE 3.13: Schematic of the calibrated and validated heat pump model at component level in TRNSYS Studio.

The accuracy of the heat pump model was quantified by Coefficient of Variation of the Root Mean Squared Error, CV(RMSE), which is expressed in Equation 3.16 according to ASHRAE Guideline 1 [74]. For optimisation-based calibration, the sum of CV(RMSE)s of outlet water temperature and COP was a cost function (Equation 3.17), used to adjust the selected parameters to minimise the uncertainties between the model and the experiment through generic optimisation tool GenOpt [59] that linked with TRNOPT type (TESS libraries) [62]. The optimisation in GenOpt was done by Hook-Jeeves algorithm which is recommended for solving continuous and differentiable cost function [75].

$$CV(RSME) = \frac{\sqrt{\frac{\sum(Y_{sim}-Y_{measure})^2}{n}}}{\overline{Y}_{measure}} \times 100 \tag{3.16}$$

where $Y_{measure}$ is measured value; Y_{sim} is simulated value; n is number of observations; $\overline{Y}_{measure}$ is arithmetic mean measured value regarding n observations.

$$f = CV(RSME)_{OWT} + CV(RSME)_{COP} \tag{3.17}$$

where f is cost function; $CV(RMSE)_{OWT}$ is CV(RMSE) of outlet water temperature; $CV(RMSE)_{COP}$ is CV(RMSE) of COP.

In order to verify the model, there were two main steps:

- First, the predicted results were calibrated and validated using the data collected from the field trial experiments. In particular, the first six days (8^{th} to 13^{rd} December 2014) were chosen for calibration, and the calibrated model was then validated in the next six days (14^{th} to 19^{th} December 2014). These periods were chosen as the weather conditions during this time were suitable to test the heat pump performance in defrosting. The

measured one-hour data intervals of weather conditions during these periods, obtained from the on-site station, are shown in Figure 3.14. The ambient temperatures altered from 0.1 °C to 11.3 °C, and the relative humidity changed between 72.1% and 100%. Although the model parameters were finely tuned based on the curves and information informed by the recorded data, the initial model results did not acquire the high coincidence with the data collection. It was found at this stage that the defrost cycles' parameters were the main cause of this difference. Therefore, such parameters related to mean cooling capacity and electric input power during defrost cycles, mentioned in above Section 3.3.1.4, were chosen for optimising the cost function f in Equation 3.17.

- Second, as the heat pump model was calibrated and validated based on the field trial results in which the outdoor air temperatures were not controlled, its reliability should be re-checked. Therefore, the heat pump model's predictions were also compared with the data obtained from the laboratory experiments.

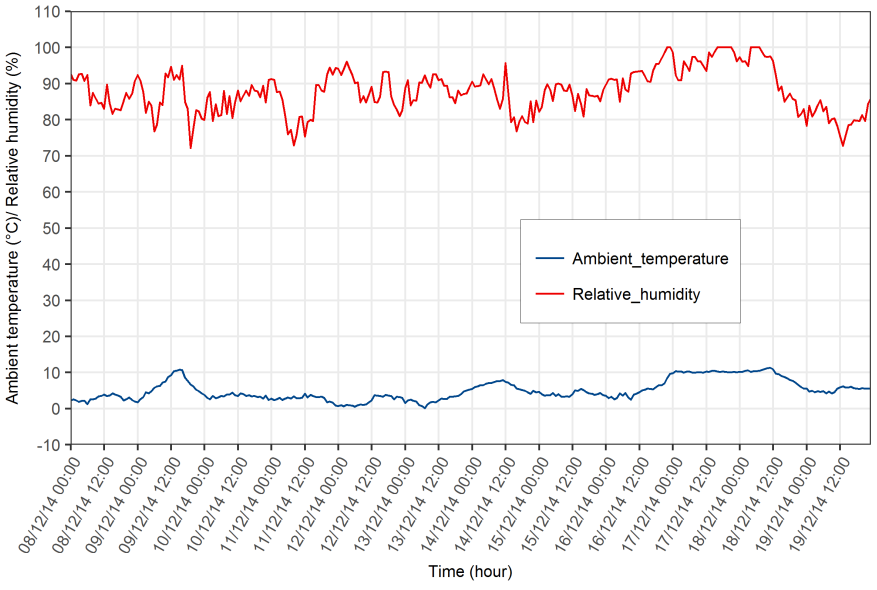

FIGURE 3.14: Real weather conditions of Belfast-Northern Ireland from 8^{th} December 2014 to 19^{th} December 2014.

Results of calibration and validation at component level:

Comparison with the field trial results: Figure 3.15 shows the quality of the calibrated simulation data versus the monitoring results in terms of outlet water temperatures at the condenser side. The figure indicates a strong correlation between the calibrated simulation results and the field trial data, with the R^2 linear of 0.961. The average cooling capacity and electric input power during defrost cycles were calibrated to be 2.17 kW and 1.75 kW, respectively.

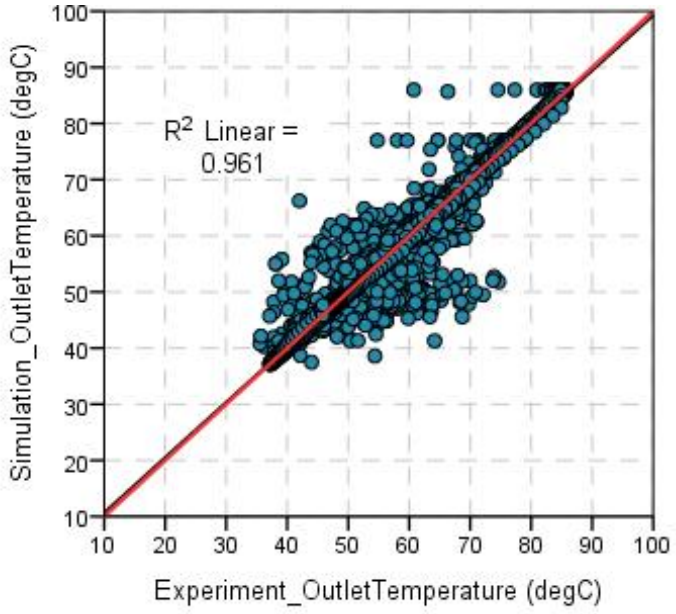

FIGURE 3.15: Comparison of calibration results of outlet water temperatures between the heat pump model and the field trial one.

In Figure 3.16, the validated outlet water temperatures highly matched with those of the recorded data, with the R^2 value of 0.955. These results indicate that the calibrated parameters could provide good results for the outlet water temperatures of the heat pump model.

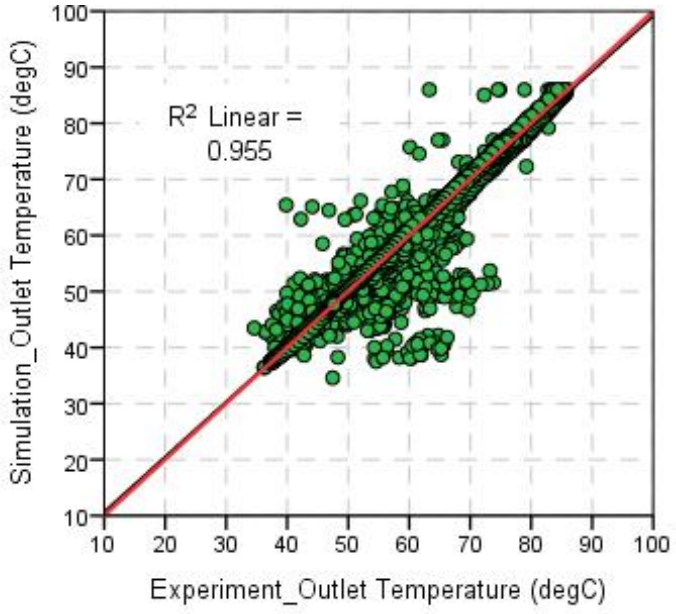

FIGURE 3.16: Comparison of validation results of outlet water temperatures between the heat pump model and the field trial one.

COPs versus external air temperatures at different outlet water temperatures were also investigated to assess if the adapted performance map of the heat pump model was acceptable with the monitored data. In Figures 3.17 and 3.18, all data points of COP values versus air temperatures at the outlet water temperatures of 55 ± 1 °C and 65 ± 1 °C are illustrated, respectively. It can be seen that all simulated COPs were likely to coincide with most of the measured COPs, except some out-of-fit points which could be described by start-up duration of the heat pump. This phenomenon is further explained in the below paragraph. TRNSYS Type 1271 could not reflect the start-up transients so that these large discrepancies remained. Looking at Figure 3.19, all COP values of the model with the outlet water temperature of 80 ± 1 °C highly correlated with those of the monitored data. In short, it can be said that the results of the performance map-based heat pump model relatively coincided with those of the monitored heat pump in steady states, whereas there remained large differences because of start-up transients.

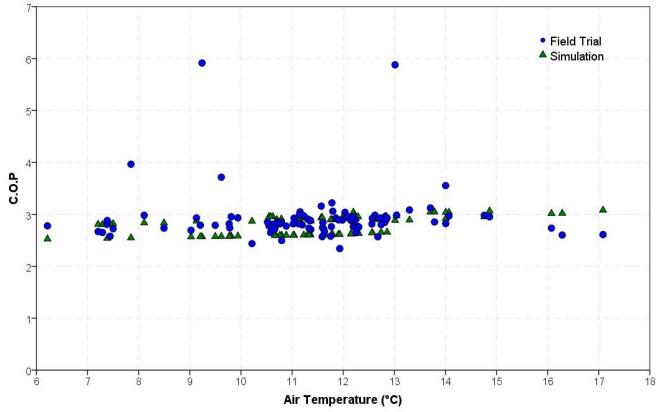

FIGURE 3.17: Validation results of COPs against ambient temperatures with outlet water temperature of 55 ± 1 °C.

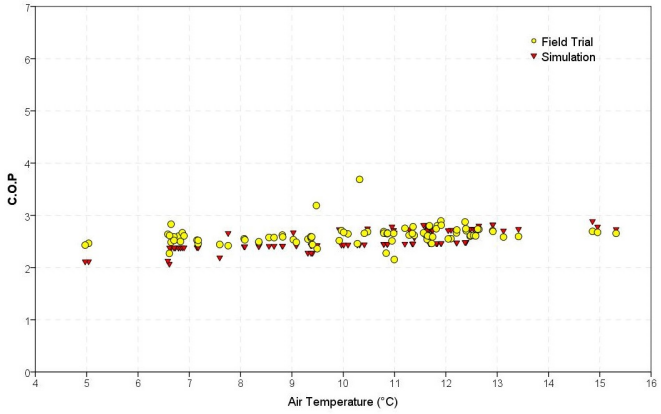

FIGURE 3.18: Validation results of COPs against ambient temperatures with outlet water temperature of 65 ± 1 °C.

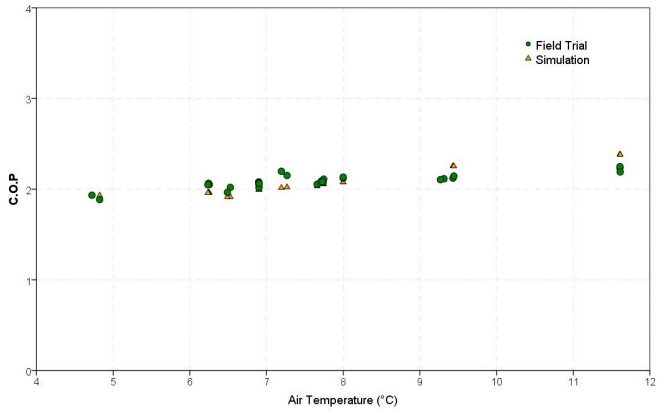

FIGURE 3.19: Validation results of COPs against ambient temperatures with outlet water temperature of 80 ± 1 °C.

The results of CV(RMSE)s of the calibration and validation simulations at component level using the field trial data are reported in Table 3.3. It can be seen in the table that the accuracy of the calibrated and validated models for both outlet water temperatures and COPs was improved, compared with those of the initial model. Particularly, CV(RMSE)s of the validated model (4.14% for outlet water temperature and 11.6% for COP) were slightly higher than those of the calibrated (3.84% for outlet water temperature and 11% for COP). As a result, it can be said that the calibrated parameters could be reliable.

TABLE 3.3: Results of calibration and validation at component level.

CV(RMSE)	Initial model	Calibrated Model	Validated Model
Outlet water temperature	6.26%	3.84%	4.14%
COP	17.69%	11%	11.6%

To discuss the discrepancies happening in start-up durations, Figures 3.20, 3.21, and 3.22 are depicted, all of which show the model and field trial results of the outlet water temperatures, heat capacity, and electric input power from 02.00 h to 09.00 h on 10^{th} May 2015, respectively. Both the outlet water temperatures and heating capacity of the monitored data observed high sudden increases in start-up transients, whereas the model results did not (Figures 3.20 and 3.21). This is because in reality, the heat transfer rate from the compressor fluid to the condenser water in start-up transients is maximum, whilst the condenser water flow rate is relatively slower in start-up transients than in steady states, all of which result in the high sudden rise of the outlet water temperatures in respective to the sudden increase of the heat capacity. In TRNSYS, however, the heat capacity and electric input power were linearly interpolated based on evaporator air temperatures with proper condenser entering water temperatures contained in the performance map, so there was not any noticeable increase in the

start-up. Additionally, the field trial heat capacity was much higher in the start-up transients than in the steady-state (Figure 3.21), whereas its consumed electric power was not much different in both states (Figure 3.22). This resulted in much higher COPs in start-up transients than in steady states, which helps to explain why the big different COPs in Figures 3.17 and 3.18 were observed.

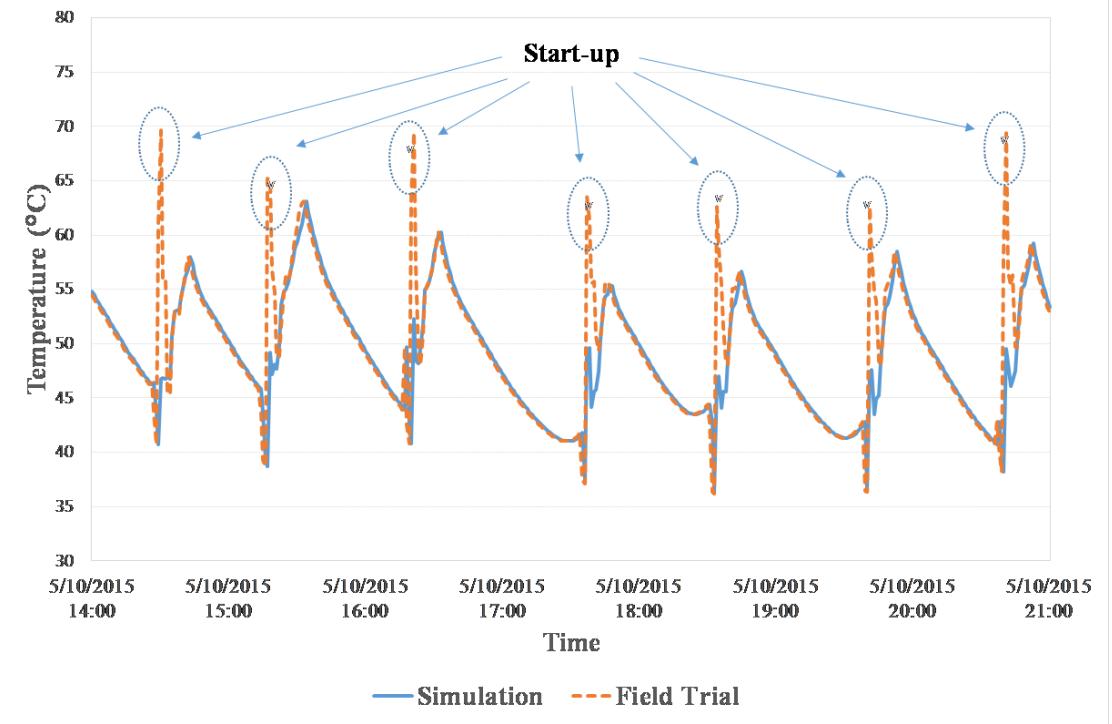

FIGURE 3.20: Outlet water temperatures of simulated and field trial results.

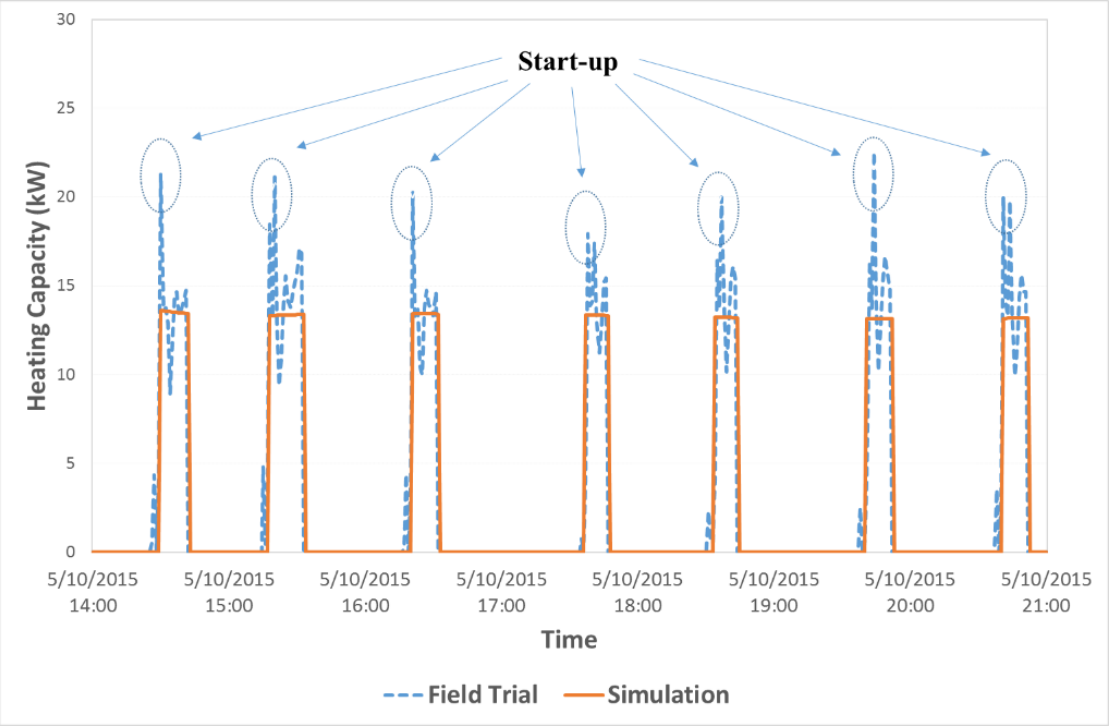

FIGURE 3.21: Heat capacity of simulated and field trial results.

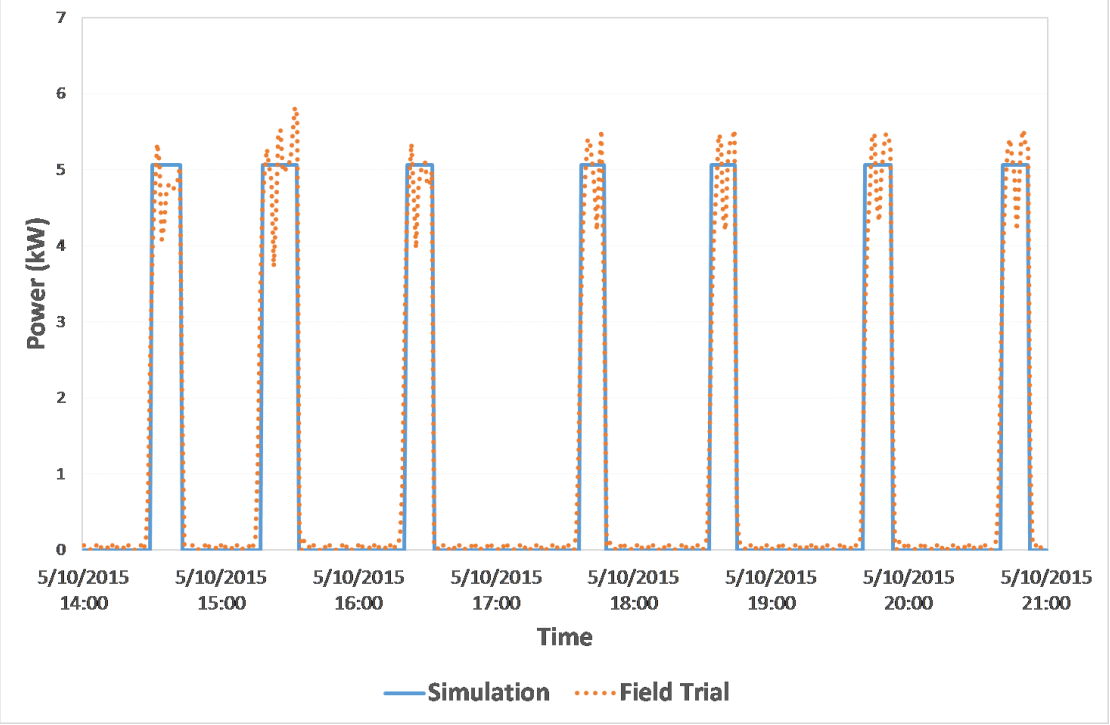

FIGURE 3.22: Electric input power of simulated and field trial results.

Comparison with the laboratory data: To re-check the reliability of the heat pump model calibrated and validated using the field trial results, the heat pump model's predictions were also compared with the data obtained from the laboratory experiments. Figure 3.23 shows the comparison results between the heat pump model and laboratory experiments. The predicted electric power was within the uncertainty range of ± 1.5% (Figure 3.20a), and the COP computed from the model was also within the difference of ± 5.59% (Figure 3.20b).

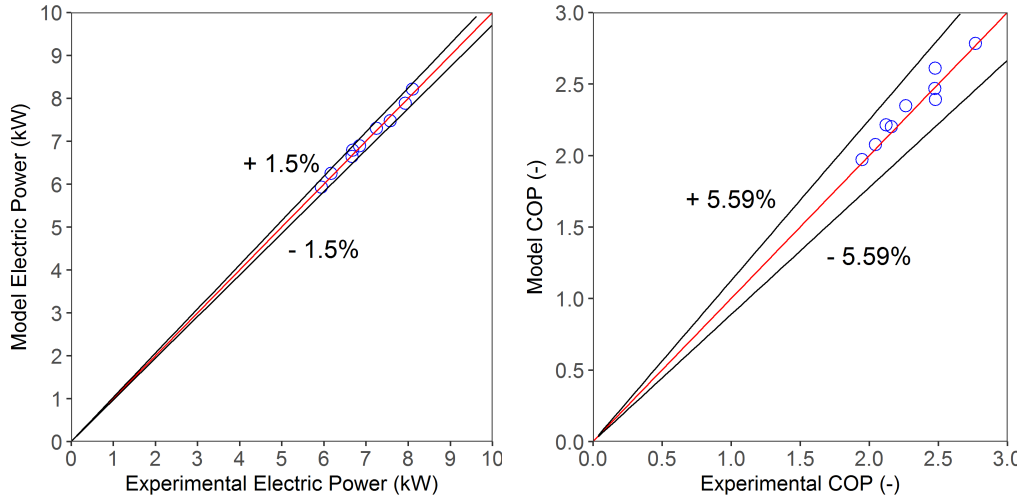

(A) (B)

FIGURE 3.23: Comparison between the heat pump model and laboratory experimental results: (a) Comparison of electric power utilisation; (b) COP comparison.

3.4.1.2 Integrated system level

Methods: After calibrating and validating the heat pump model at component level, the model was then integrated into the whole building simulation model, as depicted in Figure 3.9. The simulations at this stage were also run with one-minute intervals, and the real weather data of the on-site station were acquired to run.

While the heat pump model parameters were already calibrated and validated at component level, the initial results of the predicted daily COPs at this stage, integrated system level, were not highly matched with the measured ones. It was found that the reference values (reference heat capacity and electric input power in the performance map mentioned in Section 3.3.1.3) were the main causes of the model's errors. Therefore, these parameters were calibrated again at this step through an optimisation of a cost function, expressed in Equation 3.18, which defines the variation between the measured and simulated daily COPs. GenOpt software in combination with TRNSYS was also obtained to automatically alter the calibration parameters to attain the minimum value of the cost function ($f_{daily,COP}$). Hook-Jeeves algorithm was also adopted for optimization process in GenOpt environment.

$$f_{daily,COP} = CV(RSME)_{daily,COP} = \frac{\sqrt{\frac{\sum(COP_{daily,sim} - COP_{daily,measure})^2}{n}}}{\overline{COP_{daily,measure}}} \times 100 \quad (3.18)$$

There were two sets of the recorded data used for calibration and validation at this stage. On the one hand, the calibration was performed using the collected data of the first two monitoring sessions, direct mode (26^{th} November 2014 to 10^{th} February 2015) and indirect mode (21^{st} February to 30^{th} March 2015). On the other hand, the validation was carried out utilising the field trial results of the third monitoring session, combined mode (16^{th} April to 7^{th} June 2015).

There are some reasons why the calibration was investigated using the first two monitoring sessions, while the validation was performed based on the results of the third measuring campaign. In the direct mode, the heat pump delivered heat directly to the house, and according to the indirect mode, the heat pump charged storage all the time. This means that the collected data of these campaigns included the period of the heat pump operating as the direct heating

and the buffering system, all of which reflect the operation of the heat pump in the combined mode.

Results of calibration and validation at integrated system level: COP and COP_{sys}, defined respectively in Equations 3.19 and 3.20, were used to summarise the simulation results of calibration and validation of the heat pump model at integrated system level. Note that COP is of the heat pump only, while COP is of the whole system which accounts for all heat losses from the heat pump to the house.

$$COP = \frac{E_{q,hp}}{E_e} = \frac{\int_0^t \rho \times C_p \times \dot{m}_{hp} \times (T_{w,out,hp} - T_{w,in,hp}) \times \mathrm{d}t}{E_e} \tag{3.19}$$

$$COP_{sys} = \frac{E_{q,house}}{E_e} = \frac{\int_0^t \rho \times C_p \times \dot{m}_{house} \times (T_{w,in,house} - T_{w,out,house}) \times \mathrm{d}t}{E_e} \tag{3.20}$$

Figure 3.24 illustrates the comparison of daily COPs between the calibrated model and the monitoring results. It is worth noting that the outliers in the figure are caused by sensor malfunction mentioned in the previous Section 2.3. The statistical measures of the calibration results are reported in Table 3.4. RMSE and CV(RMSE) of daily COPs were 0.08 and 4.15%, respectively. Maximum deviation accounted for 0.24, and there was 83% of the calibrated daily COPs within the 5.59% uncertainty of the measured COP (this uncertainty number is mentioned in previous Section 2.3). In Table 3.5, the predicted COPs of the direct mode (2.06) and indirect mode (1.67) highly matched with those of the measurement (2.05 for direct mode and 1.63 for indirect mode). The reference heat capacity and electric input power were calibrated to be 15.1 kW and 6.9 kW, respectively.

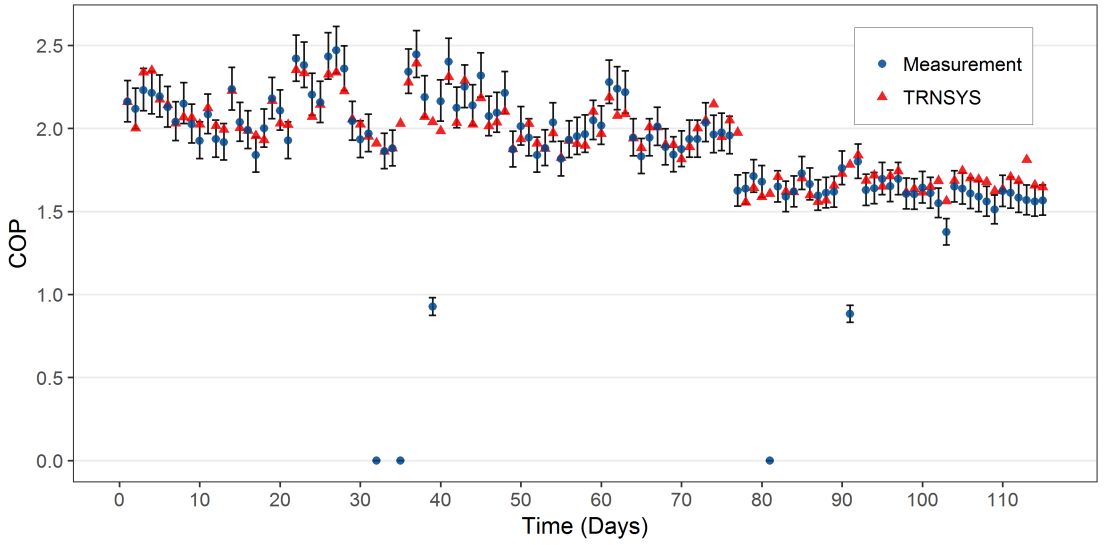

FIGURE 3.24: Calibration results of daily COPs at integrated system level (the big outliers in the figure are of the measurement due to sensor errors).

TABLE 3.4: Statistical measures of the results between the heat pump model and field trial data (the measured values in the days related to sensor fault were removed from the calculations).

	Daily COP		Daily COP_{sys}	
	Calibration	Validation	Calibration	Validation
RMSE [-]	0.08	0.07	0.09	0.12
CV(RMSE) [%]	4.15	3.31	4.88	6.03
Maximum Deviation [-]	0.24	0.2	-0.19	-0.34
Percentage of model results in	83	88	71	70
$\pm$ 5.59% of measurement uncertainty [%]				

TABLE 3.5: Seasonal COP comparison between the model's predictions and the field data of three modes (Note that the results in this table are for calibration and validation purpose only).

	COP		COP_{sys}		Mean T_a (°C)
	Model	Field trial	Model	Field trial	
Direct Mode	2.06	2.05	2.02	2.03	4.5
Indirect Mode	1.67	1.63	1.51	1.5	5.7
Combined Mode	2.26	2.24	1.97	1.94	9

The validation results of daily COPs are shown in Figure 3.25. It can be seen in the figure that the simulated daily COPs highly coincided with the monitored values, except one outlier of the monitoring due to sensor fault. Maximum daily COP deviation between the results of simulation and measurement was 0.2, as reported in Table 3.4. The values of CV(RMSE) and RMSE were 3.31% and 0.07, respectively. 88% of the model's predictions were within the permitted range of the daily COP measurement. In Table 3.5, the model predicted a seasonal COP of 2.26, equivalent the seasonal measured COP of 2.24.

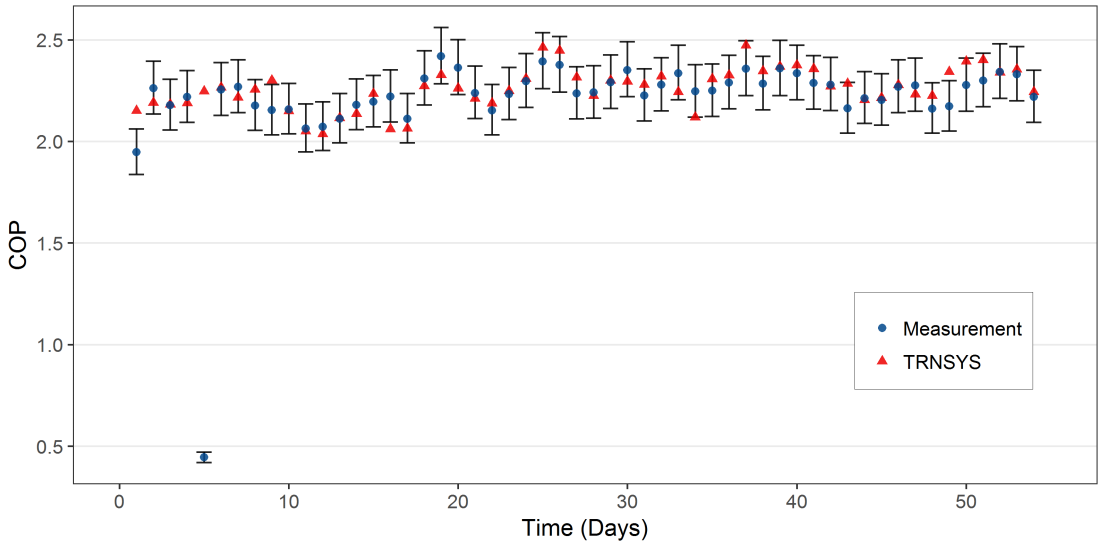

FIGURE 3.25: Validation results of daily COPs at integrated system level (the big outliers in the figure are of the measurement due to sensor errors).

It is also worthwhile to check the correlation of COP_{sys} between the model and the measurement. The validation of daily COP_{sys} for all modes is depicted in Figure 3.26. It is noted that the big outliers in the figure are caused by sensor errors. In Table 3.4, the statistical results of daily COP_{sys} are reported. Seasonal COP_{sys} are presented in Table 3.5, in which the predicted efficiency highly matched with the measured.

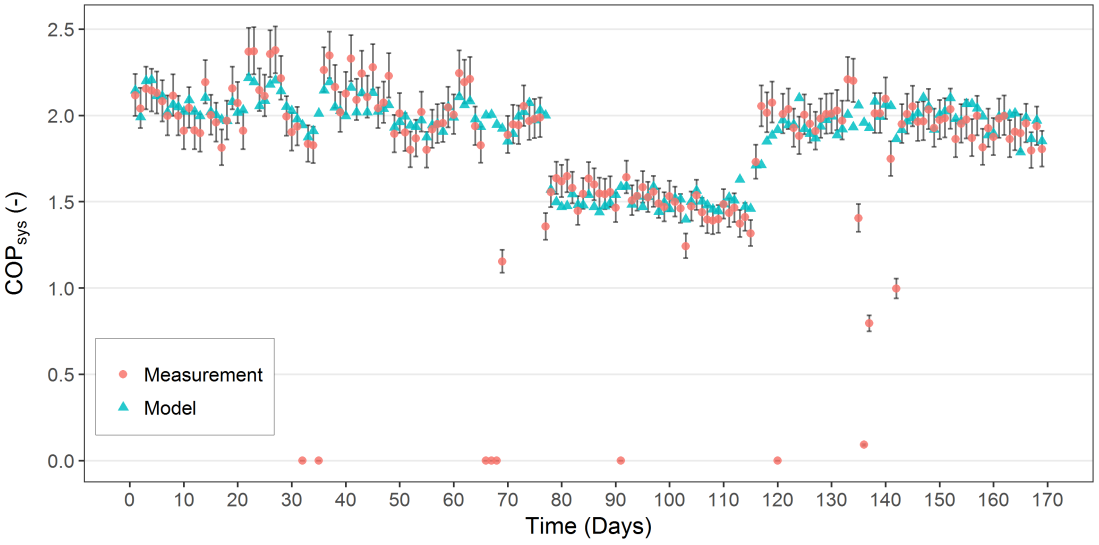

FIGURE 3.26: Daily system COP comparison between the model and the measurement for three modes (the big outliers in the figure are of the measurement due to sensor errors).

3.4.2 Calibration of thermal energy storage model

3.4.2.1 Methods

According to the third monitoring session (combined mode), the tank was heated up to 75 °C by the heat pump during the night time and then was left in standby mode (three and half hours on the average, named "Stand-by Loss 1" in Figure 3.28). When the first heating demand of the house was called, the tank discharged heat to the house until its temperature dropped to 55 °C. After that, the storage was in standby mode (the average of 17 hours), named "Stand-by Loss 2" in Figure 3.28, waiting for the heat pump charging again. Based on this operation, the experimental data could allow the storage model to be calibrated as of three modes: (1) charge, (2) discharge and (3) thermal standby losses.

Figure 3.27 depicts the schematic of the calibrated TES model in TRNSYS studio. There was a pump forcing convection of water inside the tank, according the field trial set-up. Consequently, a circulating pump Type 3d [57] was also

implemented into the model to prevent stratification effects. This pump was run only in the period of charge and discharge so that the stratification process only happened in standby mode, approximately 18 hours of a day. The inputs of the storage model were obtained as follows, using TRNSYS Type 62 [57] that read the recorded data from an excel file:

- Inlets of the charging heat exchanger were connected to the outlets of the validated heat pump model, including water flow rates and outlet water temperatures.
- Experimental results of water flow rates and inlet temperatures of the discharging heat exchanger were obtained as input data for that heat exchanger of the model.

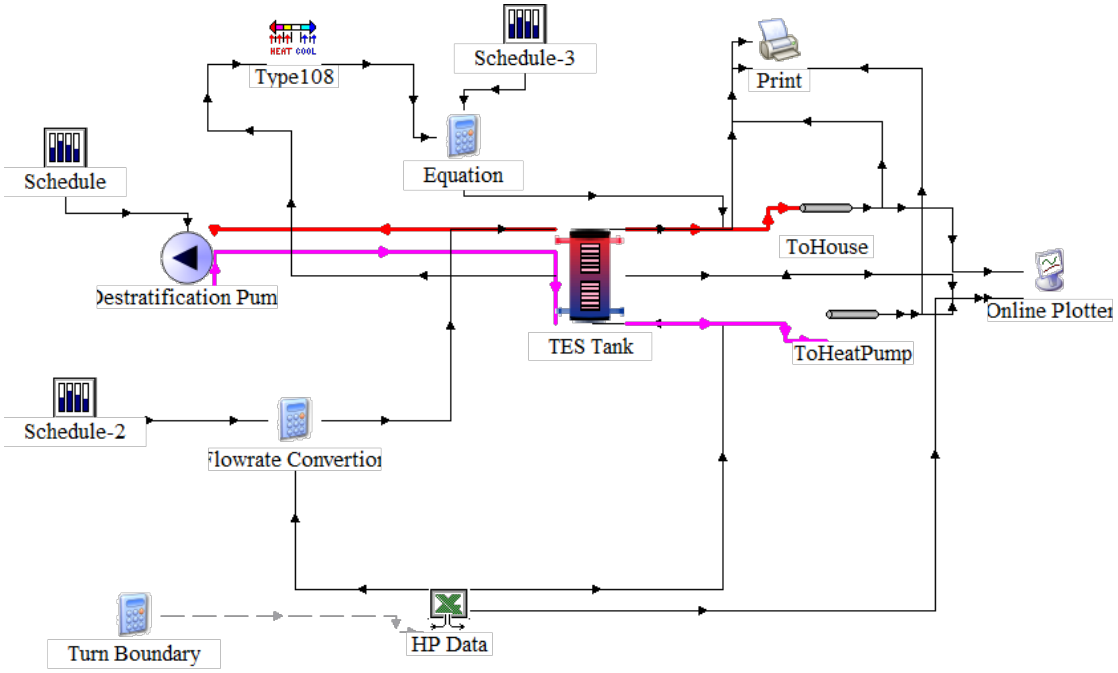

FIGURE 3.27: Schematic of calibration of TES at component level in TRNSYS Studio.

Predicted seven node temperatures as well as outlet water temperatures of charging and discharging heat exchangers were compared with the recorded

data. These parameters were chosen for the comparisons because they could affect the uncertainties of entering water temperatures of the validated heat pump in charging mode, and the inlet temperatures of radiators in discharging mode when coupled into the whole building simulation model, as shown in Figure 3.9.

3.4.2.2 Calibration results

Normal operation for charging and discharging the tank was repeatable every day, so the model results of one specific day (8^{th} May 2015) were chosen for the analysis of the model calibration. The tank node temperatures between the model and the monitoring results on 8^{th} May 2015 are illustrated in Figure 3.28, with only temperatures at the top and bottom nodes being shown to make the graph easier to look. Both the charge (1am to 2.10am) and discharge (5.30am to 6.20am) showed a good agreement between the field trial and the model. “Standby Loss 1” attained a good correlation, but there were some discrepancies during “Standby Loss 2” (after 6.20am), and stratification was noticed during this period. It is noted that during the period of "Standby Loss 1", the stratification of the tank was eliminated by the de-stratification pump on the storage, while this pump was inactive during the period of "Standby Loss 2" so that the stratification was observed.The simulated top node temperature in “Standby Loss 2” gradually overestimated the monitored top temperature with the maximum of 2.5 °C, whereas the bottom temperatures seemed to coincide within the uncertainty of 1 °C.

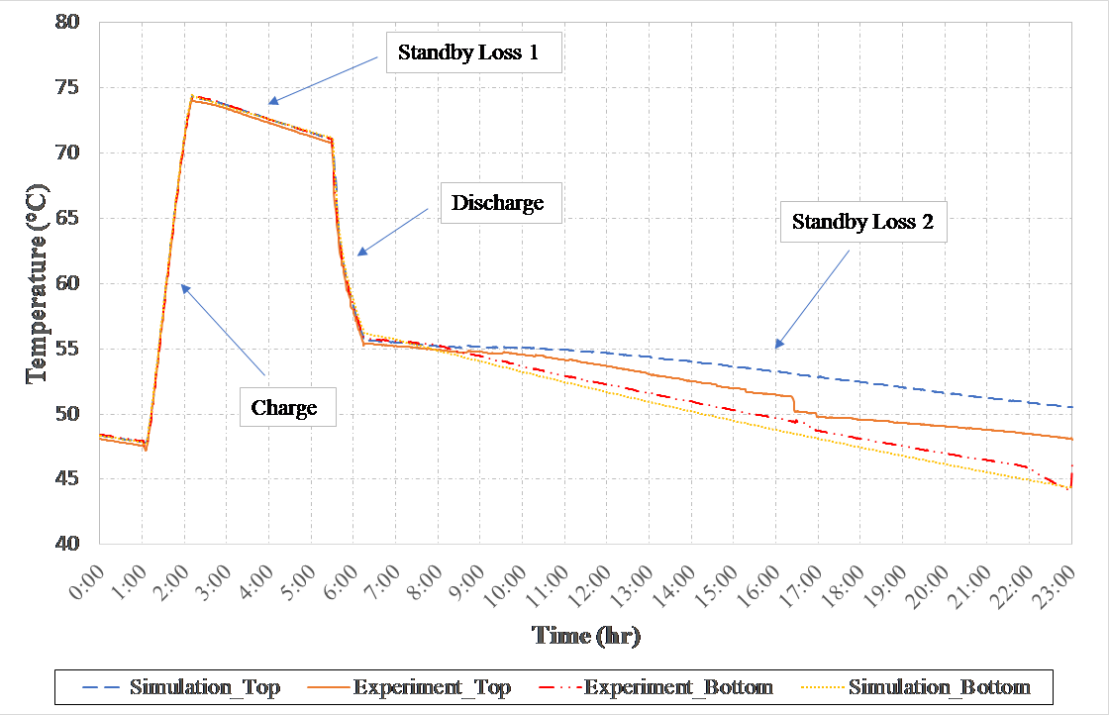

FIGURE 3.28: Comparison of the top and bottom tank node temperatures between the calibrated model and experimental results.

The differences during "Standby Loss 2" were highly challenging to address, although the model parameters were fine-tuning. This is because the tank nodes in TRNSYS were consistent, while the measuring temperatures at different heights of the tank via thermocouples were not uniform. In other words, there were inlets/outlets of the heat exchangers and supply water along the tank which caused natural heat conduction with connected pipes as well as heat convection within the tank, and therefore temperature at the thermocouples close to those pipes decreased more suddenly than temperatures at the others. For example, the top tank node temperature of the monitored data in Figure 3.28 decreased quickly after 4.00pm. Such TRNSYS tank model, in contrast, did not consider this effect. Fortunately, these discrepancies were minor, and it was also mentioned in the work of Banister et al [76].

Comparisons of outlet temperatures of the two heat exchangers are depicted in Figure 3.29. The results showed very good agreements in both charging and

discharging mode with the maximum discrepancy of 1 °C and 0.5 °C, respectively.

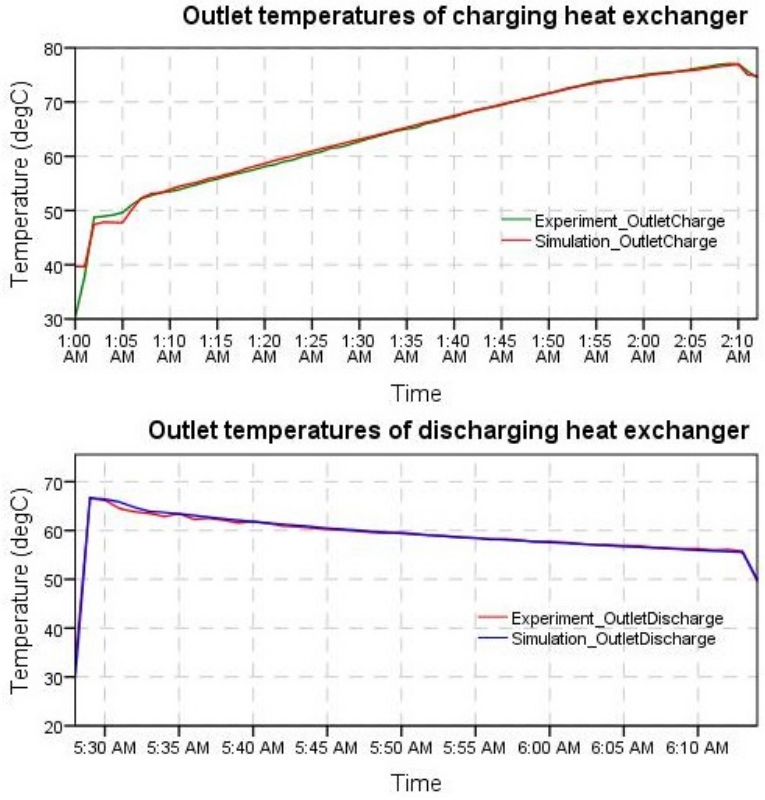

FIGURE 3.29: Comparison of outlet temperatures of charging and discharging heat exchangers between the calibrated model and the experimental results.

3.4.3 Calibration of whole building simulation model

3.4.3.1 Methods

The whole building simulation model mentioned in the previous Section 3.3.5 involved a wide range of parameters, such as building characteristics, system components, occupancy patterns, etc., all of which are complicated to determine which ones should be selected for calibration. Therefore, the hierarchy method, that was suggested and used in the works of Raftery et al. [77], Mustafaraj et al. [78], Royapoor and Roskilly [79] , and Carlon et al. [80], was adopted

for calibration in this research. This method includes two stages: former calibration stage and latter calibration stage. The first stage involves in gathering the promptly approachable information about the dwellings, such as building geometry plans, building materials, HVAC systems, etc. The second step is carried out using surveys and interviews with occupants, and specially, measurement results to alter the simulation parameters to seek their optimum values. Details of these calibration stages are explained as follows.

Former calibration stage: The former calibration stage in this research was performed following the steps suggested by Carlon et al. [80]:

- The building thermal properties of the envelops and materials, as well as the building geometry were supplied by the dwelling manufacturer. Therefore, these parameters were assumed to be trustworthy and kept unchanged.
- The parameters of the heat pump model (explained in the above Section 3.4.1) and the TES model (explained in the above Section 3.4.2) were calibrated and validated at both component level and integrated system level. Hence, these parameters were kept constant in these calibration steps.
- The DHW tank was modelled based on the specifications given by the manufacturer. As a result, the parameters related to the DHW tank were also assumed to be reliable and kept unchanged.
- The internal heat gains of the dwelling, such as occupant attendance, lights and electric appliances, were primarily estimated. Particularly, the electric lights were assumed to be turned on during occupied periods, with the heat gains given by these actions being of 15 W/m^2 [81]. The computers were assumed to generate heat gains of 230 W/m^2 for PC with

colour monitor [81]. The internal heat gains caused by occupant attendance were estimated for different thermal zones; for example, values for the standing, light work or working slowly activities were set up for the kitchen, while figures for the seated at rest were estimated for the bed rooms, all of which followed the standards of ISO 7730 [82].

Latter calibration stage: Following the former calibration process, the latter calibration was carried out using surveys and interviews with the homeowners along with the monitoring data to adjust the simulation parameters. The simulation parameters chosen for this calibration process are demonstrated as follows:

- As mentioned in the previous Section 3.3.3, the infiltration rate of the building model was initially set to one air change per hour following the standard proposed by CIBSE [73]. However, with regards to interviews with the homeowners, the windows were opened whenever the occupants preferred, making it hard to obtain the right parameter values. As a result, this parameter was included in this calibration process.
- Heat capacitances of the thermal zones were also chosen for the latter calibration. These parameters were of importance as they reflected the indoor air volume and the furniture, all of which are often difficult to estimate [80]. In particular, the dwelling had two floors, including ground floor and first floor, so that the heat capacitances of these two thermal zones were selected for calibration. The initial values of these parameters can be seen in Table 3.6.

TABLE 3.6: Values of parameters during calibration.

Parameter	Initial value	Calibration value	Calibration Step	Calibrated value	Unit
Infiltration rate	1	0.8÷1.2	0.05	1.15	ACH
Heat capacitance (ground floor)	2500	1500÷3500	20	2560	kJ/K
Heat capacitance (first floor)	2000	1000÷3000	20	2430	kJ/K

Daily house heat demand or daily thermal output to the house was the measure to calibrate the whole building simulation model. This approach was proposed by Safa et. [83] [84]. Particularly, coefficients of variation of the root mean square errors CV(RMSE) between simulated and monitored daily thermal outputs to the house were estimated. After that, the infiltration rate and heat capacitance were varied to obtain the minimisation of a non-dimensional cost function expressed in Equation 3.21.

$$f_{q,house} = CV(RSME)_{q,house} = \frac{\sqrt{\frac{\sum(Q_{house,sim} - Q_{house,measure})^2}{n}}}{\overline{Q_{house,measure}}} \times 100 \qquad (3.21)$$

GenOpt software linked with TRNSYS environment was also utilised to automatically adjust the calibrated parameters (infiltration rate and heat capacitance) to achieve the minimisation of the cost function $f_{q,house}$ in Equation 3.21. The optimisation was processed in GenOpt using the hybrid generalised pattern search algorithm with particle swarm optimisation algorithm and Hooke-Jeeves pattern search method, as suggested by Silva et al. [85]. The calibrated ranges for each parameter and the steps of each optimisation routine are also reported in Table 3.5.

3.4.3.2 Calibration results of whole building simulation model

Figure 3.30 shows the comparison of daily heat demand or daily thermal output to the house between the model and the field trial over three periods. The curve depicting monitored daily building heat demand with regards to daily mean ambient temperature was also compared with the one illustrating simulated daily building heat demand versus daily mean outdoor temperature, as depicted in Figure 3.31, following the approach proposed by Safa et al. [83] [84].

In Figure 3.30, the relationship between daily heat demand versus daily mean ambient temperatures of the model's predictions highly coincided with that of the field collected data, according to the linear regressions. It is noted that the outliers caused by sensor malfunction in Figure 3.30 were removed in Figure 3.31. Consequently, RMSE and CV(RMSE) were calculated to be 16.39 and 18.14%, respectively.

The parameters founded in calibration were: 1.15 air change per hour (ACH) for infiltration rate; 2560 kJ/K for heat capacitance of the first floor; and 2430 kJ/K for heat capacitance of the second floor, as presented in Table 3.5.

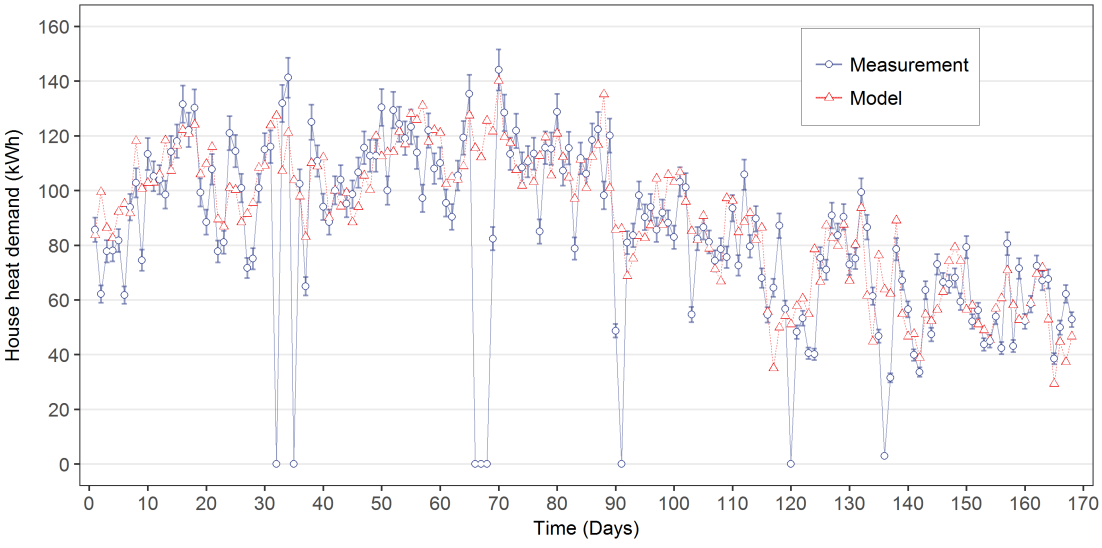

FIGURE 3.30: Daily building heat demand comparison between the model and the field trial data for three periods.

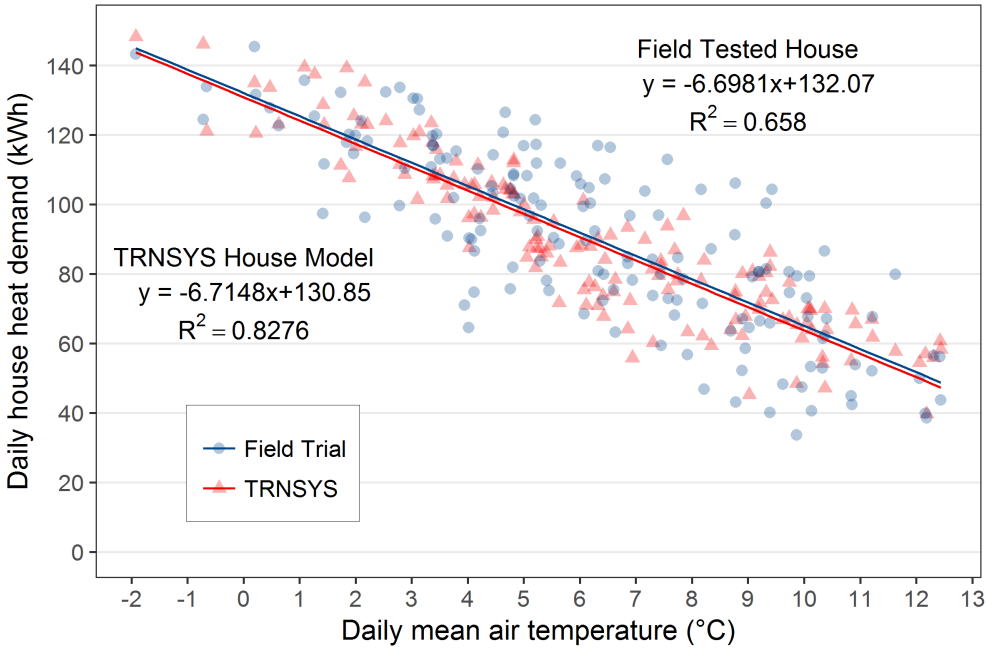

FIGURE 3.31: Comparison of daily thermal output to the house between the model and the field trial.

3.5 Summary

This chapter discusses how the models of the variable capacity CAWHP, the TES tank and the whole integrated building simulation were developed, calibrated and validated based on the field trial results and the laboratory data.

Firstly, the heat pump model, TRNSYS Type 1271, was developed using the performance map informed by the field monitoring data. The defrost cycle model, accounting for frost and defrost effects, was created separately and incorporated outside the heat pump model. The developed heat pump model coupled with the defrost cycle model was then successfully calibrated and validated against the field trial data and the laboratory results at component level and integrated system level. At component level, CV(RMSE)s of outlet water temperatures and COPs respectively accounted for 3.84% and 11% during calibration, while 4.14% and 11.6% during validation. The mismatch between the model

and the field trial data during transient states is also discussed in this chapter. At integrated system level, the results of the model highly correlated with the monitoring data for both calibration and validation processes, with CV(RMSE) of daily COP of 4.15% for calibration and 3.31% for validation.

Secondly, the TES model was developed using TRNSYS Type 534 based on the technical documents of the field trial custom design storage. Then, the model was calibrated accordingly. The calibrated temperatures at the top and bottom of the storage in charging, discharging and standby mode were within 2.5 °C uncertainty of the measured tank node temperatures.

Finally, the whole building simulation model, including the building model, the DHW water model and other component models coupled with the CAWHP and TES models, was sucessfully developed and calibrated.

Chapter 4

Performance Assessment of Cascade Air-to-water Heat Pump Retrofitted into UK Residential Buildings

4.1 Introduction

In this chapter, an evaluation of the techno-economic performance of the CAWHP system when retrofitted into UK residential buildings, especially endeavoring to quantify carbon and energy savings compared with oil and gas fired boilers, is presented. The retrofit CAWHP system was investigated with different scenarios, including various property types and ages, different locations across the UK, and varied control strategies (fixed flow water temperature and weather compensation). The rest of this chapter includes:

- Section 4.2: Methodology is given.
- Section 4.3: Results are presented along with discussion.
- Section 4.4: This chapter is summarised.

4.2 Methodology

After developing and validating the models, as described in Chapter 3, the whole incorporated building model was simulated with one-minute intervals in order to capture the high accurate operation of the system. Three main series of the simulations were done interchangeably, as explained below.

4.2.1 Different property types and ages

The first series of the simulations were carried out with various building types and ages. Archetypes that were run in the simulations are shown in Table 4.1. There were nine different archetypes, combining between three distinct housing types (mid-terraced, semi-detached, and detached) and three varied building ages (1900s, 1970s, and 1990s). These properties were selected because according to the report of Department for Business, Energy and Industrial Strategy in [17], CAWHPs are typically specialised for retrofitting into hard-to-heat or ageing residential buildings (high heat loss properties). Also, these properties are often in off-gas grid area and running with oil, where cost savings might be obtained if CAWHPs are retrofitted.

TABLE 4.1: Overview of archetypes carried out in the simulations.

	Building type	Building age
Archetype	Mid-terraced, semi-detached, detached	1900s, 1970s, 1990s
Number of archetypes	3	3
Total number of simulated archetypes	9	

Apart from the mid-terraced building depicted in Figure 3.6, the overviews of the semi-detached and detached houses drawn in SketchUp software are shown

in Figure 4.1. The dwellings were organised to have two thermal zones, including ground floor (GF) and first floor (FF). The GF comprised the living, kitchen and store areas, while the FF was the spaces of three bedrooms and a bathroom. Both floors had an area of 55 m^2 in accordance with the height of 2.7 m. As the storeroom located at the GF did not need heating, the heated volume of the GF was calculated to be 120 m^3, whilst 150 m^3 was accounted for the heated volume of the FF. Each thermal zone was heated by the retrofit CAWHP via wet traditional radiators (high heat distribution systems).

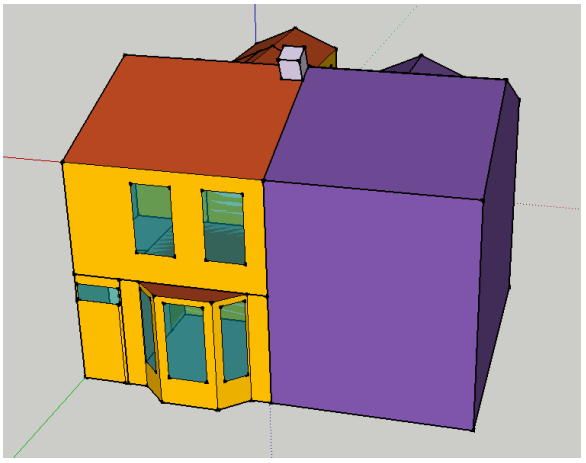

(A)

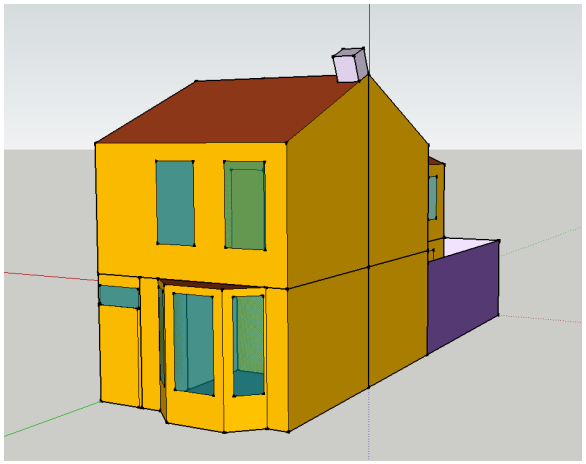

(B)

FIGURE 4.1: Investigated buildings drawn in SketchUp environment: (a) Semi-detached; (b) detached.

The adjacent houses of the mid-terraced (Figure 3.6) and semi-detached (Figure 4.1a) are shown as the shading objects. The party-walls between the buildings were set up as boundaries, with the surface temperatures being assumed as the space temperatures of the adjacent rooms. These temperature profiles were obtained from the measurements of the field trial adjacent house, as mentioned in Chapter 2.

The thermal characteristics of the buildings, that were set up in the simulations, followed the 1900s, 1970s, and 1990s building regulation standards in line with the report of Energy Saving Trust [8] mentioning U-values of existing houses in Northern Ireland. Summary of the thermal characteristics of the three reference buildings can be seen in Table 4.2.

TABLE 4.2: The thermal characteristics of the reference buildings based on the building regulation standards of the Energy Saving Trust [8].

Building age	External wall U-value (W/m^2K)	Roof U-value (W/m^2K)	Floor U-value (W/m^2K)	Window U-value (W/m^2K)	Infiltration (Air changes per hour)	Heat capacitance (kJ/K)	
						Ground floor	First floor
1900s	1.65	1.42	0.67	4.8	1.15	2560	2430
1970s	1	0.68	0.6	4.8	1	2560	2430
1990s	0.6	0.35	0.45	4.8	0.5	2560	2430

4.2.2 Different locations

The second series of annual simulations were run with different climatic conditions across the UK, including Belfast, Aviemore, Camborne, and Bracknell. The geographical map of these locations is illustrated in Figure 4.2. These locations range from northern Scotland to southern England, which represent the variations from severe to mild weather in the UK. The meteonorm weather profiles available in TRNSYS database were used. In Table 4.3, the heating degree

days (HDDs) along with the maximum and minimum hourly average external air temperatures are reported to indicate the heat demands of the selected locations. HDDs were computed based on the chosen weather files in TRNSYS with the base temperature of 15.5 °C that is the standard in the UK [86]. It is clear in Figures 4.2 and 4.3 that Aviemore (latitude of 57.2 °N and longitude of -3.83 °E) was the coldest location with the HDDs of 3203, while Camborne (latitude of 50.22 °N and longitude of -5.32 °E) had the mildest climate with the HDDs of 1840. Also, Belfast (latitude of 54.65 °N and longitude of -6.22 °E) had 2475 HDDs followed by Bracknell (latitude of 51.38 °N and longitude of -0.78 °E) requiring HDDs of 1840.

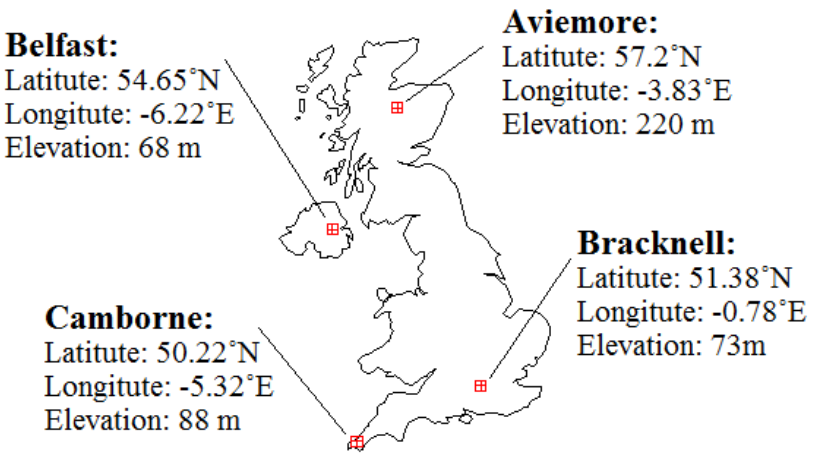

FIGURE 4.2: Geography map of the selected UK locations investigated in the simulations.

TABLE 4.3: Heating degree days and hourly maximum and minimum air temperatures of the selected locations carried out in the simulations.

Location	HDD	Hourly max. air temperature [°C]	Hourly min. air temperature [°C]
Belfast	2475	23.8	-5.6
Aviemore	3203	24.3	-11.2
Camborne	1840	23.7	-4.09
Bracknell	2092	29.5	-6.2

4.2.3 Different control strategies

The third set of simulations was run interchangeably with the cascade heat pump adopting fixed outlet water temperature and weather compensation strategy. These simulations aimed at assessing how the efficiency of the cascade heat pump could improve when it adopted weather compensation compared with the fixed flow temperature.

Regarding the constant flow temperature strategy, the outlet water temperature was fixed to 75°C that imitated the outlets of conventional boilers. As for the weather compensation control, the minimum flow temperature was set at 55 °C if the ambient temperature was 15 °C and above, while the maximum flow was set at 75 °C corresponding to the ambient temperature of 0 °C and below, as shown in Figure 4.3.

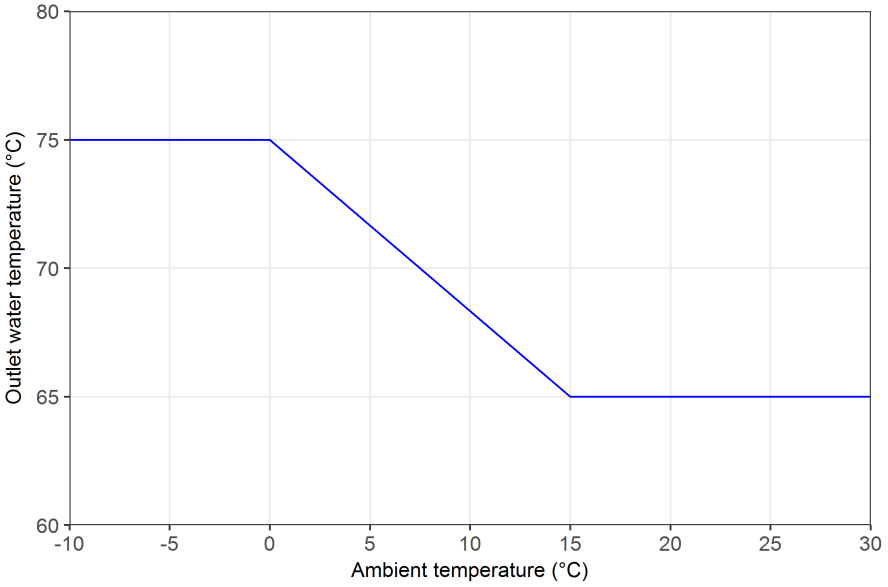

FIGURE 4.3: Weather compensation set-up for the heat pump model.

4.3 Results and Discussion

4.3.1 Performance of the cascade heat pump retrofitted into 1900s mid-terraced dwellings

4.3.1.1 In Northern Ireland

The predicted performance of the CAWHP retrofitted into the 1900s mid-terraced buildings with and without weather compensation in Belfast - Northern Ireland are summarised in Table 4.4, with summer months (June to August) being of the DHW demands only.

Considering the fixed outlet water temperature, the annual heat output of the cascade heat pump was approximately 89.96GJ (24989 kWh), and the yearly electric consumption accounted for roundly 42.39GJ (11777 kWh). The annual COP_{sys} was thus computed equal 2.12, with the monthly COP_{sys} ranging from 1.98 to 2.54 where the mean COP_{sys} of winter period (December to March) accounted for 2.02.

TABLE 4.4: Summary of simulation results of the CAWHP retrofitted into the 1900s mid-terraced building in Belfast - Northern Ireland.

	Jan	Feb	Mar	Apr	May	Jun	Jul	Aug	Sep	Oct	Nov	Dec	**Annual**
Air temperature [°C]	3.6	3.9	5.5	7.3	10.2	13	14.7	14.5	12.2	9.9	5.9	4.7	**8.8**
a) Fixed outlet water temperature (75 °C)													
COP_{sys} [-]	1.98	2.00	2.07	2.17	2.31	2.44	2.54	2.51	2.42	2.29	2.10	2.04	**2.12**
Electric use [kWh]	1808	1615	1459	1062	734	139	115	134	624	953	1448	1686	**11777**
Heat output [kWh]	3588	3230	3025	2308	1697	339	291	337	1513	2186	3040	3435	**24989**
b) Weather compensation													
COP_{sys} [-]	2.09	2.12	2.24	2.43	2.66	3.02	3.14	3.11	2.85	2.62	2.27	2.17	**2.32**
Electric use [kWh]	1675	1500	1312	911	607	109	89	107	505	793	1300	1552	**10460**
Heat output [kWh]	3504	3177	2940	2213	1613	328	280	332	1439	2075	2951	3362	**24216**

Regarding the heat pump adopted weather compensation strategy, the annual COP_{sys} was about 9.4% higher than the one with fixed outlet water temperature (Table 4.4). This resulted in around 11.2% of annual energy savings which could be achieved with the weather compensation strategy. Details of the monthly COP_{sys} improvements, indicating the enhancement of the cascade heat pump when adopting weather compensation compared to fixed outlet water temperature, can be seen in Figure 4.4. The higher mean air temperatures corresponded to the higher monthly COP_{sys} enhancements, and vice versa. The monthly COP_{sys} improvements ranged from approximately 5.4% to 23.9%, with the highest in summer period and the lowest in winter months.

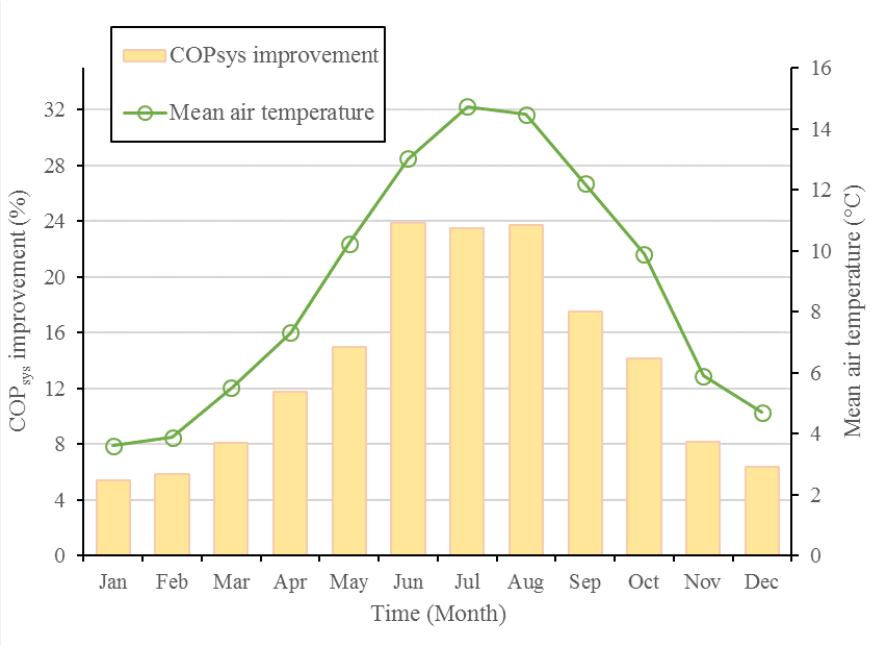

FIGURE 4.4: Influence of weather compensation on monthly COP_{sys} improvements in Belfast-Northern Ireland of the CAWHP in the 1900s mid-terraced dwelling.

4.3.1.2 In different locations across the UK

The annual COP_{sys} of the CAWHP primarily depended on weather conditions. In Table 4.5, as for the fixed outlet water temperature, the CAWHP retrofitted into the 1900s mid-terraced buildings had the best performance in Camborne

(yearly COP_{sys} of 2.24) thanks to the mildest weather condition (HDDs of 1840 reported in 4.3) compared to the other locations. In contrast, the cascade heat pump performed most badly in Aviemore (annual COP_{sys} of 2.03) due to the extreme weather condition where the external air temperatures dropped to -11.2 °C along with the highest HDDs of 3203 (Table 4.3). The cascade heat pump's performance in Bracknell and Belfast were better than the one in Aviemore but worse than that in Camborne, with annual COP_{sys} of 2.17 and 2.12, respectively. Regarding the heat pump with weather compensation, the yearly COP_{sys} also ranged from the highest (2.5) in milder condition Camborne to the lowest (2.17) in severe condition Aviemore. These yearly figures indicate that the retrofit CAWHP is unlikely to be suitable for the renewable heat incentive scheme in the UK requiring a seasonal performance factor of 2.5 [87].

TABLE 4.5: Annual simulation results of the stand-alone CAWHP in different climates.

Location	Fixed outlet water temperature (75°C)			Weather compensation		
	Yearly COP_{sys} [-]	Total electric use [kWh]	Total delivered heat [kWh]	Yearly COP_{sys} [-]	Total electric use [kWh]	Total delivered heat [kWh]
Belfast	2.12	11777	24989	2.32	10460	24216
Aviemore	2.03	13962	28396	2.17	12728	27615
Camborne	2.24	9427	21100	2.5	8105	20299
Bracknell	2.17	10740	23335	2.38	9321	22144

The employment of weather compensation strategy permitted the retrofit CAWHP to acquire the better performance. Besides, milder weather conditions could allow this strategy to improve the heat pump's performances further. To better explain this effect, Figure 4.5 depicts the relationship between the annual COP_{sys} enhancement and the weighted mean of hourly ambient temperature (T_{wma}) in different locations, following the approach proposed by Madonna and Bazzocchi [8]. The improvement of yearly COP_{sys} changed relatively according

to the climatic variations. In particular, it was approximately 6.7% in Aviemore (T_{wma} of 6 °C), just below 9.1% in Belfast (T_{wma} of 8.4 °C), 9.3% in Bracknell (Twma of 10.2 °C) and 11.9% in Camborne (T_{wma} of 10.6 °C).

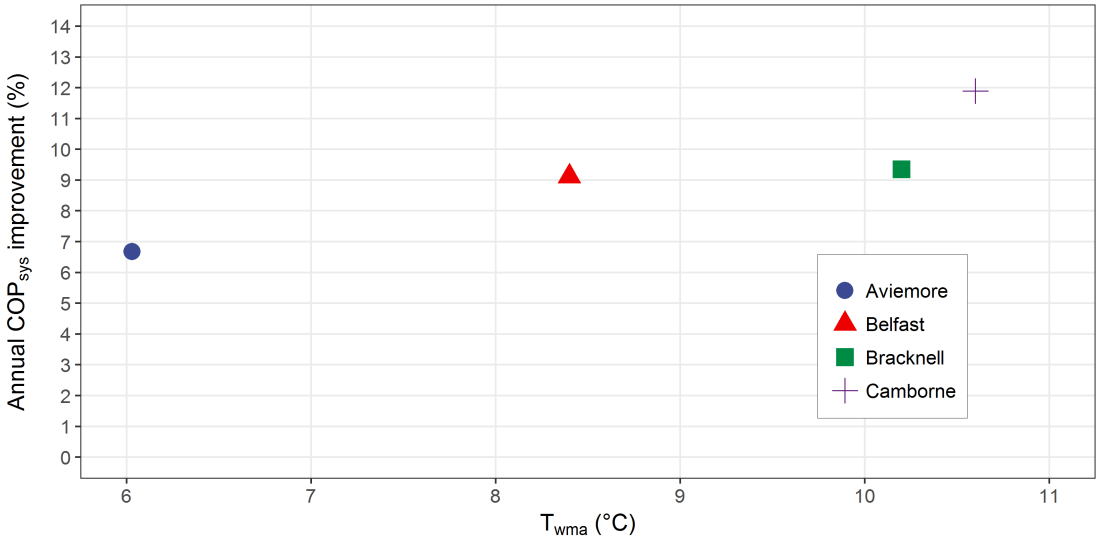

FIGURE 4.5: Influence of weather compensation on annual COP_{sys} improvements as a function of T_{wma}.

4.3.2 Performance of the cascade heat pump retrofitted into different property types and ages

This section presents the performance analysis of the retrofit CAWHP in different scenarios. Particularly, an evaluation on annual COP_{sys} and annual energy consumption of the CAWHP retrofitted into the different property types and ages along with the four selected locations and the two control strategies is discussed.

4.3.2.1 Annual COP_{sys}

Tables 4.6, 4.7, and 4.8 report the summaries of the predicted annual heat output, energy consumption, and COP_{sys} of the retrofit CAWHPs for the nine

archetypes in line with the four selected locations and the two control strategies. Additionally, Figure 4.6 shows the percentages of annual COP_{sys} improvement of the CAWHPs with weather compensation control compared to those with the fixed flow water temperature.

TABLE 4.6: Summary results of the CAWHP retrofitted into mid-terraced buildings with different ages and varied locations.

Mid-terraced building							
Building age	**Location/HDDs**	**Annual useful heat output [kWh]**		**Annual Electric Use [kWh]**		**Annual COP_{sys} [-]**	
		Fixed flow	**Weather compensation**	**Fixed flow**	**Weather compensation**	**Fixed flow**	**Weather compensation**
1900s	Belfast/2475	24989	24216	11777	10460	2.12	2.32
	Aviemore/3203	28396	27615	13962	12728	2.03	2.17
	Bracknell/2092	23335	22144	10740	9321	2.17	2.38
	Camborne/1840	21100	20299	9427	8105	2.24	2.5
1970s	Belfast/2475	22631	21997	10726	9543	2.11	2.31
	Aviemore/3203	25899	25332	12774	11760	2.03	2.15
	Bracknell/2092	21036	20045	9724	8509	2.16	2.36
	Camborne/1840	18956	18417	8518	7433	2.23	2.48
1990s	Belfast/2475	15354	15047	7293	6616	2.11	2.27
	Aviemore/3203	17895	17727	8828	8283	2.03	2.14
	Bracknell/2092	14073	13482	6548	5819	2.15	2.32
	Camborne/1840	12408	12166	5583	4991	2.22	2.44

TABLE 4.7: Summary results of the CAWHP retrofitted into semi-detached buildings with different ages and varied locations.

Semi-detached building							
Building age	**Location/HDDs**	**Annual useful heat output [kWh]**		**Annual Electric Use [kWh]**		**Annual COP_{sys} [-]**	
		Fixed flow	**Weather compensation**	**Fixed flow**	**Weather compensation**	**Fixed flow**	**Weather compensation**
1900s	Belfast/2475	29078	28155	12810	11830	2.27	2.38
	Aviemore/3203	31524	30783	14731	13866	2.14	2.22
	Bracknell/2092	26885	25923	11588	10624	2.32	2.44
	Camborne/1840	25963	24609	10661	9538	2.3	2.58
1970s	Belfast/2475	26087	25213	11895	10761	2.41	2.34
	Aviemore/3203	28890	28195	13868	12910	2.08	2.18
	Bracknell/2092	23963	23071	10699	9590	2.24	2.41
	Camborne/1840	22683	21681	9759	8546	2.32	2.54
1990s	Belfast/2475	19884	19181	9121	8162	2.18	2.35
	Aviemore/3203	22522	21937	10828	9971	2.08	2.2
	Bracknell/2092	18062	17366	8099	7206	2.23	2.41
	Camborne/1840	16892	16129	7344	6350	2.3	2.54

TABLE 4.8: Summary results of the CAWHP retrofitted into detached buildings with different ages and varied locations.

Detached building							
Building age	**Location/HDDs**	**Annual useful heat output [kWh]**		**Annual Electric Use [kWh]**		**Annual COP_{sys} [-]**	
		Fixed flow	**Weather compensation**	**Fixed flow**	**Weather compensation**	**Fixed flow**	**Weather compensation**
1900s	Belfast/2475	33339	31524	15303	13684	2.18	2.38
	Aviemore/3203	34937	34289	16667	15383	2.1	2.23
	Bracknell/2092	31347	30525	14001	12472	2.24	2.45
	Camborne/1840	31037	30119	13534	11802	2.29	2.55
1970s	Belfast/2475	30467	29891	14115	12743	2.16	2.35
	Aviemore/3203	32967	32444	15835	14723	2.08	2.2
	Bracknell/2092	28160	27533	12710	11416	2.22	2.41
	Camborne/1840	26963	26297	11833	10421	2.28	2.52
1990s	Belfast/2475	22161	22013	10324	9530	2.15	2.31
	Aviemore/3203	25592	25597	12409	11841	2.06	2.16
	Bracknell/2092	20008	19813	9118	8397	2.19	2.36
	Camborne/1840	18385	18122	8118	7308	2.26	2.48

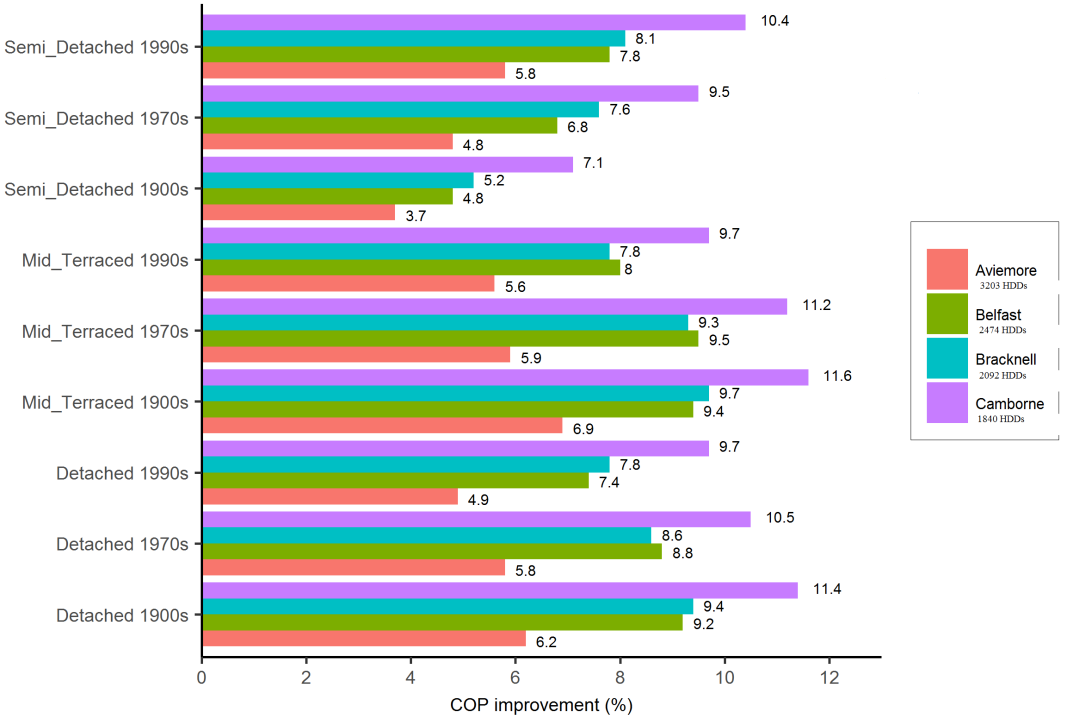

FIGURE 4.6: COP improvement of the CAWHP adopted weather compensation control compared with those adopted fixed flow temperature.

With regards to the mid-terraced buildings, annual COP_{sys} was from 2.03 to 2.24 with the fixed flow water temperature heat pumps, while yearly COP_{sys} was between 2.15 and 2.48 with the weather compensation control (Table 4.6).

COP_{sys} improvements of 5.6% to 11.6% were obtained if the cascade heat pump adopted weather compensation control compared to those with the fixed flow temperature (Figure 4.6).

As for the semi-detached houses, from 2.08 to 2.41 of COP_{sys} was seen with the fixed outlet water temperature CAWHPs, whereas between 2.18 and 2.58 of COP_{sys} was observed with the weather compensation control (Table 4.7), which accounted for the enhancements of 3.7% to 10.4% (Figure 4.6) when the cascade heat pumps took advantage of weather compensation control strategy.

Considering the detached dwellings, maximum COP_{sys} of 2.29 and 2.55 was obtained with the fixed flow water temperature and weather compensation, respectively. Minimum COP_{sys} of 2.06 was seen with the fixed outlet temperature heat pumps, whilst minimum COP_{sys} of 2.16 was observed with the weather compensation ones. In Figure 4.6, the efficiency enhancements ranging from 4.9% to 11.4% were accounted for the CAWHPs employed weather compensation in comparison to those with fixed outlet water temperature.

In general, the thermal inertia of the buildings affected the annual efficiency of the retrofit CAWHPs. Particularly, if the cascade heat pumps were retrofitted into the newer dwellings, their efficiency was slightly reduced, and vice versa (see Tables 4.6, 4.7, and 4.8). For example, looking at the mid-terraced buildings in Belfast, annual COP_{sys} of the 1900s house with the fixed flow water temperature was 2.12 followed by annual COP_{sys} of 2.11 regarding the 1970s and 1990s buildings. With the weather compensation control, annual COP_{sys} of the cascade heat pump retrofitted into the 1900s dwelling accounted for 2.32, while it was 2.31 for the 1970s house followed by 2.29 for the 1990s building. This performance could be explained that the better house thermal inertia tended to make the heat pumps operate, on average, mostly when external air temperatures were low. In other words, the thermal energy requirement of the newer buildings tended to be zero when external air temperatures were above certain

points (e.g. 16 °C), resulting in making the heat pumps work mostly with lower ambient temperatures.

4.3.2.2 Energy consumption

The energy utilisation of the CAWHPs retrofitted into nine archetypes in the selected locations along with two control strategies can also be seen in Tables 4.6, 4.7, and 4.8. It is clear in the tables that all factors, including property types and ages, weather conditions, and control approaches, affected the annual energy consumption of the retrofit CAWHPs.

Different building types and ages yielded different energy consumption. In particular, the buildings with the higher heat losses consumed more energy than those with the better thermal inertia. For example, the cascade heat pumps in the 1900s detached buildings, which had the highest heat losses, consumed more energy than those in the other buildings. In contrast, the CAWHPs retrofitted into the 1990s mid-terraced dwellings, which had the best thermal inertia, used the least energy.

Weather conditions also affected the energy utilisation of the retrofit CAWHPs. If the cascade heat pumps were installed in the locations where the weather was milder, the electric use was lower compared to those in the severe weather locations. For instance, looking at Table 4.7 for the 1990s semi-detached building retrofitted with the fixed flow water temperature heat pump, the electric consumption in Camborne (the mildest climate) was lowest (7344 kWh), while that in Aviemore (the most severe weather) was highest (10828 kWh).

The CAWHPs employing weather compensation control could obtain energy savings compared with the fixed flow water temperature heat pumps. In Figure 4.7, from 4.6% to 14% of the yearly energy savings could be acquired if the cascade heat pumps employed weather compensation control.

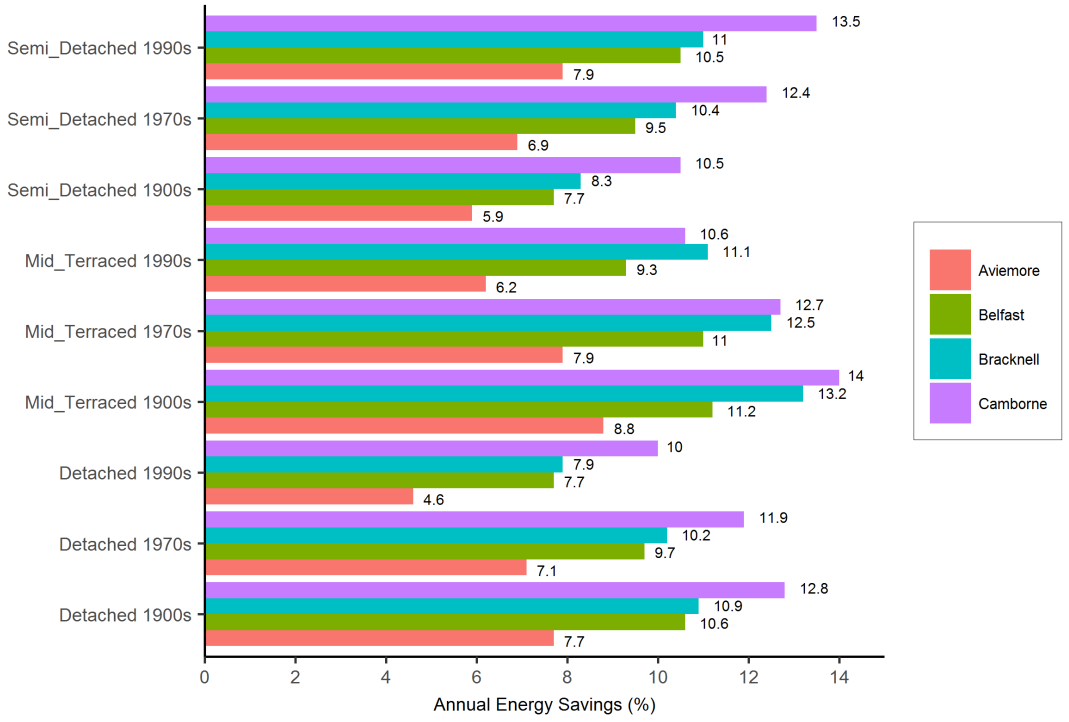

FIGURE 4.7: Annual energy consumption savings of the CAWHP adopted weather compensation control compared with fixed flow temperature.

4.3.3 Retrofit assessment of the cascade heat pump system

To evaluate the retrofit performance of the selected CAWHP, the operating costs and CO_2 emissions of the cascade heat pump were compared to those of the 60%, 70%, 80% and 90% efficiency oil- and gas-fired boilers (representing from old heavy weight boilers to new condensing boilers that are popular in the UK housing stock). Tables 4.9, 4.10, and 4.11 report these results of the cascade heat pump and the boilers in the mid-terraced, detached, and semi-detached buildings, respectively. The price of electricity was £0.175/kWh [88]. The oil price per kWh was £0.068 [89]. The gas price was £0.06508/kWh for the first 2000 kWh, and £0.0459/kWh for the after 2000 kWh [90]. The carbon conversion factor for grid electricity was 0.3844 $kgCO_2$/kWh (including electricity generation and transmission and distribution factors [91]). The carbon emissions factors were 0.2 $kgCO_2$/kWh for gas and 0.243 $kgCO_2$/kWh for oil [91].

TABLE 4.9: Annual energy consumption, running costs and carbon emissions of the retrofit CAWHP along with gas and oil boilers in the mid-terraced buildings.

	Mid-terraced building											
	1900s				1970s				1990s			
	Belfast	Aviemore	Bracknell	Camborne	Belfast	Aviemore	Bracknell	Camborne	Belfast	Aviemore	Bracknell	Camborne
1) Retrofit CAWHP												
a) Fixed flow water temperature												
Annual electric use [kWh]	11777	13962	10740	9427	10726	12774	9724	8518	7293	8828	6548	5583
Annual running cost [£]	2061	2443	1880	1650	1877	2236	1702	1491	1276	1545	1146	977
Annual CO_2 emissions [kg]	4527	5367	4129	3624	4123	4910	3738	3274	2803	3393	2517	2146
b) Weather compensation control												
Annual electric use [kWh]	10460	12728	9321	8105	9543	11760	8509	7433	6616	8283	5819	4991
Annual running cost [£]	1831	2227	1631	1418	1670	2058	1489	1301	1158	1450	1018	873
Annual CO_2 emissions [kg]	4021	4893	3583	3116	3668	4520	3271	2857	2543	3184	2237	1919
2) Oil boiler												
a) 60% efficiency												
Annual oil use [kWh]	34895	39754	32669	29540	31683	36259	29450	26538	21496	25053	19702	17371
Annual running cost [£]	2379	2703	2221	2009	2154	2466	2003	1805	1462	1704	1340	1181
Annual CO_2 emissions [kg]	8501	9660	7939	7178	7699	8811	7156	6449	5223	6088	4788	4221
b) 70% efficiency												
Annual oil use [kWh]	32486	36915	30336	27430	29420	33669	27347	24643	19960	23264	18295	16130
Annual running cost [£]	2209	2510	2063	1865	2001	2289	1860	1676	1357	1582	1244	1097
Annual CO_2 emissions [kg]	7894	8970	7372	6665	7149	8181	6645	5988	4850	5653	4446	3920
c) 80% efficiency												
Annual oil use [kWh]	29987	34075	28002	25320	27157	31079	25243	22747	18425	21474	16888	14890
Annual running cost [£]	2039	2317	1904	1722	1847	2113	1717	1547	1253	1460	1148	1012
Annual CO_2 emissions [kg]	7287	8280	6804	6153	6599	7552	6134	5528	4477	5218	4104	3618
d) 90% efficiency												
Annual oil use [kWh]	27488	31236	25669	23210	24894	28489	23140	20852	16889	19685	15480	13649
Annual running cost [£]	1869	2124	1745	1578	1693	1937	1573	1418	1148	1339	1053	928
Annual CO_2 emissions [kg]	6680	7590	6237	5640	6049	6923	5623	5067	4104	4783	3762	3317
3) Gas boiler												
a) 60% efficiency												
Annual gas use [kWh]	34895	39754	32669	29540	31683	36259	29450	26538	21496	25053	19702	17371
Annual running cost [£]	1646	1865	1539	1396	1494	1704	1392	1258	1020	1190	944	837
Annual CO_2 emissions [kg]	6997	7951	6534	5908	6335	7252	5890	5308	4272	5011	3941	3474
b) 70% efficiency												
Annual gas use [kWh]	32486	36915	30336	27430	29420	33669	27347	24643	19960	23264	18295	16130
Annual running cost [£]	1531	1734	1432	1299	1390	1585	1295	1171	950	1108	880	780
Annual CO_2 emissions [kg]	6497	7383	6067	5486	5883	6734	5469	4929	3967	4653	3660	3226
c) 80% efficiency												
Annual gas use [kWh]	29987	34075	28002	25320	27157	31079	25243	22747	18425	21474	16888	14890
Annual running cost [£]	1416	1604	1325	1202	1286	1466	1198	1084	880	1025	815	723
Annual CO_2 emissions [kg]	5997	6815	5600	5064	5430	6216	5049	4549	3662	4295	3378	2978
d) 90% efficiency												
Annual gas use [kWh]	27488	31236	25669	23210	24894	28489	23140	20852	16889	19685	15480	13649
Annual running cost [£]	1301	1474	1218	1105	1182	1347	1102	997	810	943	750	666
Annual CO_2 emissions [kg]	5498	6247	5134	4642	4978	5698	4628	4170	3357	3937	3097	2730

TABLE 4.10: Annual energy consumption, running costs and carbon emissions of the retrofit CAWHP along with gas and oil boilers in the semi-detached buildings.

	Semi-detached building											
	1900s				**1970s**				**1990s**			
	Belfast	**Aviemore**	**Bracknell**	**Camborne**	**Belfast**	**Aviemore**	**Bracknell**	**Camborne**	**Belfast**	**Aviemore**	**Bracknell**	**Camborne**
1) Retrofit CAWHP												
a) Fixed flow water temperature												
Annual electric use [kWh]	12810	14731	11588	10661	11895	13868	10699	9759	9121	10828	8099	7344
Annual running cost [£]	2242	2578	2028	1866	2082	2427	1872	1708	1596	1895	1417	1285
Annual CO_2 emissions [kg]	4924	5663	4455	4098	4572	5331	4113	3751	3506	4162	3113	2823
b) Weather compensation control												
Annual electric use [kWh]	11830	13866	10624	9538	10761	12910	9590	8546	8162	9971	7206	6350
Annual running cost [£]	2070	2427	1859	1669	1883	2259	1678	1496	1428	1745	1261	1111
Annual CO_2 emissions [kg]	4547	5330	4084	3667	4137	4962	3687	3285	3137	3833	2770	2441
2) Oil boiler												
a) 60% efficiency												
Annual oil use [kWh]	40709	44134	37639	35970	36521	40446	33548	31757	27837	31530	25287	23649
Annual running cost [£]	2768	3001	2559	2446	2483	2750	2281	2159	1893	2144	1719	1608
Annual CO_2 emissions [kg]	9892	10725	9146	8741	8875	9828	8152	7717	6764	7662	6145	5747
b) 70% efficiency												
Annual oil use [kWh]	37801	40981	34950	33401	33913	37557	31152	29488	25849	29278	23480	21960
Annual running cost [£]	2570	2787	2377	2271	2306	2554	2118	2005	1758	1991	1597	1493
Annual CO_2 emissions [kg]	9186	9958	8493	8116	8241	9126	7570	7166	6281	7115	5706	5336
c) 80% efficiency												
Annual oil use [kWh]	34894	37829	32262	30831	31304	34668	28755	27220	23861	27026	21674	20271
Annual running cost [£]	2373	2572	2194	2097	2129	2357	1955	1851	1623	1838	1474	1378
Annual CO_2 emissions [kg]	8479	9192	7840	7492	7607	8424	6988	6614	5798	6567	5267	4926
d) 90% efficiency												
Annual oil use [kWh]	31986	34677	29573	28262	28695	31779	26359	24952	21872	24774	19868	18581
Annual running cost [£]	2175	2358	2011	1922	1951	2161	1792	1697	1487	1685	1351	1264
Annual CO_2 emissions [kg]	7773	8426	7186	6868	6973	7722	6405	6063	5315	6020	4828	4515
3) Gas boiler												
a) 60% efficiency												
Annual gas use [kWh]	40709	44134	37639	35970	36521	40446	33548	31757	27837	31530	25287	23649
Annual running cost [£]	1908	2066	1767	1691	1716	1896	1580	1497	1318	1487	1200	1125
Annual CO_2 emissions [kg]	8142	8827	7528	7194	7304	8089	6710	6351	5567	6306	5057	4730
b) 70% efficiency												
Annual gas use [kWh]	37801	40981	34950	33401	33913	37557	31152	29488	25849	29278	23480	21960
Annual running cost [£]	1775	1921	1644	1573	1596	1764	1470	1393	1226	1384	1118	1048
Annual CO_2 emissions [kg]	7560	8196	6990	6680	6783	7511	6230	5898	5170	5856	4696	4392
c) 80% efficiency												
Annual gas use [kWh]	34894	37829	32262	30831	31304	34668	28755	27220	23861	27026	21674	20271
Annual running cost [£]	1641	1776	1521	1455	1477	1631	1360	1289	1135	1280	1035	970
Annual CO_2 emissions [kg]	6979	7566	6452	6166	6261	6934	5751	5444	4772	5405	4335	4054
d) 90% efficiency												
Annual gas use [kWh]	31986	34677	29573	28262	28695	31779	26359	24952	21872	24774	19868	18581
Annual running cost [£]	1508	1631	1397	1337	1357	1498	1250	1185	1044	1177	952	893
Annual CO_2 emissions [kg]	6397	6935	5915	5652	5739	6356	5272	4990	4374	4955	3974	3716

TABLE 4.11: Annual energy consumption, running costs and carbon emissions of the retrofit CAWHP along with gas and oil boilers in the detached buildings.

	Detached building											
	1900s				1970s				1990s			
	Belfast	Aviemore	Bracknell	Camborne	Belfast	Aviemore	Bracknell	Camborne	Belfast	Aviemore	Bracknell	Camborne
1) Retrofit CAWHP												
a) Fixed flow water temperature												
Annual electric use [kWh]	15303	16667	14001	13534	14115	15853	12710	11833	10324	12409	9118	8118
Annual running cost [£]	2678	2917	2450	2368	2470	2774	2224	2071	1807	2172	1596	1421
Annual CO_2 emissions [kg]	5882	6407	5382	5203	5426	6094	4886	4549	3969	4770	3505	3120
b) Weather compensation control												
Annual electric use [kWh]	13684	15383	12472	11802	12743	14723	11416	10421	9530	11841	8397	7308
Annual running cost [£]	2395	2692	2183	2065	2230	2576	1998	1824	1668	2072	1469	1279
Annual CO_2 emissions [kg]	5260	5913	4794	4537	4898	5659	4388	4006	3663	4552	3228	2809
2) Oil boiler												
a) 60% efficiency												
Annual oil use [kWh]	46675	48911	43886	43452	42653	46154	39424	37748	31026	35829	28011	25739
Annual running cost [£]	3174	3326	2984	2955	2900	3138	2681	2567	2110	2436	1905	1750
Annual CO_2 emissions [kg]	11342	11885	10664	10559	10365	11215	9580	9173	7539	8706	6807	6255
b) 70% efficiency												
Annual oil use [kWh]	43341	45418	40751	40349	39607	42857	36608	35051	28810	33269	26010	23901
Annual running cost [£]	2947	3088	2771	2744	2693	2914	2489	2384	1959	2262	1769	1625
Annual CO_2 emissions [kg]	10532	11037	9903	9805	9624	10414	8896	8518	7001	8084	6321	5808
c) 80% efficiency												
Annual oil use [kWh]	40007	41924	37617	37254	36560	39561	33792	32355	26594	30710	24010	22062
Annual running cost [£]	2720	2851	2558	2533	2486	2690	2298	2200	1808	2088	1633	1500
Annual CO_2 emissions [kg]	9722	10188	9141	9050	8884	9613	8211	7862	6462	7463	5834	5361
d) 90% efficiency												
Annual oil use [kWh]	36673	38430	34482	34141	33513	36264	30976	29659	24377	28151	22009	20224
Annual running cost [£]	2494	2613	2345	2322	2279	2466	2106	2017	1658	1914	1497	1375
Annual CO_2 emissions [kg]	8912	9339	8379	8296	8144	8812	7527	7207	5924	6841	5348	4914
3) Gas boiler												
a) 60% efficiency												
Annual gas use [kWh]	46675	48911	43886	43452	42653	46154	39424	37748	31026	35829	28011	25739
Annual running cost [£]	2182	2285	2054	2034	1998	2158	1849	1772	1464	1684	1326	1221
Annual CO_2 emissions [kg]	9335	9782	8777	8690	8531	9231	7885	7550	6205	7166	5602	5148
b) 70% efficiency												
Annual gas use [kWh]	43341	45418	40751	40349	39607	42857	36608	35051	28810	33269	26010	23901
Annual running cost [£]	2029	2124	1910	1892	1858	2007	1720	1649	1362	1567	1234	1137
Annual CO_2 emissions [kg]	8668	9084	8150	8070	7921	8571	7322	7010	5762	6654	5202	4780
c) 80% efficiency												
Annual gas use [kWh]	40007	41924	37617	37254	36560	39561	33792	32355	26594	30710	24010	22062
Annual running cost [£]	1876	1964	1766	1749	1718	1856	1591	1525	1260	1449	1142	1052
Annual CO_2 emissions [kg]	8001	8385	7523	7449	7312	7912	6758	6471	5319	6142	4802	4412
d) 90% efficiency												
Annual gas use [kWh]	36673	38430	34482	34141	33513	36264	30976	29659	24377	28151	22009	20224
Annual running cost [£]	1723	1804	1623	1607	1578	1704	1462	1401	1159	1332	1050	968
Annual CO_2 emissions [kg]	7335	7686	6896	6828	6703	7253	6195	5932	4875	5630	4402	4045

4.3.3.1 Running costs

As for the mid-terraced buildings, the CAWHP's operating costs per year ranged from £977 to £2443 if its flow water temperature was fixed to 75 °C, while they

were between £873 and £2227 if weather compensation control was adopted (Table 4.9).

Considering the semi-detached dwellings (Table 4.10), the annual operating costs of the retrofit CAWHP were in the range from £1285 to £2578 as well as from £1111 to £2427 for fixed flow water temperature and weather compensation control, respectively.

Regarding the detached houses, running the retrofit CAWHP costed from £1421/year to £2917/year for fixed outlet water temperature, while it was between £1279/year and £2692/year for weather compensation control (Table 4.11).

Figures 4.8, 4.9, 4.10, 4.11, 4.12, 4.13, 4.14, and 4.15 depict the percentages of the running cost savings when the gas and oil boilers were retrofitted by the reference CAWHP. The positive values in the figures indicate that operating the retrofit CAWHP was cheaper than running the boilers, while the negative values show that the cascade heat pumps were more expensive to run than the boilers.

It is clear in Figures 4.8, 4.9, and 4.10 that there were cost savings if the 60%, 70% and 80% efficiency oil boilers were retrofitted by the reference CAWHP, except the fixed flow water temperature heat pump in Aviemore and Belfast when replacing 80% efficiency oil boiler (Figure 4.10). However, there were not money savings if the CAWHP was retrofitted for the 90% efficiency oil boiler and all gas boilers (Figures 4.11, 4.12, 4.13, 4.14, and 4.15). Since the recent prices of oil and gas in the UK were relatively low compared to that of electricity, it presented challenges for retrofitting the reference CAWHP into residential dwellings. Therefore, to allow the retrofit CAWHP become more competitive than boilers, the future electricity costs would decrease, or the prospective gas and oil prices would increase to certain levels.

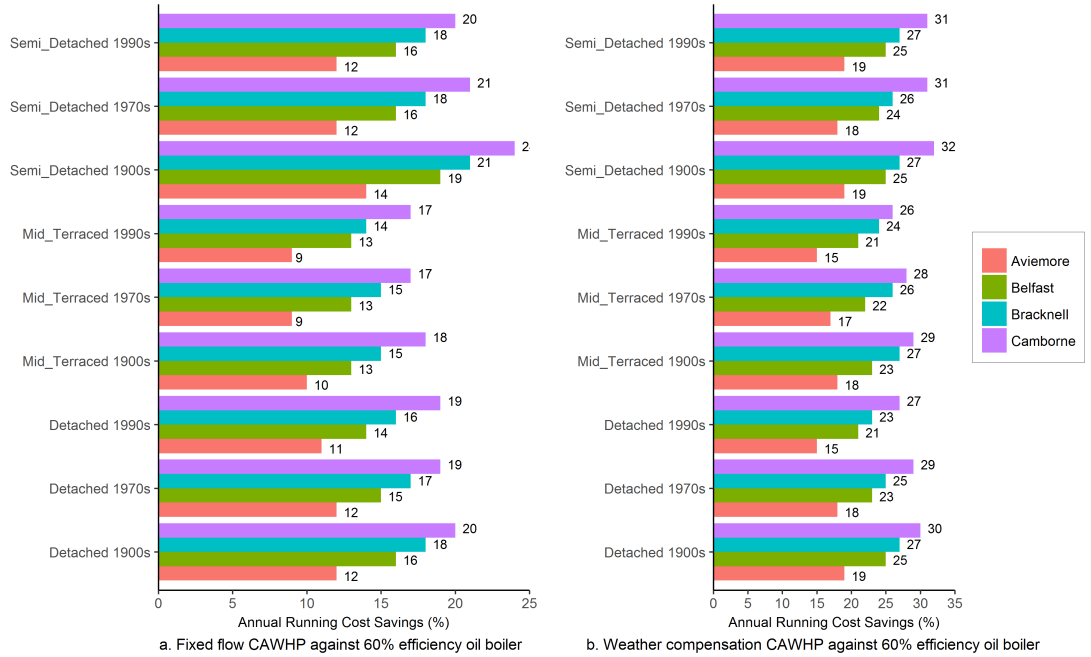

FIGURE 4.8: Annual operating cost savings of the retrofit CAWHPs compared with 60% efficiency oil boilers (Positive values indicate CAWHP's running costs are lower than those of boilers).

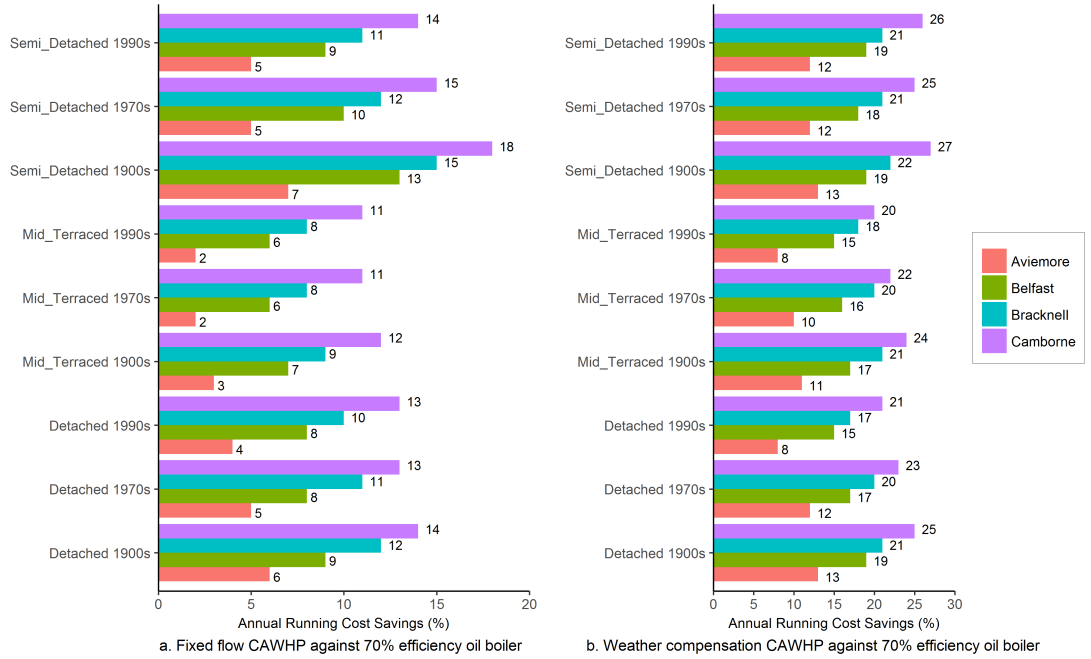

FIGURE 4.9: Annual operating cost savings of the retrofit CAWHPs compared with 70% efficiency oil boilers (Positive values indicate CAWHP's running costs are lower than those of boilers).

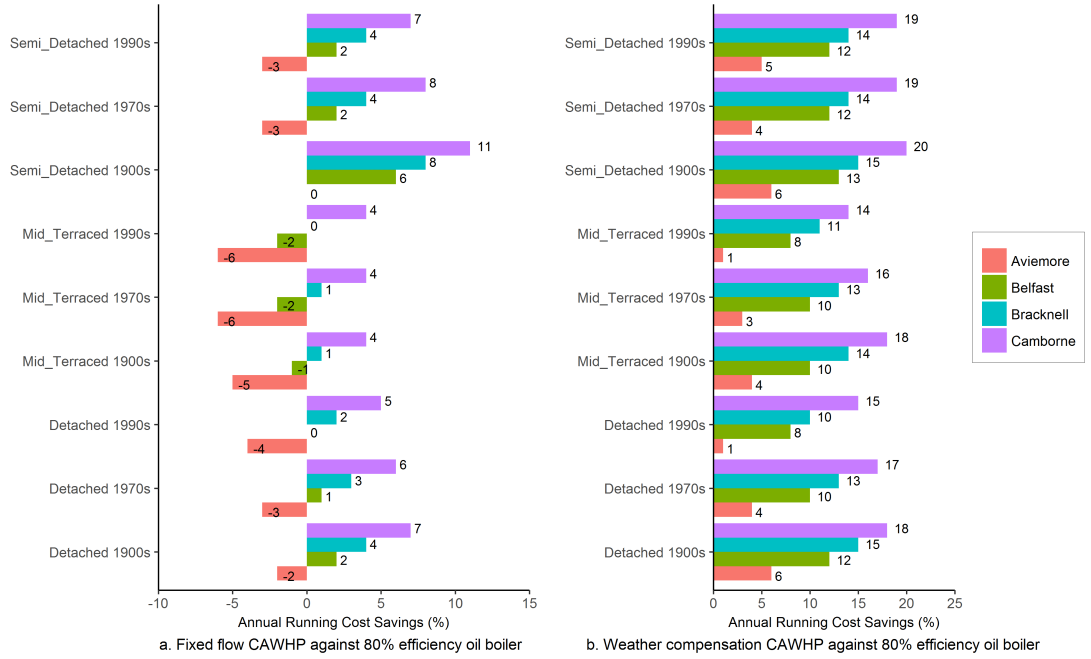

FIGURE 4.10: Annual operating cost savings of the retrofit CAWHPs compared with 80% efficiency oil boilers (Positive values indicate CAWHP's running costs are lower than those of boilers).

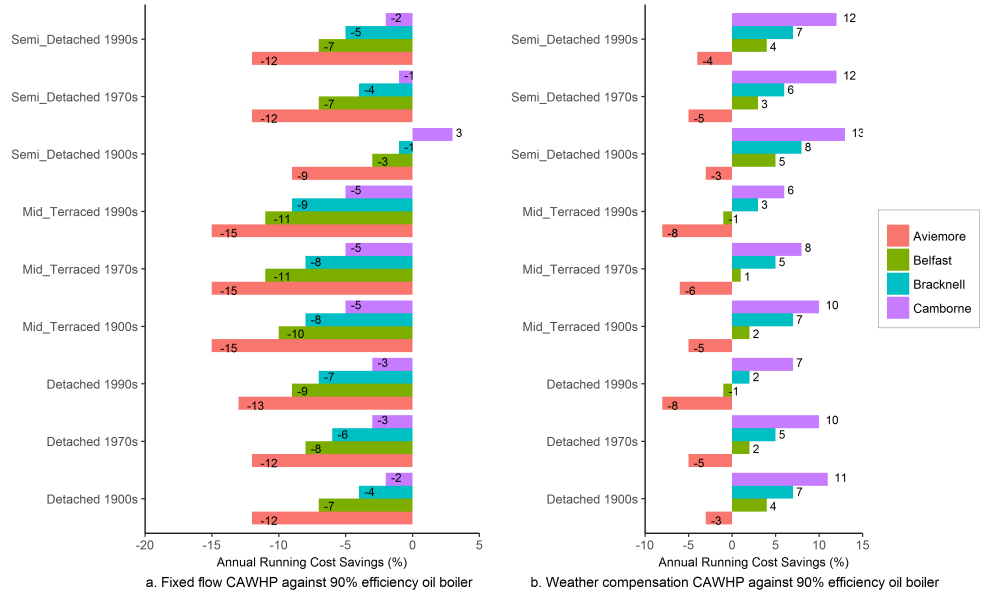

FIGURE 4.11: Annual operating cost savings of the retrofit CAWHPs compared with 90% efficiency oil boilers (Positive values indicate CAWHP's running costs are lower than those of boilers).

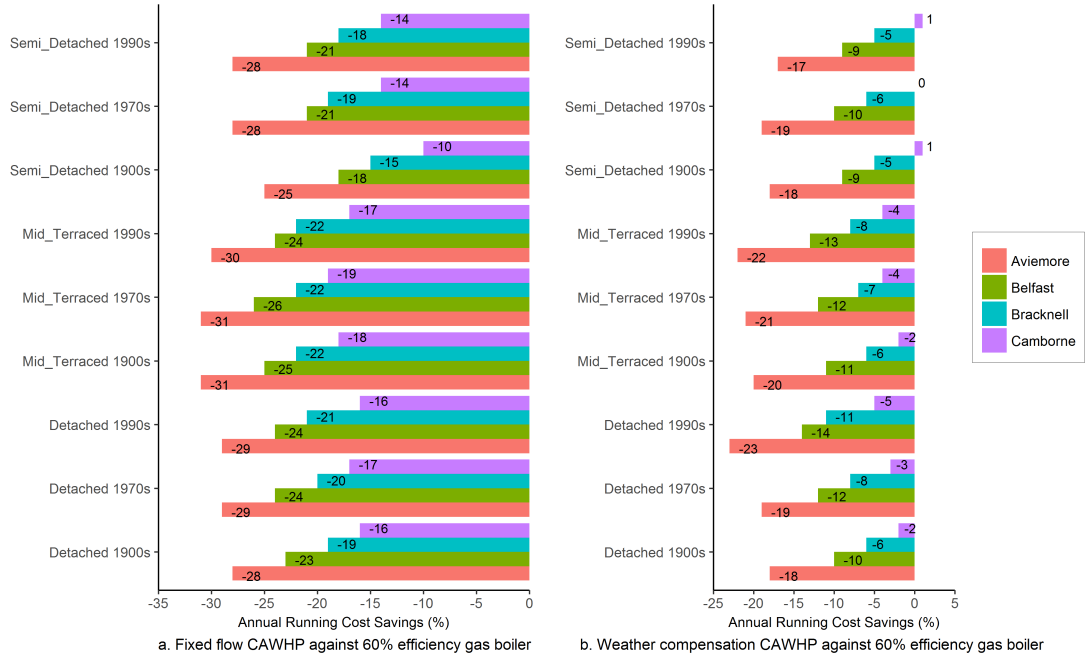

a. Fixed flow CAWHP against 60% efficiency gas boiler

b. Weather compensation CAWHP against 60% efficiency gas boiler

FIGURE 4.12: Annual operating cost savings of the retrofit CAWHPs compared with 60% efficiency gas boilers (Positive values indicate CAWHP's running costs are lower than those of boilers; negative values indicate CAWHP's operating costs are higher).

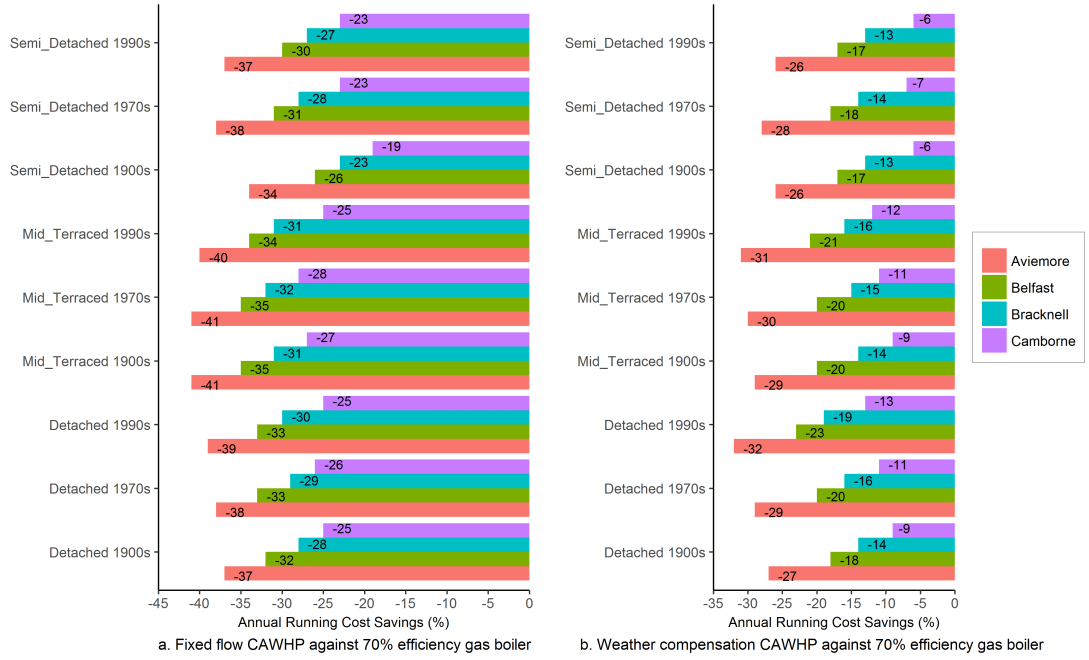

a. Fixed flow CAWHP against 70% efficiency gas boiler

b. Weather compensation CAWHP against 70% efficiency gas boiler

FIGURE 4.13: Annual operating cost savings of the retrofit CAWHPs compared with 70% efficiency gas boilers (Negative values indicate CAWHP's operating costs are higher than those of boilers).

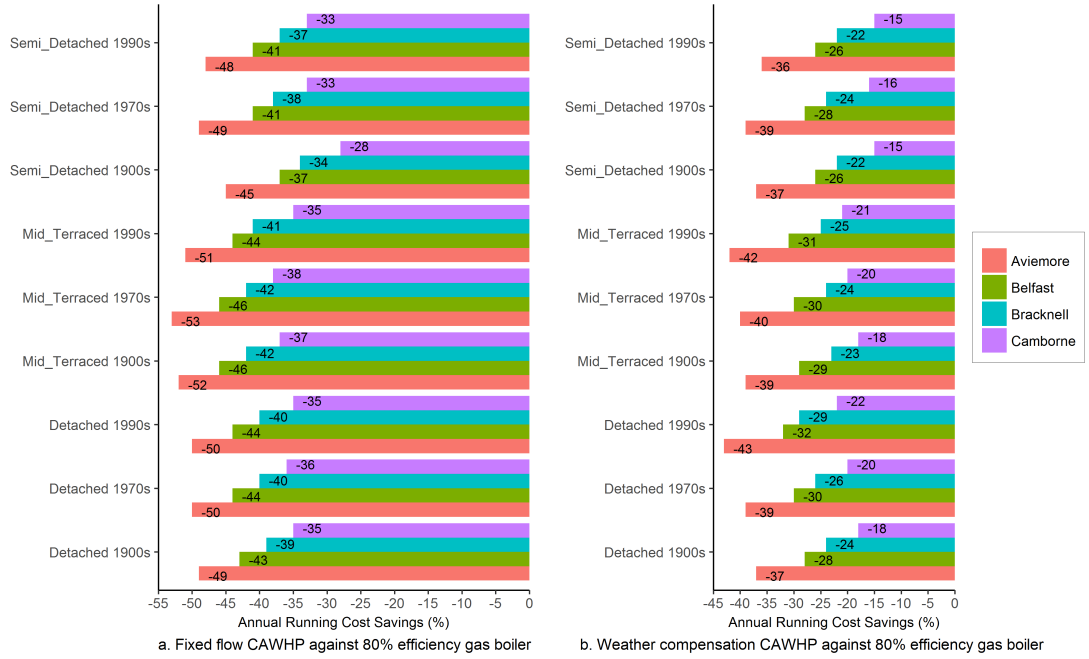

FIGURE 4.14: Annual operating cost savings of the retrofit CAWHPs compared with 80% efficiency gas boilers (Negative values indicate CAWHP's operating costs are higher than those of boilers).

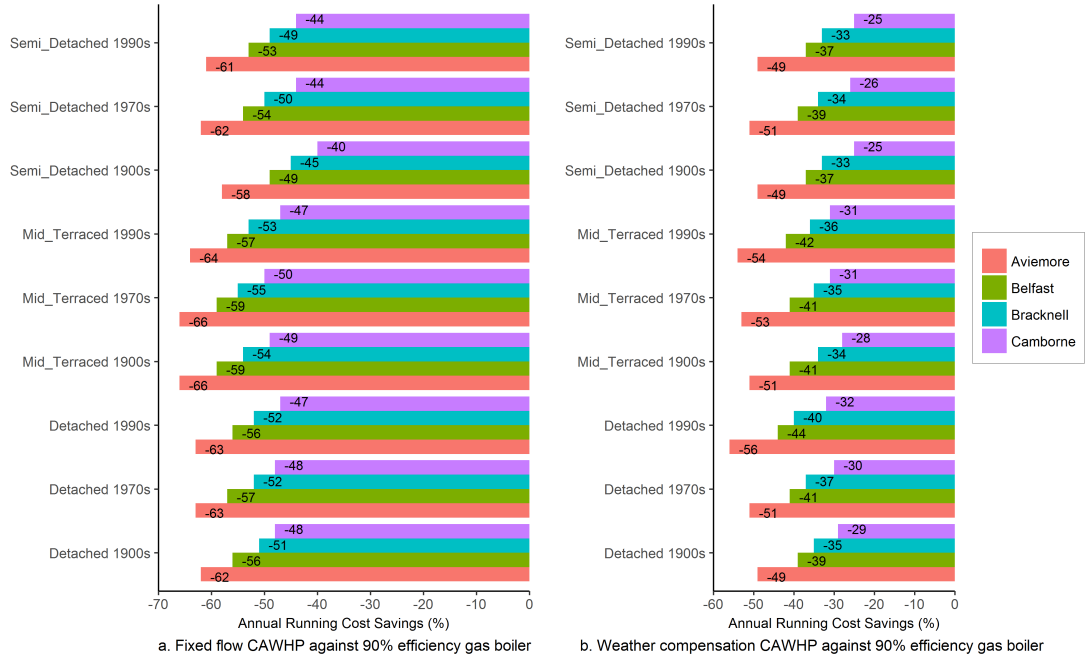

FIGURE 4.15: Annual operating cost savings of the retrofit CAWHPs compared with 90% efficiency gas boilers (Negative values indicate CAWHP's operating costs are higher than those of boilers).

4.3.3.2 Payback Time

Based on the running costs analysis of the retrofitted CAWHP above, it is necessary to calculate the payback time in case the heat pump produced operational savings. As mentioned in Section 1.1.4, the capital costs for the reference 11-kW CAWHP were £9900, including product itself and installation costs, so that it was used to calculate the payback time in Equation 4.1. It is assumed that the maintenance costs were not accounted fo.

$$PaybackTime(year) = \frac{9900}{OperationalSavingsPerYear} \tag{4.1}$$

Table 4.12 reports the payback time of the CAWHP with weather compensation control retrofitted into the buildings running with 60%, 70% and 80% efficiency oil boilers. Since there were not cost savings if the 90% efficiency oil boiler and all gas boilers were retrofitted by the reference CAWHP, the payback time was not considered. It is clear that the minimum payback time was 12.7 years when the heat pump was retrofitted into 1900s semi-detached houses.

TABLE 4.12: Payback time of the CAWHP with weather compensation control retrofitted into buildings running with oil boilers.

Building Type	Building Age	Location	Payback Time of Oil Boilers Retrofitted by CAWHPs (year)		
			60% efficiency	70% efficiency	80% efficiency
Mid-Terraced	1900s	Belfast	18	26.1	47.4
		Aviemore	20.8	35	110
		Bracknell	16.8	22.9	36.3
		Camborne	16.8	22.1	32.6
	1970s	Belfast	20.5	30	56.2
		Aviemore	24.3	42.9	180
		Bracknell	19.3	26.7	43.4
		Camborne	19.6	26.4	40.2
	1990s	Belfast	32.6	49.7	104.2
		Aviemore	39	75	990
		Bracknell	30.7	43.8	76.2
		Camborne	32.1	44.2	70.7
Detached	1900s	Belfast	12.7	17.9	30.5
		Aviemore	15.6	25	62.3
		Bracknell	12.4	16.8	26.4
		Camborne	11.1	14.6	21.2
	1970s	Belfast	14.8	21.4	38.7
		Aviemore	17.6	29.4	87.6
		Bracknell	14.5	20.2	33
		Camborne	13.3	17.7	26.3
	1990s	Belfast	22.4	34	70.7
		Aviemore	27.2	52.1	618.8
		Bracknell	22.7	33	60.4
		Camborne	21	28.6	44.8
Semi_Detached	1900s	Belfast	14.2	19.8	32.7
		Aviemore	17.2	27.5	68.3
		Bracknell	14.1	19.1	29.6
		Camborne	12.7	16.4	23.1
	1970s	Belfast	16.5	23.4	40.2
		Aviemore	20.2	33.6	101
		Bracknell	16.4	22.5	35.7
		Camborne	14.9	19.4	27.9
	1990s	Belfast	21.3	30	50.8
		Aviemore	24.8	40.2	106.5
		Bracknell	21.6	29.5	46.5
		Camborne	19.9	25.9	37.1

4.3.3.3 Carbon emissions

Carbon emissions of the retrofit CAWHP and boilers in the mid-terraced, detached and semi-detached buildings can be seen in Tables 4.9, 4.11, and 4.10, respectively. Furthermore, the figures of carbon emissions savings when the gas and oil boilers were retrofitted by the CAWHP are illustrated in Figures 4.16, 4.17, 4.18, 4.19, 4.20, 4.21, 4.22, and 4.23. The positive values in the figures indicate that operating the retrofit CAWHP emitted less carbon than running the boilers, while the negative values show that more CO_2 was released to the environment if the CAWHP was retrofitted.

It is clear from all tables (Table 4.9 to 4.11) and all figures (Figure 4.16 to 4.23) that the retrofit CAWHP could attain relative carbon cut (from 14% to 58%) compared to the figures of gas and oil boilers. The future UK grid with more proportions of renewable energy sources would make the retrofit CAWHP more competitive than fossil-fuelled boilers to help the UK achieve the binding target of carbon emissions reduction.

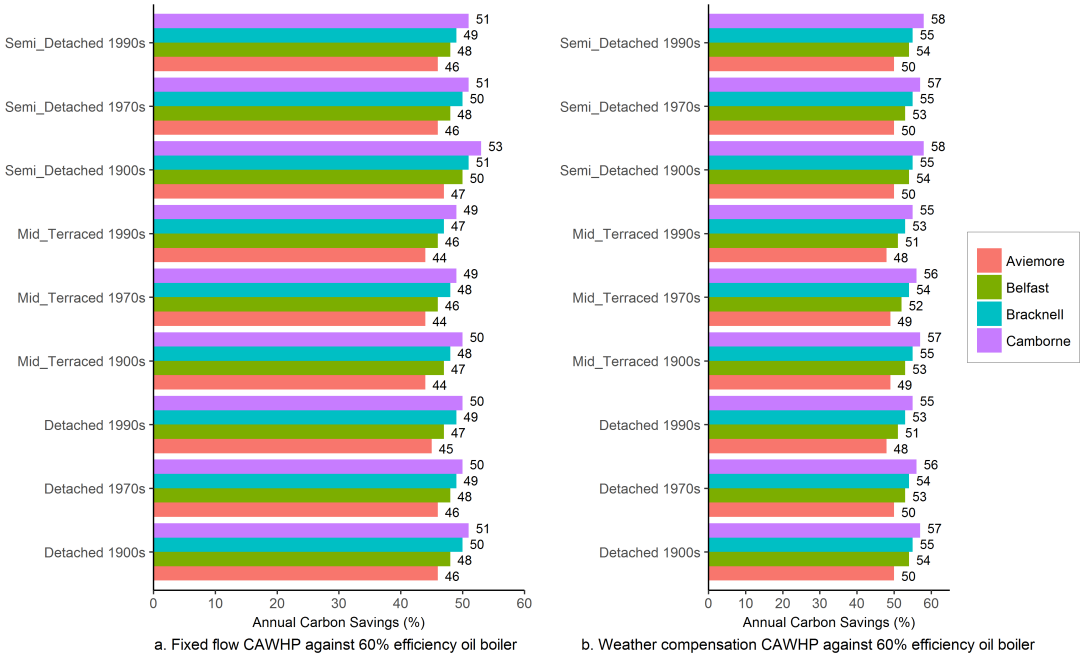

a. Fixed flow CAWHP against 60% efficiency oil boiler

b. Weather compensation CAWHP against 60% efficiency oil boiler

FIGURE 4.16: Annual carbon emissions savings of the retrofit CAWHPs compared with 60% efficiency oil boilers (Positive values indicate CAWHP's carbon emissions are lower than those of boilers).

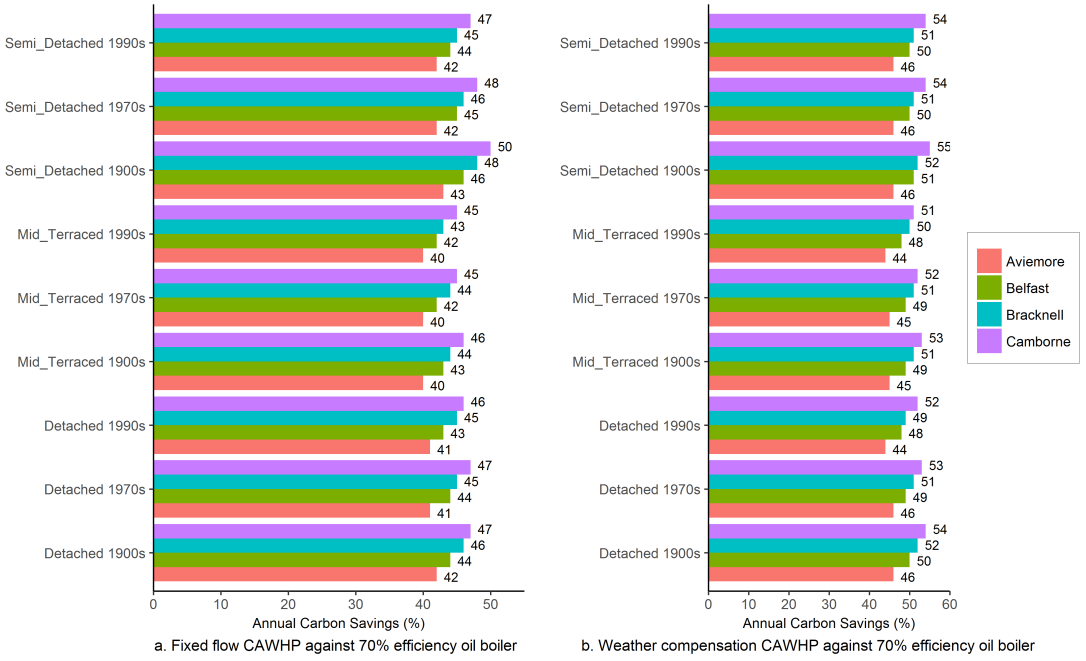

a. Fixed flow CAWHP against 70% efficiency oil boiler

b. Weather compensation CAWHP against 70% efficiency oil boiler

FIGURE 4.17: Annual carbon emissions savings of the retrofit CAWHPs compared with 70% efficiency oil boilers (Positive values indicate CAWHP's carbon emissions are lower than those of boilers).

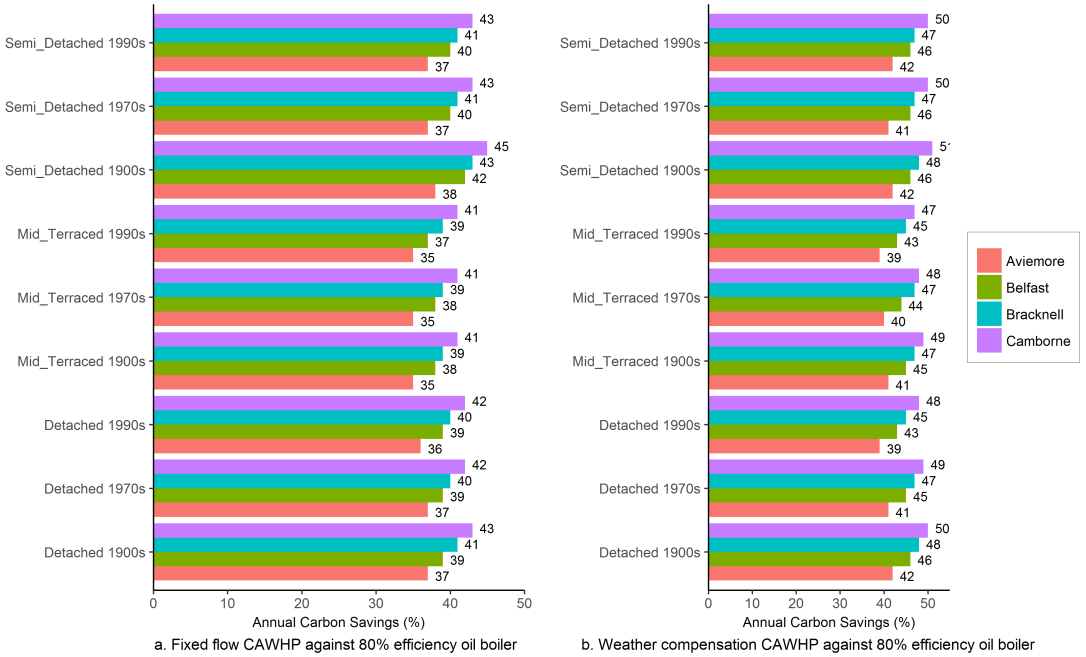

a. Fixed flow CAWHP against 80% efficiency oil boiler

b. Weather compensation CAWHP against 80% efficiency oil boiler

FIGURE 4.18: Annual carbon emissions savings of the retrofit CAWHPs compared with 80% efficiency oil boilers (Positive values indicate CAWHP's carbon emissions are lower than those of boilers).

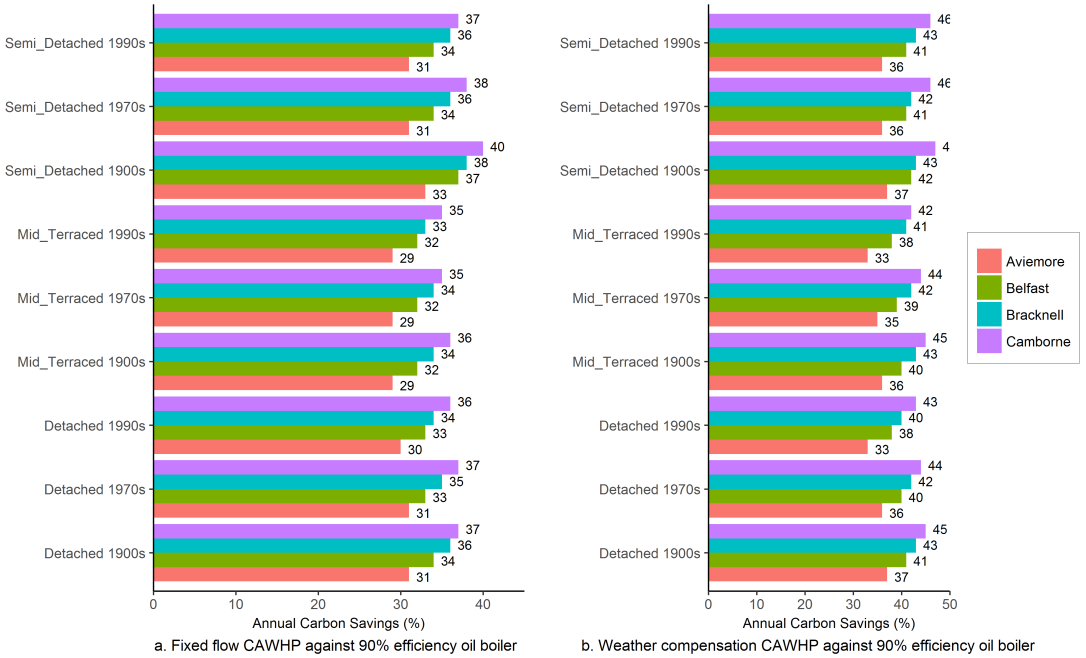

a. Fixed flow CAWHP against 90% efficiency oil boiler

b. Weather compensation CAWHP against 90% efficiency oil boiler

FIGURE 4.19: Annual carbon emissions savings of the retrofit CAWHPs compared with 90% efficiency oil boilers (Positive values indicate CAWHP's carbon emissions are lower than those of boilers).

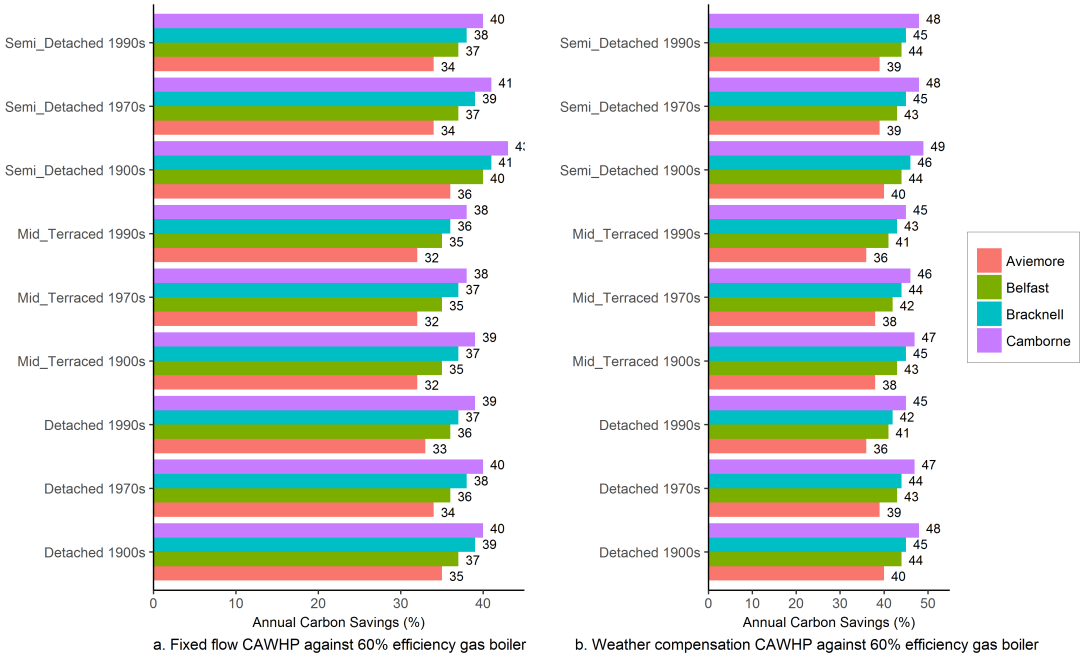

a. Fixed flow CAWHP against 60% efficiency gas boiler

b. Weather compensation CAWHP against 60% efficiency gas boiler

FIGURE 4.20: Annual carbon emissions savings of the retrofit CAWHPs compared with 60% efficiency gas boilers (Positive values indicate CAWHP's carbon emissions are lower than those of boilers).

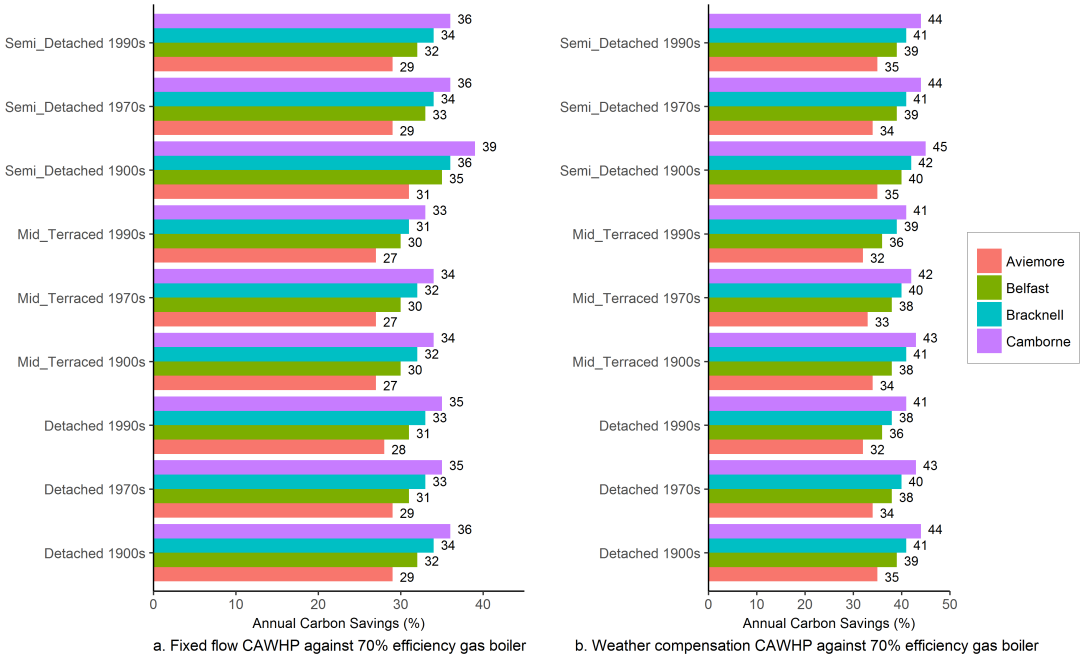

a. Fixed flow CAWHP against 70% efficiency gas boiler

b. Weather compensation CAWHP against 70% efficiency gas boiler

FIGURE 4.21: Annual carbon emissions savings of the retrofit CAWHPs compared with 70% efficiency gas boilers (Positive values indicate CAWHP's carbon emissions are lower than those of boilers).

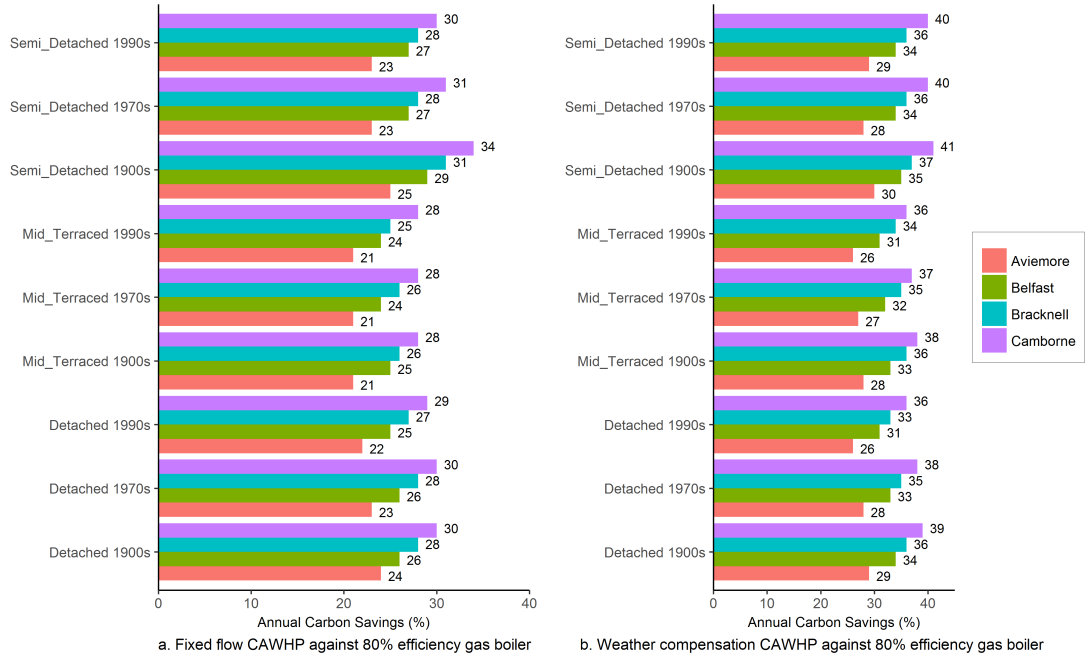

FIGURE 4.22: Annual carbon emissions savings of the retrofit CAWHPs compared with 80% efficiency gas boilers (Positive values indicate CAWHP's carbon emissions are lower than those of boilers).

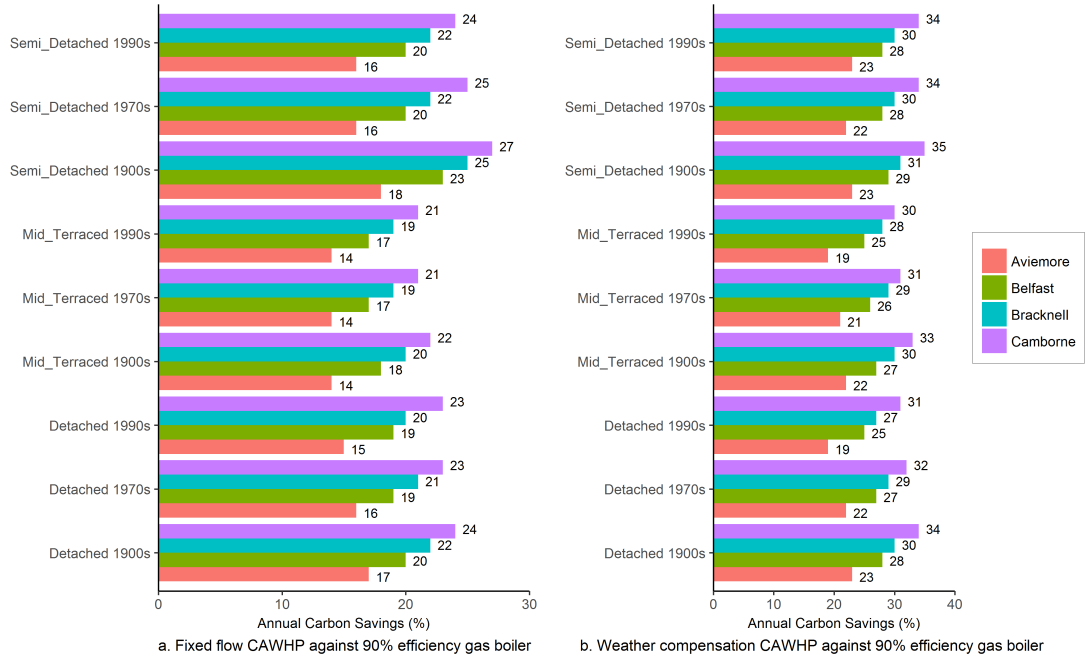

FIGURE 4.23: Annual carbon emissions savings of the retrofit CAWHPs compared with 90% efficiency gas boilers (Positive values indicate CAWHP's carbon emissions are lower than those of boilers).

4.3.3.4 Limitations of the work

The investigated houses in this work were mid-terraced, detached and semi-detached. Due to time and cost limitations, there was only heat demand validation of the mid-terraced building model was carried out. Therefore, the retrofit analysis of the detached and semi-detached buildings in this study was not highly accurate as their model parameters were just assumed and not verified against measured data. Future work should address these limitations.

4.4 Summary

In this chapter, the experimentally validated TRNSYS dynamic building simulation models were used to assess the annually techno-economic performance of the CAWHP when retrofitted into nine property types and ages in four locations across the UK. The performance of the retrofit CAWHP adopting fixed flow water temperature and weather compensation control was also investigated. The main outcomes of the simulation results are listed as follows:

- Regarding the hard-to-heat mid-terraced properties, the annual COP_{sys} of the retrofit CAWHP was lowest (2.03) in Aviemore and highest (2.24) in Camborne with the fixed outlet water temperature of 75 °C. With weather compensation control, the annual COP_{sys} could improve at least 6.7% and up to 11.9%, with the highest improvement being seen in Camborne where was milder than other locations, and the lowest being observed in the severe climate Aviemore.
- Considering the nine investigated archetypes in the four locations, the retrofit CAWHP could not defeat the gas boilers and 90% efficiency oil boilers in terms of running costs. However, there were cost savings if

the 60%, 70%, and 80% efficiency oil boilers were replaced by the retrofit CAWHP. In addition, the retrofit CAWHP could reduce carbon emissions from 14% to 58% compared to the figures of gas and oil boilers.

Based on the retrofit results above, it can be concluded that the reference CAWHP is a good candidate for retrofitting the domestic built environment in off-gas grid area, where most of the properties are old or high heat losses and running with low efficiency oil boilers (below 80% efficiency) for thermal heating demands. Furthermore, although operating the CAWHP was more expensive than running the condensing oil boilers (high efficiency) and all gas boilers, the reduced figures of carbon emissions of the retrofit CAWHP would be a good sign for the future uptake of this renewable-based technology.

Chapter 5

Comparative Performance of Cascade Heat Pump Coupled with Thermal Energy Storage in Different System Configurations

5.1 Introduction

This chapter presents the compared performance of the CAWHP integrated with the TES tank in the residential dwelling in terms of different system configurations. In particular, three operation modes were carried out, including direct heating, buffering system, and combined mode, as mentioned in Chapter 2. TRNSYS software was also utilised to simulate the systems. The validated dynamic building simulations were run with the same one-year period, which is different from the field trials that were conducted in the different periods. The rest of this chapter includes:

- Section 5.2: Methodology is presented.

- Section 5.3: Results and discussion are shown.
- Section 5.4: This chapter is summarised.

5.2 Methodology

To compare the performance of the system of the CAWHP coupled with the TES tank in terms of different configurations, three sets of annual simulations were investigated, including direct mode (stand-alone CAWHP system), indirect mode (buffering system) and combined mode (load shifting). These system configurations are mentioned clearly in Chapter 2 and now summarised as follows:

- **Direct Mode** (stand-alone CAWHP system): The CAWHP delivered heat directly to the house. The flow water temperature of the cascade heat pump was fixed to 75 °C.
- **Indirect Mode** (buffering system): The CAWHP provided heat to the TES tank, and that heat was then transferred to the house. The cascade heat pump was switched on to reheat the tank if the tank temperature was below 65 °C, and it was off when the tank reached 70 °C.
- **Combined Mode** (the load shifting): The heat pump was switched on at 1.00 am (at night) to store energy in the storage, bringing the water tank temperature to 75 °C. When the house required the first heating demand of the day, the stored energy was delivered to the house until its temperature dropped to 55 °C. After that, the cascade heat pump took over to provide heat to the house in the rest of the day. This operation can be assigned as demand-side management in which the heat pump was shifted to off-peak hours (at night) with cheap electricity prices (Economy 7 tariff)

to store the energy which was later used in the peak demand of the day (in the early morning).

Three sets of the annual simulations above were run with the same weather file (Belfast) available in TRNSYS data base. Also, the other boundary conditions (e.g. internal heat gains) were kept similar for all simulations, allowing the extracted annual results to be equally compared. It is noted that these simulations just limited to the cascade heat pump with fixed flow temperature, while weather compensation was not investigated.

5.3 Results and Discussion

5.3.1 Energy performance

The annual simulation results of three modes' energy performance are summarised in Table 5.1. Furthermore, the simulated results of three modes in two typical winter days are illustrated in Figure 5.1 in order to investigate how these modes performed in detail.

TABLE 5.1: Annual simulation results of energy performance of three modes' operations.

	Direct Mode	Indirect Mode	Combined Mode
Annual COP [-]	2.14	1.66	2.11
Annual COP_{sys} [-]	2.12	1.41	1.88
Storage efficiency [%]	-	85	53
Annual electric use [kWh]	11777	17304	13296 (Day: 10045; Night: 3251)
Annual useful heat [kWh]	24989	24343	24964
Average room temperature [°C]	19.7	19.6	19.8

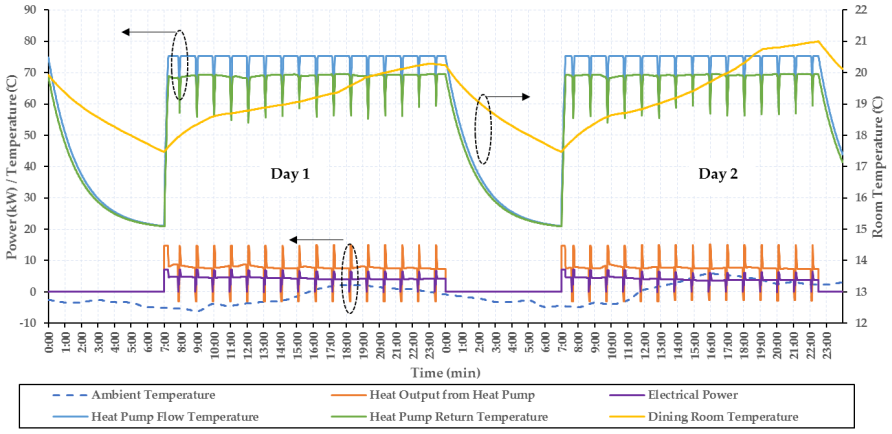

(A)

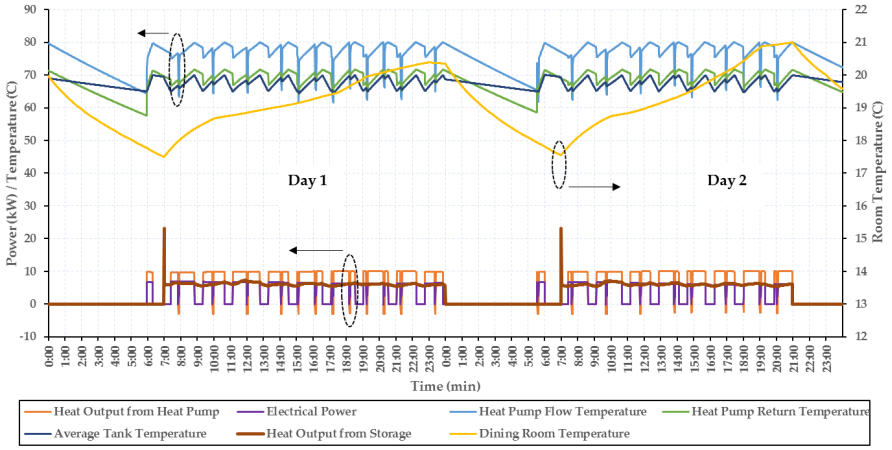

(B)

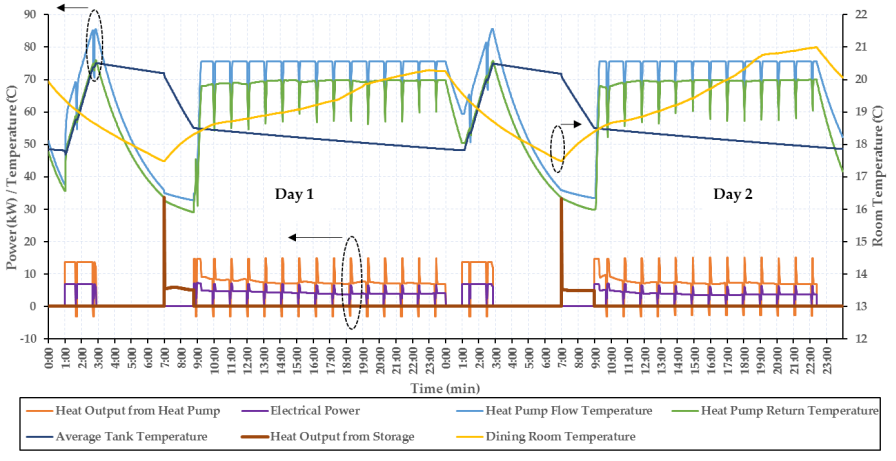

(C)

FIGURE 5.1: Simulated results of three modes in the same two typical winter days: (a) Direct mode; (b) indirect mode; (c) combined mode.

For comparison between the direct mode and the buffering system, the direct mode had a higher yearly COP than the buffering, as shown in Table 5.1. The cascade heat pump in the buffering system produced higher flow temperatures that were about 4 °C higher than the outlet water temperature of the cascade heat pump in the direct mode (75 °C) to charge the storage (Figures 5.1a and 5.1b). This is because the temperature at which heat provided to the storage via a heat exchanger needs to be higher to top up the tank. This behavior was also mentioned for the integrated system of a single-stage AWHP and TES by Kelly et al. [92]. This higher flow temperature led to the lower COP of the buffering system. Additionally, due to the parasitic losses of the storage tank, the buffering system yielded a yearly COP_{sys} of 1.41, which was about 33% lower efficiency compared to the direct heating (Table 5.1).

Regarding the direct mode and the combined mode, the direct mode also had a better performance. This is again due to the required higher water flow temperatures to charge the storage associated with the cascade heat pump in the combined mode (see Figures 5.1a and 5.1c). Furthermore, the CAWHP in the combined mode was active to top up the storage tank at night when the external air temperatures were lower than in daytime, resulting in its COP reduction. The higher water lift temperature combined with the COP decrease at night caused a lower annual COP (2.11) of the combined mode in comparison to the direct system (2.14), as reported in Table 5.1. For the system efficiency, again because of the parasitic losses of the storage tank, the yearly COP_{sys} of the combined mode was roughly 11.3% lower than that of the direct mode.

Comparing the buffering to the combined mode, the yearly COP of the buffering (1.66) was lower than the one of the combined mode (2.11). This is because the cascade heat pump in the combined mode charged the storage at night and then provided heat directly to the house in the day time (Figure 5.1c), meaning that its COP deterioration due to the required high flow temperature was only

affected for about two hours at night. Meanwhile, the CAWHP in the storage mode delivered high water flow temperature all the time.

Although all systems could maintain the same comfort (Table 5.1), there was an electric use penalty of the buffering (17304 kWh) which was approximately 46.9% and 30.1% higher than the heat pump in the direct mode and the combined mode, respectively. There are two main reasons why the buffering system consumed more energy than the night shifted load and the direct heating. Firstly, the heat pump had lower COP in the buffering system than in the direct mode and the combined mode. Secondly, the parasitic losses of the storage subjecting to the buffering system led the heat pump to consume more energy to compensate the supplied heat to the house, while this did not occur in the direct mode and happened in the shorter time during a day in the combined mode.

5.3.2 Running costs

Running costs of the CAWHP in three modes are calculated and presented in Table 5.2 based on the simulated energy consumption presented in Table 5.1. To calculate the operating costs, the electricity price of £0.175 per kWh [88] was used for the cascade heat pump in the direct mode and the indirect mode. As for the combined mode that applied the Economy 7 tariff, the day rate was £0.1666/kWh, while the night rate was £0.0931/kWh [93].

TABLE 5.2: Annual operating costs of the retrofit CAWHP in three modes.

	Annual running cost [£]
Direct mode	2061
Indirect mode	3028
Combined mode	1976

It is clear in Table 5.2 that the combined mode could help homeowners to pay less money than the other modes thanks to the benefit of the Economy 7 tariff. As for the direct mode and indirect mode, the cascade heat pump in the direct heating was cheaper to run (about 46.9%) than the one in the buffering mode. The reason for this is due to the lower efficiency of the cascade heat pump and the parasitic losses of the tank, as mentioned above Section 5.3.1.

In Figure 5.2, it is clear that there was cost penalty associated with the cascade heat pump in the buffering system (indirect mode). Although the load shifting (combined mode) could attain the cost savings compared to the other modes as mentioned above, its operating cost was still higher than those of gas boilers and 90% efficiency oil boiler. Therefore, a better demand-side management strategy should be carried out to make this CAWHP more cost competitive than the boilers, which is presented in the next chapter.

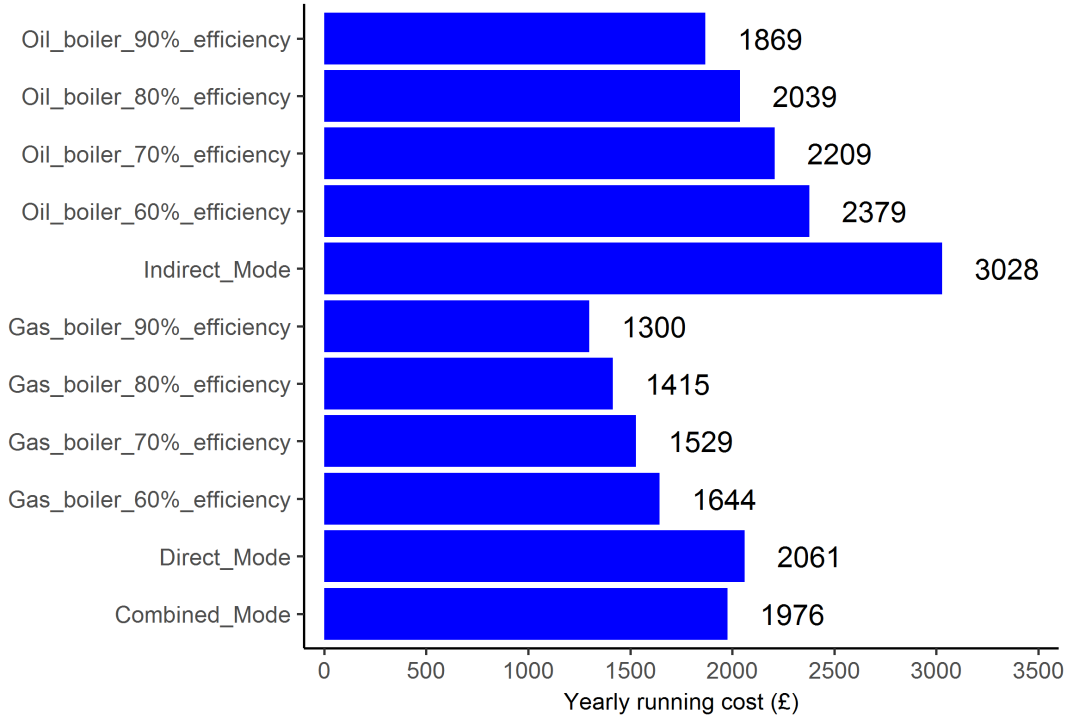

FIGURE 5.2: Annual running costs of the retrofit CAWHP in three operating modes and boilers.

5.3.3 Summary of advantages and disadvantages of three system operations

A summary of the advantages and disadvantages of three mode operations is stated in Table 5.3. In the direct mode, it took longer time to reach the set-point room temperature compared to the other modes. This is evidenced by looking at day 2 in Figure 5.1, in which the room temperature reached 21 °C at 22.31 h (direct mode), 20.58 h (indirect mode) and 22.24 h (combined mode). There were two main reasons why this happened. First, the cascade heat pump in the direct mode operated with cold start in the morning, while the high heat output from the TES in both the indirect mode and combined mode could allow the room temperature to reach its set-point earlier. Second, during the operation of a defrost cycle, heat was taken from the house to melt the ice on the outdoor coils according to the direct mode and combined mode, whilst regarding the indirect mode, this heat was taken from the TES. This also explains why the period to reach thermal comfort of the combined mode was shorter than the indirect mode but longer than the direct mode.

TABLE 5.3: Summary of pros and cons of three mode operations.

	Advantage	Disadvantage
Direct Mode	- High efficiency	- High running cost
	- Low energy utilisation	- Longer time to reach thermal comfort
		- Heat for defrost taken from house
Indirect Mode	- Faster to reach thermal comfort	- High flow temperature to charge TES
	- Heat for defrost taken from TES	- Low efficiency
		- Parasitic losses of TES
		- High running cost
		- High energy utilisation
Combined Mode	- Good efficiency	- High flow temperature to charge TES
	- Take advantage of low electricity rate	- Charge TES at night where ambient temperature is low
	- Low running cost	- Parasitic losses of TES
	- Faster to reach thermal comfort	- High energy utilisation
		- Heat for defrost taken from house

5.4 Summary

In this chapter, the system performance of the retrofit CAWHP coupled with the TES tank was compared by means of the annual extracted simulations under the same boundary conditions. Three operating modes, including direct mode, indirect mode, and combined mode, were investigated. The direct mode obtained the highest annual efficiency (COP_{sys} of 2.12) followed by the shifted load (COP_{sys} of 1.88), whereas the buffering system had the worst performance (COP_{sys} of 1.41). The reasons behind the low efficiencies in the buffering (indirect mode) and the load shifting (combined mode) were mainly due to the high outlet water temperature required to top up the tank in line with the parasitic losses of the storage. With regards to the running costs, the combined mode was a promising system as its operating cost was lowest thanks to the Economy 7 tariff. However, its operating cost was still higher than those of gas boilers and 90% efficiency oil boiler.

Chapter 6

Load Shifting for Cascade Heat Pump Coupled with Thermal Energy Storage: Tariff-based Schedule Approach

6.1 Introduction

In this chapter, different operation strategies for the CAWHP coupled with the TES were designed to shift both space heating and hot water demands from peak to off-peak periods. The operation of the cascade heat pump was blocked to off-peak periods identified by a time-of-use tariff. There were three main objectives of this investigation. The first was to find the best schedule to operate the cascade heat pump efficiently with minimised running costs and reduced wind energy curtailment, while shifting wholly the electrical heating loads to off-peak periods. The second was to find the optimum system design, storage

tank sizing and temperature set points in particular. Finally, a retrofit assessment was carried out to evaluate how the designed load shifting strategy could help the cascade heat pump save operating costs and carbon emissions when compared with the performance of gas and oil boilers. The remain of this chapter is organised as follows:

- Section 6.2: Methods are discussed.
- Section 6.3: Results and discussion are presented.
- Section 6.4: Summary of this chapter is drawn.

6.2 Methodology

6.2.1 Structure of the simulations

Figure 6.1 shows the structure of the simulations carried out to obtain the results in this chapter. It contained two main parts: TRNSYS simulation tool and load shifting strategies. The load shifting strategy component acquired the information inputs from the grid demand, the available electricity tariffs, the wind energy, the weather conditions, the tank sizes, the tank temperature set points, and the starting time to charge the storage tank. The TRNSYS simulation tool received the inputs from the load shifting strategy part, the developed and validated building models, and the weather conditions. Then, the TRNSYS tool provided the results of energy consumption, thermal output, running costs and system efficiency.

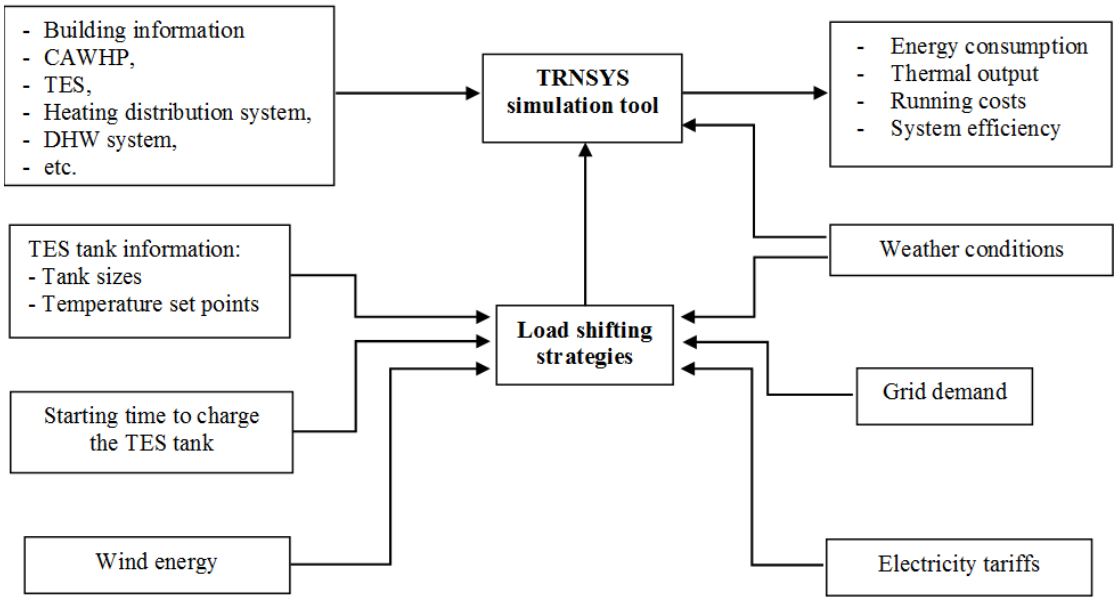

FIGURE 6.1: Structure of the investigated simulations.

6.2.2 Case study

The building investigated in this chapter was the mid-terraced hard-to-heat house representing typical ageing house stock in the UK, as shown in Figure 2.2 in Chapter 2. The heating system was the selected CAWHP coupled with the TES tank, transferring heat to the DHW and wet radiator systems for the space heating demand with the nominal flow of 75 °C, as illustrated in Figure 2.3 in Chapter 2. The sizes of the TES carried out in this chapter were in the range from 0.6 m^3 to 1.1 m^3. The tanks' height was 2 m, but the diameters were changed in accordance with the storage sizes.

The heating system was controlled on/off, based on a scheduled programmer to maintain the dining room temperature at 19.5 – 21 °C and the DHW temperature at 50 – 60 °C during the occupied hours. The periods of active occupancy and operation of the heating system are shown in Figure 6.2, in which the data were adapted from the work of Kelly et al. [4] representing typical occupants' behaviours in the UK. In particular, the active occupancy was assumed to be

07.00 – 08.00 h and 18.00 – 23.00 h every day, and the heating system was turned on during the periods of 06.00 – 09.00 h and 16.00 – 11.00 h. The heating system was operated one hour earlier in the morning and evening than the occupancy periods to preheat the house.

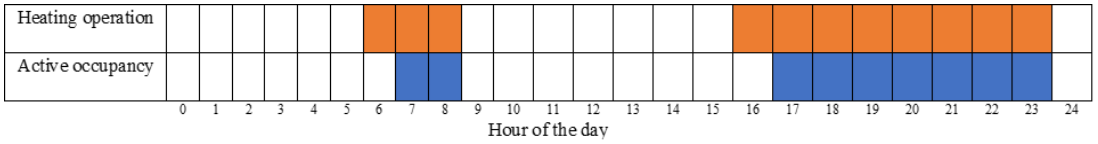

FIGURE 6.2: Daily operating hours of heating system and active occupancy (data are adapted from [4]).

6.2.3 TRNSYS simulations

The developed TRNSYS whole building simulation models validated against the laboratory and field trial data, explained in Chapter 3, were utilised to carry out the load shifting strategies in this chapter. The test and boundary conditions investigated in the TRNSYS simulations are explained as follows.

Grid demand: In Figure 6.3, the two-consecutive-day electrical demand in winter in Northern Ireland illustrates that the peak hours were from 16.00 h to 19.00 h, whereas the low demand was between midnight and 06.00 h. The control algorithms were designed to shift the house heating demands from peak hours to off-peak periods. Therefore, the TES tank played an important role. In particular, the TES supplied heat to the house during the period of 16.00 – 19.00 h, while it was charged to store the energy by the cascade heat pump at any time outside of that period. The start-up time to top up the TES was determined depending on the designed load shifting strategies, as explained in the next sections.

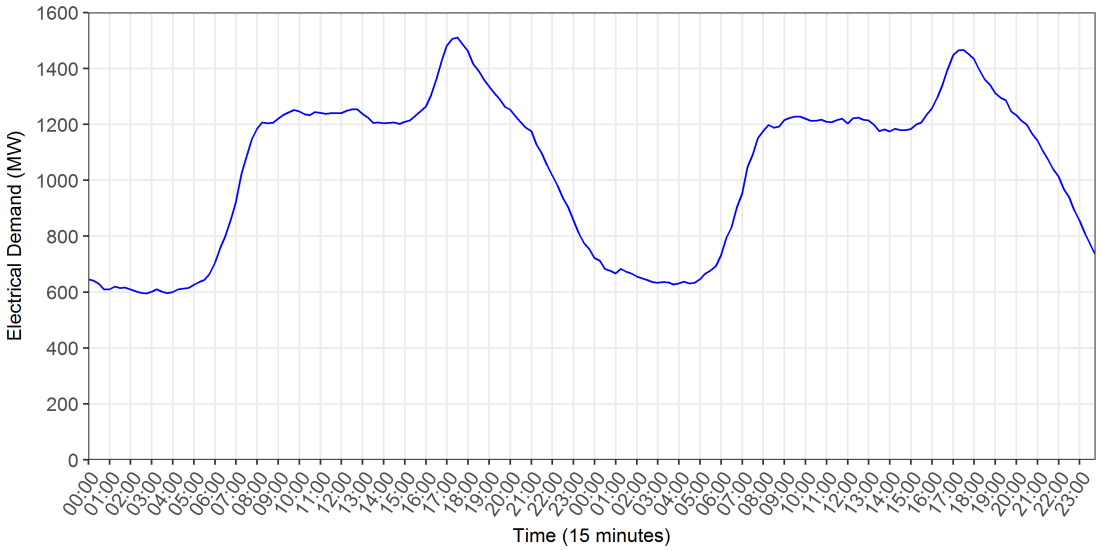

FIGURE 6.3: Two-consecutive-day grid demand in winter in Northern Ireland (data are adapted from [5]).

Electricity tariffs: In the UK, there are three main electricity tariffs, namely standard tariff, Economy 7 and Economy 10 in England (or Powershift tariff in Northern Ireland). In Northern Ireland particularly, the standard tariff is called a flat rate tariff in which the electricity rates are the same every day. The Economy 7 is a tariff in which the electricity price is much cheaper at night (01.00 – 08.00 h) compared to the flat rate, while the price in the daytime (09.00 – 24.00 h) is more expensive than the flat one. The Powershift can be defined as a time-of-use tariff, including three distinct rates: low rate applies between midnight and 08.00 h; normal rate is between 08.00 – 16.00 h and 19.00 – 24.00 h; peak rate applies from 16.00 – 19.00 h. In this study, the aims of the demand response control were to shift the heating demands from peak hours (16.00 -19.00 h) to off-peak periods. Therefore, the Powershift was an appropriate tariff for calculating the running costs of the cascade heat pumps in this study. Furthermore, for comparison purposes, the flat rate tariff was applied to the reference case in which the heat pump was not controlled to shift the house heating demands, and the TES was not used. The electricity prices of the flat rate and the Powershift in Northern Ireland can be seen in Figure 6.4.

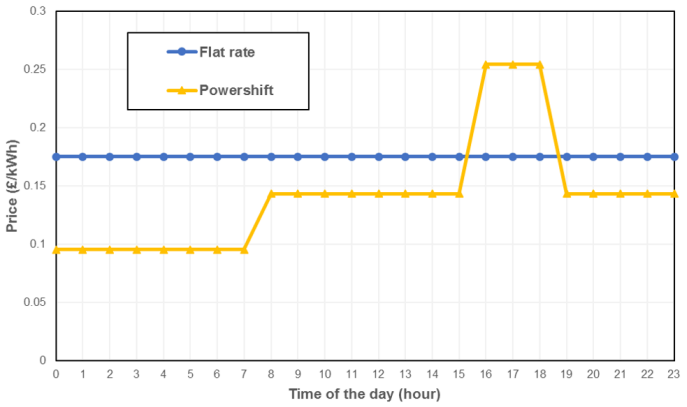

FIGURE 6.4: Electricity prices of the flat rate and the Powershift tariff in Northern Ireland [6].

Wind energy: In Northern Ireland (the UK), there are high proportions of wind energy dispatch-down, according to the report of EIRGRID [27]. In Figure 6.5, the highest figures are seen at night and in the afternoon. Therefore, the load shifting control strategies in this study were also designed to operate the cascade heat pump during the periods of the high wind curtailment power, which in turn can help more proportions of wind energy to be integrated into the grid.

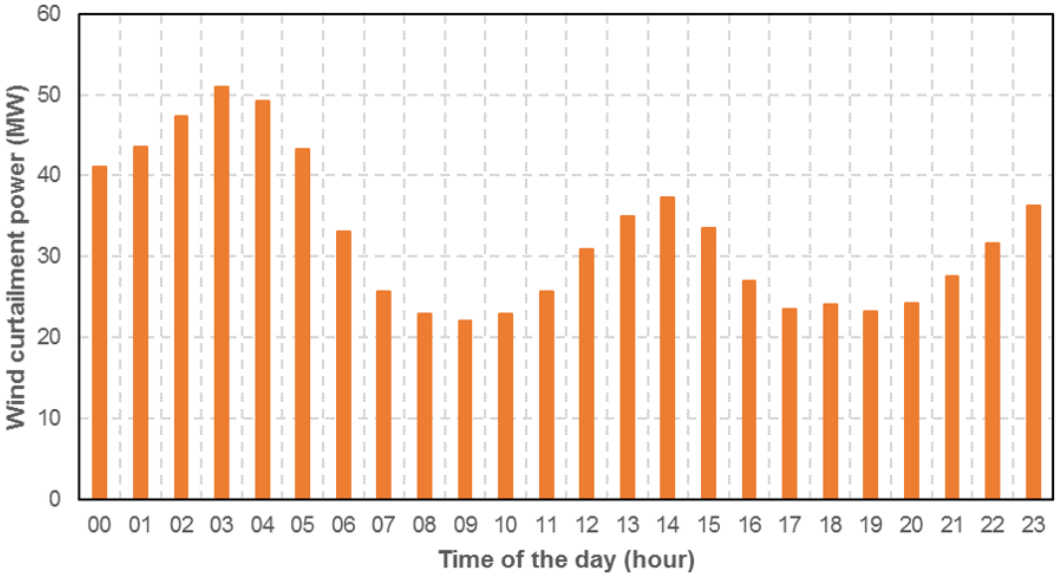

FIGURE 6.5: Average wind curtailment by hour of the day across the year 2018 in Northern Ireland (data are adapted from [7]).

Weather data: The weather data used to run the simulations were the Meteonorm data of Belfast - Northern Ireland (the UK), available in TRNSYS files. The average ambient temperatures versus 24 hours of winter, spring, summer and autumn are depicted in Figure 6.6. The periods of each season in the UK can be defined as follows: winter is from December to February; spring is March – May; summer is between June and August; and autumn is September – November. It can be seen in the figure that, the trends of average temperatures of all seasons are similar. They are lower in the night than in the daytime, and the highest air temperatures occur from 13.00 h to 16.00 h.

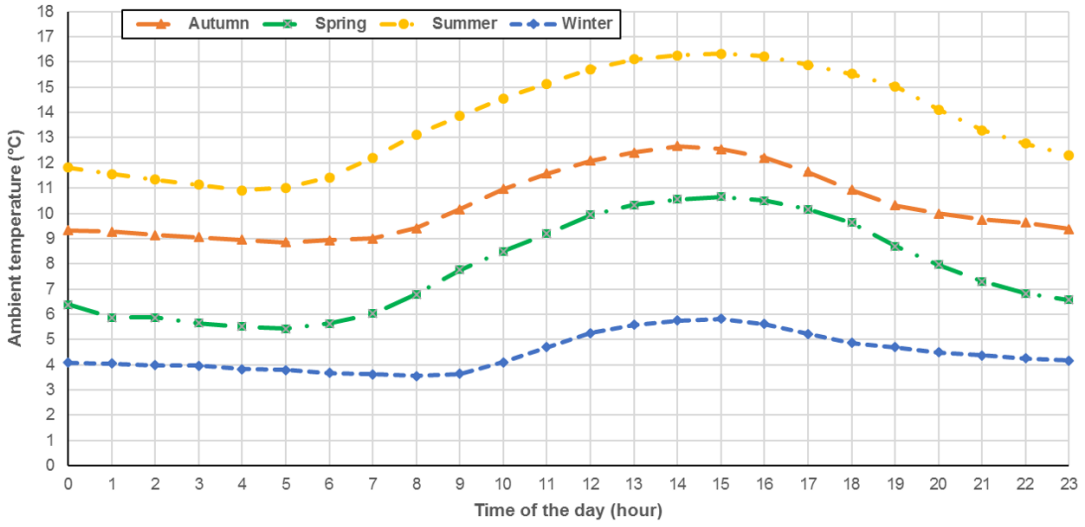

FIGURE 6.6: Average hourly ambient temperatures in each season in Belfast, Northern Ireland obtained from TRNSYS weather data.

The storage sizes and temperature set points: Seven tank sizes were investigated in this study to evaluate the performance of the designed load shifting strategies. The sizes ranged from 0.6 m^3 to 1.2 m^3 with an increment of 0.1 m^3. Additionally, three different temperature set points of the tank were conducted, including 65 °C, 70 °C and 75 °C. There are two main reasons why the investigated tank set points were limited from 65 °C to 75 °C. First, if the tank set point is higher than 75 °C, the heat pump needs to lift its outlet water temperatures approximately over 80 °C (about 5 °C difference to the set point of the tank)

to maintain the heat transfer rate between the heat pump and the storage via the heat exchanger, as stated in [4]. This hence makes the heat pump reduce its efficiency. Second, if the tank set point is reduced below 65 °C, it would result in the larger tanks to store enough energy to shift wholly the heating demand to off-peak hours. Since the real TES was custom made, its heat losses were higher than the units that are currently available in the UK market. Its average heat loss coefficient found in the experimentally validated model mentioned in Chapter 3 was about 2.5 W/m^2K. Therefore, the average heat loss coefficient of the TES carried out in the simulations with the applied DSM strategies was improved to 0.6 W/m^2K [50].

Periods of the storage tanks to get fully charged: To decide what time of a day the cascade heat pump should be turned on to charge the TES, a set of simulations was initially run to determine the periods the TES could reach its temperature set points from the cut-off temperature (55 °C). The times for the TES tanks to get fully charged are detailed in Table 6.1. The smaller tanks with the lower set points could get fully charged in shorter periods than the larger tanks with the higher set points. The times to fully top up the TES ranged from 54 minutes to 164 minutes.

TABLE 6.1: Time for the TES fully charged and the determined starting time to top up the TES for different tank sizes and temperature set points.

Tank size (m^3)	Tank temperature set point (°C)	Time for the TES fully charged	Starting time to charge the TES (hour)		
			Strategy A	Strategy B	Strategy C
0.6	65	54	4 am	2 pm	4 am and 2 pm
	70	68	4 am	2 pm	4 am and 2 pm
	75	84	4 am	2 pm	4 am and 2 pm
0.7	65	62	4 am	2 pm	4 am and 2 pm
	70	79	4 am	2 pm	4 am and 2 pm
	75	97	4 am	2 pm	4 am and 2 pm
0.8	65	70	4 am	2 pm	4 am and 2 pm
	70	89	4 am	2 pm	4 am and 2 pm
	75	111	4 am	2 pm	4 am and 2 pm
0.9	65	79	4 am	2 pm	4 am and 2 pm
	70	100	4 am	2 pm	4 am and 2 pm
	75	124	3 am	1 pm	3 am and 2 pm
1	65	87	4 am	2 pm	4 am and 2 pm
	70	112	4 am	2 pm	4 am and 2 pm
	75	137	3 am	1 pm	3 am and 2 pm
1.1	65	95	4 am	2 pm	4 am and 2 pm
	70	120	4 am	2 pm	4 am and 2 pm
	75	150	3 am	1 pm	3 am and 2 pm
1.2	65	104	4 am	2 pm	4 am and 2 pm
	70	132	3 am	1 pm	3 am and 2 pm
	75	164	3 am	1 pm	3 am and 2 pm

6.2.4 Load shifting strategies

The investigation in this chapter aimed to seek the best schedule of operation of the CAWHP coupled with the TES to improve system efficiency with minimised

running costs and reduced wind energy curtailment, while avoiding the peak demand periods as well as guaranteeing the thermal comfort of the end-users. Therefore, three load shifting rule-based control strategies, namely Strategy A, Strategy B and Strategy C, were designed based on the available electricity tariff (Powershift tariff), the outdoor ambient temperatures, the utility peak hours (16.00 – 19.00 h), and the periods of high wind curtailment.

6.2.4.1 Strategy A

In this strategy, the cascade heat pump was turned on to charge the TES at night when the electricity rate was lowest according to the Powershift tariff (Figure 6.4), and the stored energy was later used during peak hours to satisfy the house heat demands. Other than that period, the heat pump provided heat directly to the house when the space and DHW demands were required. Flow chart of this strategy is shown in Figure 6.7. By this strategy, the system could take advantage of the lowest electricity while reducing the utility power demand during peak hours.

To determine when the TES was charged at the night, there were four main factors to consider. First, in Figure 6.6, the ambient temperatures did not change much during these hours, within 1 °C difference. Therefore, COPs of the heat pump were not much different during this period. Second, it took about one hour to three hours, depending on the tank sizes and temperature set points, to get it fully charged (Table 6.1). Meanwhile, it needed to be sure that the TES got fully charged before the first house heat demands were called at 06.00 h (Figure 6.2). Third, as the TES was charged at night and then used in the afternoon, its efficiency due to standing heat losses should be minimised. Finally, the percentages of the wind power curtailment were highest from 03.00 h to 05.00 h (Figure 6.5). If the cascade heat pumps were used during these hours, it could help more proportions of this renewable energy to be integrated into the grid.

Based on these factors, the hours to start charging the TES were at 03.00 h and 04.00 h depending on the tank sizes and temperature set points, as mentioned in Table 6.1.

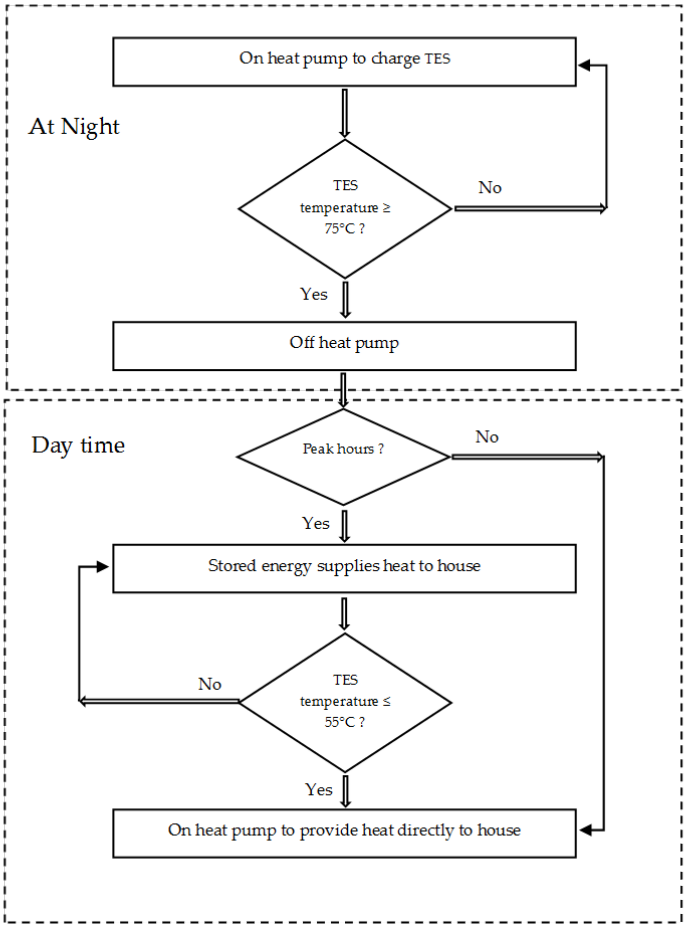

FIGURE 6.7: Flow chart of Strategy A.

6.2.4.2 Strategy B

In this strategy, the CAWHP was on to top up the TES at daytime between 09.00 h and 16.00 h to take advantage of the high ambient temperatures (Figure 6.6) while getting the normal rate electricity price (Figure 6.4). Then, the stored energy was used during peak hours. This operation could help the cascade heat pump improve its efficiency and shift the peak grid demand. Flow chart of this strategy can be seen in Figure 6.8

There were four main factors to determine what time the TES was topped up. The first factor was due to the ambient temperatures. Looking at Figure 6.6, the ambient temperatures in 09.00 – 16.00 h were highest from 13.00 h to 16.00 h, so the TES should be charged during these hours. The second was of wind energy curtailment. In Figure 6.5, the highest wind dispatch-down power was from 13.00 h to 15.00 h. The third and fourth factors were the standby losses of the TES and the times for the tank to get fully charged. As a result, the time to start the CAWHP to charge the TES was at 13.00 h and 14.00 h depending on the tank sizes and temperature set points, as reported in Table 6.1.

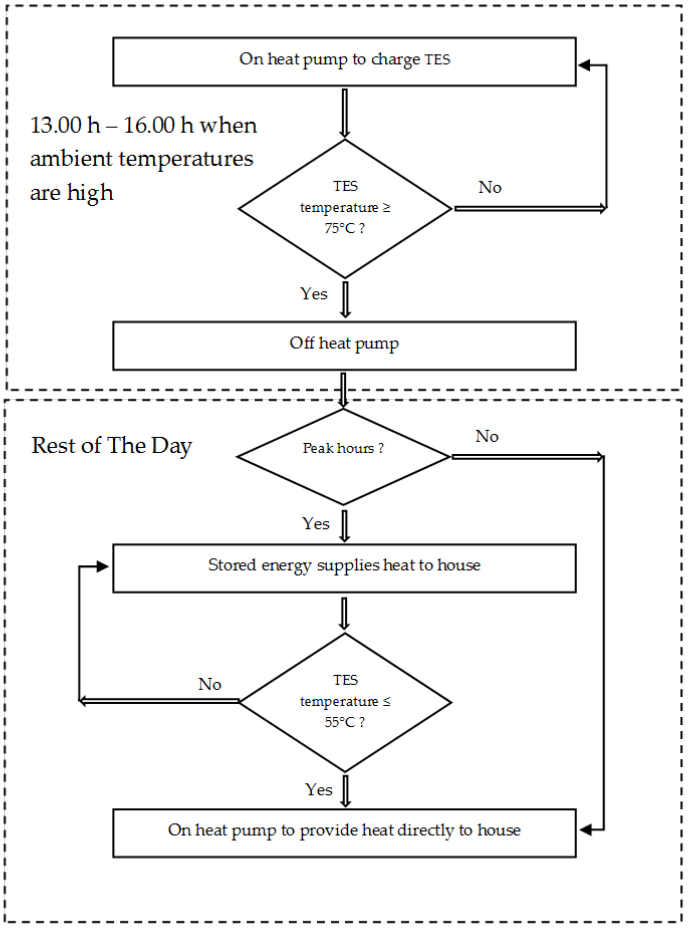

FIGURE 6.8: Flow chart of Strategy B.

6.2.4.3 Strategy C

In this strategy, the cascade heat pump was on to top up the TES at both the night time and the daytime to take advantage of both the low electricity rates and the high ambient temperatures. Particularly, the night time stored energy was used for the house heat demands in the morning (06.00 – 09.00 h). As the electricity price was still lowest from 06.00 h to 08.00 h (Figure 6.4) in the period of the morning demands, the cascade heat pump provided heat directly to the house for two hours (06.00 - 08.00 h), while the stored energy at the night time was used for only one hour (08.00 – 09.00 h) to satisfy the house demands. Additionally, the daytime stored energy was used during peak hours. Flow chart of this strategy is illustrated in Figure 6.9

Considering the same factors as the above Strategy A and Strategy B, the hours to start the CAWHP to top up the TES were at 04.00 h and 14.00 h for the lower tank sizes and set points, while at 03.00 h and 14.00 h for the larger tanks and higher temperature set points. These are detailed in Table 6.1.

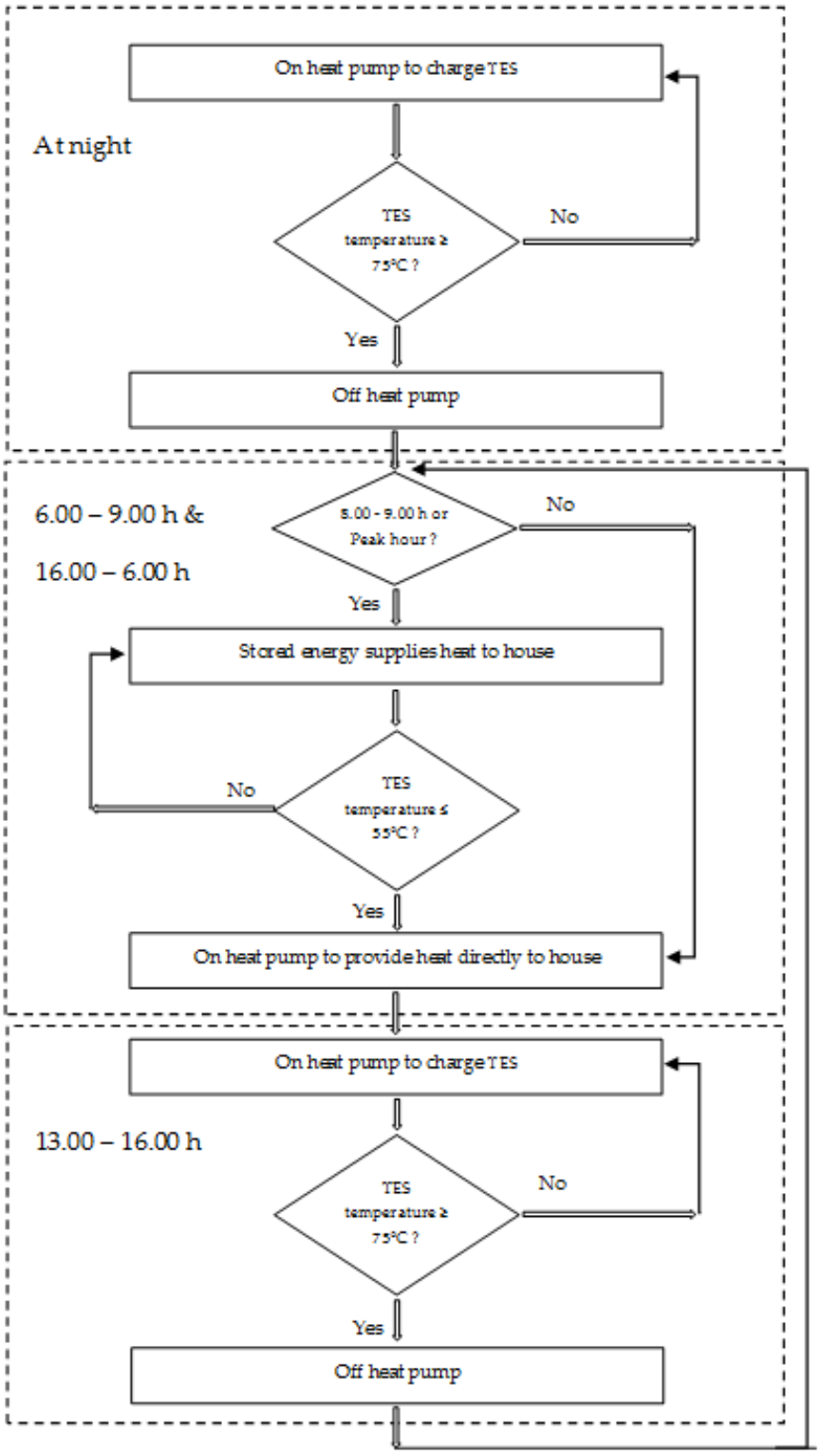

FIGURE 6.9: Flow chart of Strategy C.

6.3 Simulation results and Discussion

6.3.1 Optimal tank sizes and temperature set points

To find the optimal tank sizes and temperature set points for the designed load shifting control strategies, a set of simulations was carried out. 63 simulations in total were run interchangeably with different tank sizes and set points and three different control strategies. The simulations were run with one-minute steps for two winter months, January and February, where the ambient conditions were most severe in the year.

The summary of the simulation results is shown in Table 6.2. It includes the total running costs and the total energy consumption of the cascade heat pumps during peak hours. Looking at each control strategy in the table, if the tank sizes and temperature set points were lower, the running costs were higher. Similarly, the CAWHPs consumed more energy during peak hours if the tank sizes and temperature set points were lower. Therefore, the optimum tank size was 1.2 m^3, and the optimum temperature set points of the storage was 75 °C. With this system design, Strategy B and Strategy C could wholly shift three-hour peak demands.

TABLE 6.2: Total running costs and energy consumption during peak hours of the cascade heat pump in two winter months applied the three load shifting strategies with different tank sizes and temperature set points.

Tank temperature set point (°C)	Tank size (m^3)	Total running costs of the heat pump (£)			Total energy use of the heat pump during peak hours (kWh)		
		Strategy A	Strategy B	Strategy C	Strategy A	Strategy B	Strategy C
65	0.6	401	406	392	657	615	631
	0.7	397	403	388	625	581	597
	0.8	392	400	383	592	546	563
	0.9	388	396	379	560	511	528
	1	383	393	374	526	476	493
	1.1	378	389	369	493	440	458
	1.2	373	386	364	459	404	422
70	0.6	388	396	379	564	517	530
	0.7	381	391	372	513	465	478
	0.8	373	385	365	463	412	425
	0.9	366	380	358	412	358	372
	1	358	375	351	400	305	320
	1.1	351	369	343	309	250	265
	1.2	344	364	336	256	196	216
75	0.6	374	386	367	469	417	427
	0.7	364	379	357	401	347	357
	0.8	355	371	347	334	276	285
	0.9	345	365	338	268	209	219
	1	335	357	328	197	135	148
	1.1	324	349	318	123	59	73
	1.2	314	344	309	49	0	0

6.3.2 Comparison of three load shifting strategies

In order to compare the performance of the designed load shifting strategies, another set of simulations was run. The optimum tank size of 1.2 m^3 and the optimum tank temperature set point of 75 °C found in the previous Section 6.3.1 were selected in these simulations. The simulations were run with one-minute intervals for a whole year period. Apart from the simulations for the three

control strategies, one simulation, named Base Case, was run with the CAWHP providing heat directly to the house without the TES. This means that there was not load shifting in this Base Case.

Table 6.3 summaries the annual results of the investigated simulations. Note that the useful heat output accounts for the heat losses of the whole system.

TABLE 6.3: Summary of simulation results of three control strategies and Base Case.

	Base Case	Strategy A	Strategy B	Strategy C
Annual useful heat output [kWh]	21412	23442	23503	23619
Annual energy consumption [kWh]	9646	11911	11518	11869
Annual wind curtailment prevention [kWh]	8707	10687	10332	10697

As for energy consumption, the CAWHP in Base Case consumed least energy compared to the ones in the other control strategies, 9646 kWh per year (Table 6.3). The energy utilisation of the cascade heat pump was lower in Strategy B (11518 kWh/year) than in Strategy C (11869 kWh/year). The heat pump in Strategy A used the highest energy (11911 kWh/year).

With regards to running costs, although Strategy C made the cascade heat pump consume more energy than the ones in Base Case and Strategy B, its annual running cost was lowest (£1345), as shown in Figure 6.10. Note that the flat rate tariff (£0.175/kWh) was applied to calculate the running cost of the heat pump in Base Case, while the Powershift tariff (low rate: £0.0953/kWh, normal rate: £0.143/kWh, peak rate: £0.254/kWh) was used for the cascade heat pump in three load shifting strategies. Strategy C was designed to take advantage of both the low electricity rates and the higher ambient temperatures, thereby improving its overall efficiency and reducing its running costs. Compared to Strategy B (£1545 per annum), Strategy A (£1368 per annum) obtained

lower operating cost, meaning that the lower electricity rates played a more important role than the higher ambient temperatures. Base Case was the worst system operation as its yearly operating cost was highest (£1688).

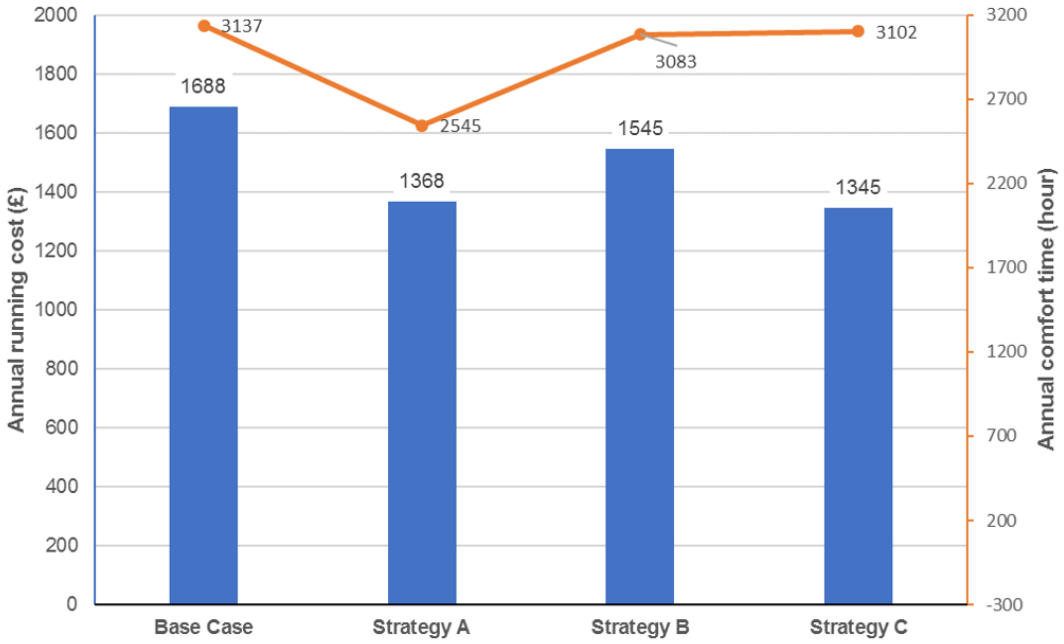

FIGURE 6.10: Annual operating costs of three control strategies and Base Case.

In terms of thermal comfort, Figure 6.10 also illustrates the total comfort time in the year of three load shifting strategies and Base Case. The total hours of comfort were calculated based on the time in which the room temperature was over the set point during the occupied periods. Considering three load shifting strategies, Strategy C could maintain better thermal comfort than the other two strategies. While Base Case was the most expensive operation as mentioned above, its thermal comfort was just slightly higher than the levels of Strategy B and Strategy C.

To see how the designed control algorithms affected the utility demand power, the one-day impact figure of the CAWHPs applied the load shifting strategies along with the breakdown of energy consumption of the cascade heat pumps

during off-peak and peak hours in the one-year period are illustrated in Figure 6.11 and Figure 6.12, respectively. Note that cascade heat pumps are more suitable to be retrofitted into ageing and high heat loss houses rather than new buildings [17], the cascade heat pump electrical demand in Figure 6.11 is therefore assumed to be aggregated with 10% of the current old housing stock in Northern Ireland (10% of 211270 buildings [94]). The breakdown of energy utilisation in each figure in Figure 6.12 accounted for only one single cascade heat pump. In Figure 6.11, it can be seen that the CAWHP without the load shifting would pose challenges to the grid as there was an added peak demand (maximum of about 120 MW) from 16.00 h to 19.00 h. Considering the cascade heat pumps with three load shifting strategies in the same figure, their operation was totally avoided during peak hours. In Figure 6.12, the annual energy use was separated into four periods representing the electricity rates in the Powershift tariff: low rate (0.00 – 08.00 h), normal rate (08.00 – 16.00 h and 19.00 – 24.00 h), peak rate (16.00 – 19.00 h). It can be seen in the figure that Strategy B and Strategy C could shift wholly the house demands from peak to off-peak hours for the whole year period, which in turn was beneficial for the utility power demand. Furthermore, according to Strategy C, the cascade heat pump consumed the highest level of energy during the nighttime (0.00 - 08.00 h) where the low grid demand was observed.

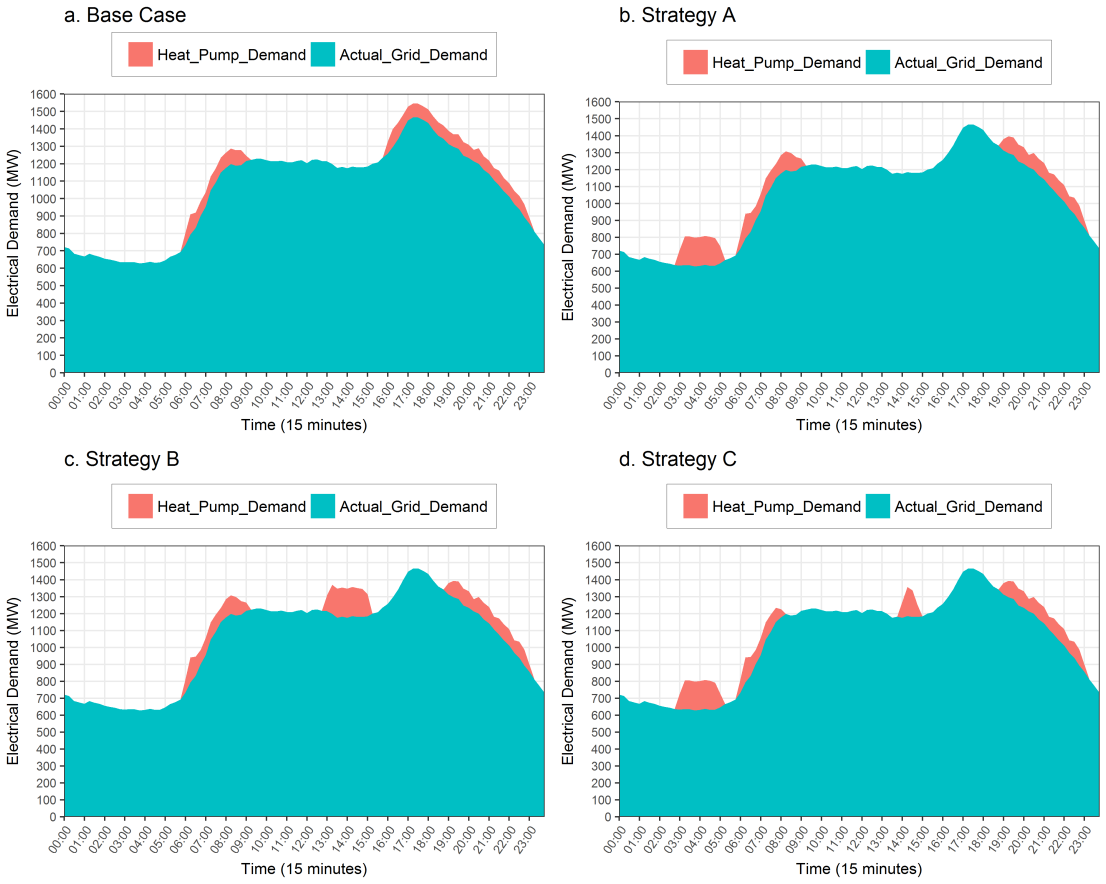

FIGURE 6.11: One-day impact of the cascade heat pump applied the load shifting strategies on the grid (the electrical power of the heat pump is aggregated with 10% of the current ageing houses in Northern Ireland).

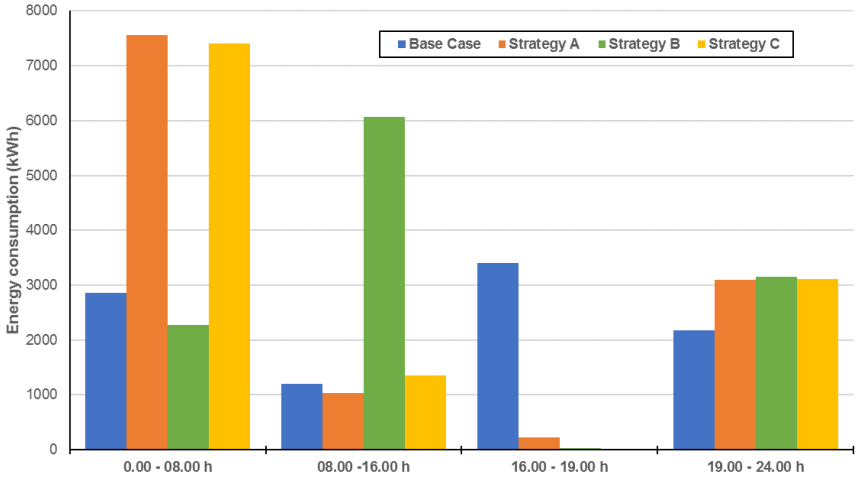

FIGURE 6.12: Breakdown of energy consumption of the cascade heat pump in peak and off-peak hours.

How much wind energy curtailment could be prevented in Northern Ireland was also evaluated for the load shifting strategies. Figure 6.13 shows an example of one-day wind curtailment power and the power consumption of the cascade heat pump to illustrate how the numbers of the wind curtailment prevention was calculated in Table 6.3. In particular, if the heat pumps operated during the periods of wind dispatch-down, it was assumed that wind energy would be used by the heat pumps. In Table 6.3, the amount of wind energy curtailment prevention was highest (10679 kWh) with the cascade heat pump applied the load shifting Strategy C, while that was lowest (8707 kWh) with the cascade heat pump operating without load shifting.

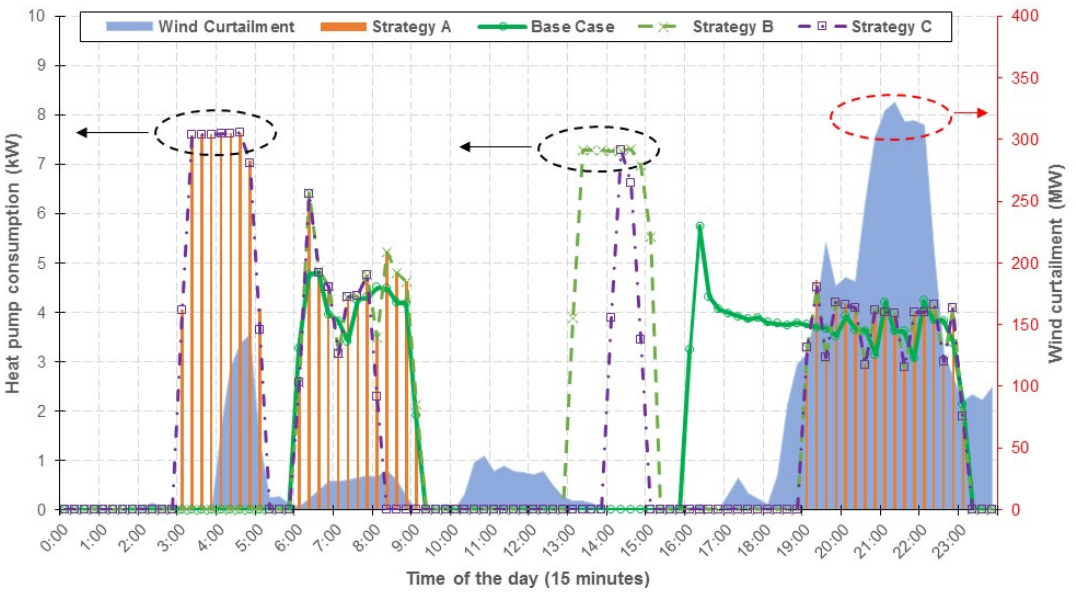

FIGURE 6.13: Example of one-day heat pump power consumption in three control strategies and Base Case along with wind curtailment power in Northern Ireland (wind dispatch-down data are of 2018 and adapted from [7]).

In short, it can be said that Strategy C was the best load shifting control strategy because it could help the CAWHP reduce annual running costs, maintain better levels of thermal comfort, perfectly avoid the grid power demand during peak hours, and allow the highest proportions of wind energy to be integrated into the grid.

6.3.3 Retrofit assessment of the cascade heat pump applied Strategy C

Since Strategy C yielded the best system operation compared to the other two strategies, as mentioned in the previous section, the performance of the CAWHP applied Strategy C was compared to the performance of gas and oil boilers to assess its retrofit ability in the UK. In particular, the running costs and carbon emissions of the 60%, 70%, 80% and 90% efficiency gas and oil boilers were the measures to compare with the results of the cascade heat pump applied Strategy C. These boilers represent from old heavy weight boilers to new condensing boilers that are popular in the UK housing stock.

The summary of the comparison results can be seen in Table 6.4. The oil price was £0.068/kWh [89]. The gas price was £0.06508/kWh for the first 2000 kWh, and £0.0459 /kWh for the after 2000 kWh [90]. The carbon emissions factors were 0.2 $kgCO_2$/kWh and 0.243 $kgCO_2$/kWh for gas and oil, respectively [91]. Time-series carbon intensity on the grid of all Ireland in 2018 [5] was used to calculate the carbon emissions of the cascade heat pump. One-week example of 15-minute carbon intensity data can be seen in Figure 6.14.

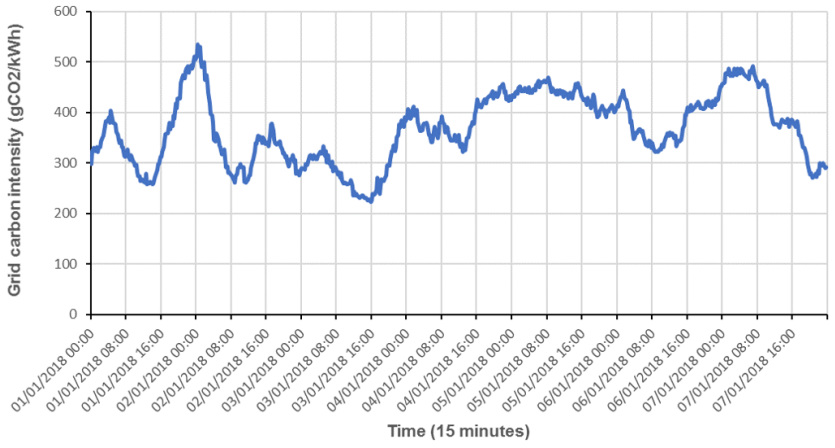

FIGURE 6.14: One-week carbon intensity on the grid of all Ireland in 2018 (data are adapted from [5]).

TABLE 6.4: Annual results of energy consumption, running costs and carbon emissions of the cascade heat pump applied Strategy C and boilers.

	Efficiency (%)	Annual energy use (kWh)	Annual running cost (£)	Annual carbon emissions (kg)
Strategy C	-	11869	1345	4562
Oil boiler	60	29977	2038	7284
	70	27836	1893	6764
	80	25694	1747	6244
	90	23553	1602	5723
Gas boiler	60	29977	1414	5995
	70	27836	1316	5567
	80	25694	1218	5139
	90	23553	1119	4711

Figure 6.15 depicts the percentages of yearly operating cost savings of gas and oil boilers compared to the heat pump applied Strategy C. The positive values in the figure indicate that the heat pump can obtain running cost savings compared to boilers, while negative values indicate the heat pump is more expensive to run than boilers. It can be seen in the figure that, if the CAWHP was retrofitted into the houses using oil boilers or low efficiency gas boiler (60%), Strategy C could help the homeowners to save the running costs (from 5% to 34%).

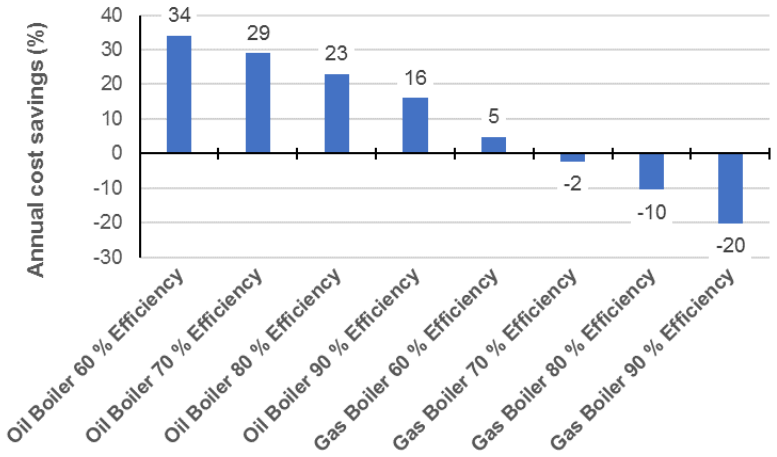

FIGURE 6.15: Annual running cost savings of the retrofit CAWHP applied Strategy C compared with boilers (positive values indicate the heat pump can obtain running cost savings, while the negative indicates it is more expensive to run).

In Figure 6.16, the percentages of annual carbon savings of gas and oil boilers compared to the CAWHP with Strategy C. The positive values in the figure indicate that operating the heat pump emits less carbon than running boilers. It can be seen in the graph that there were carbon emission savings ranging from 3% to 37% if all oil and gas boilers were replaced by the heat pump applied Strategy C.

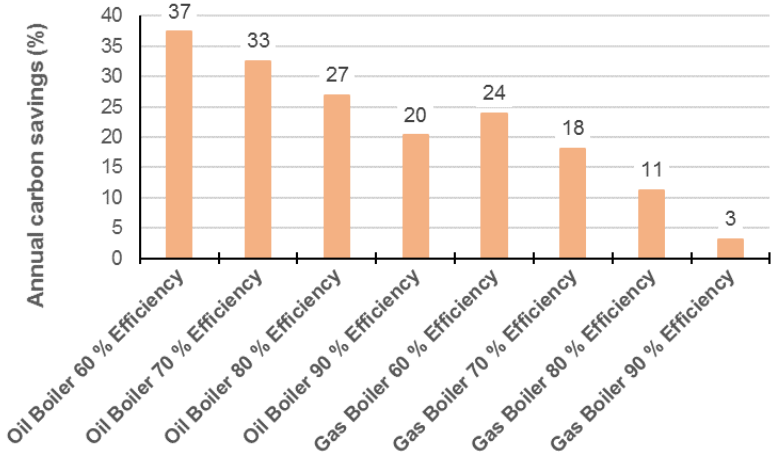

FIGURE 6.16: Annual carbon savings of the CAWHP applied Strategy C compared with boilers (positive values indicate that running the heat pump emits less CO_2 than running boilers).

Although Strategy C could not help the cascade heat pump to acquire cost savings compared to the high efficiency gas boilers (over 70%), there were cost benefits and carbon emissions savings if the CAWHP applied Strategy C was retrofitted into the houses using oil boilers. As of the simulation results mentioned in Chapter 5, the CAWHP with and without TES could not defeat high efficiency oil boilers (90%) in terms of running costs. Therefore, the results in this chapter indicates that Strategy C could help increase the retrofit rates of CAWHPs into the domestic buildings in off-gas grid areas, where the heating systems highly rely on oil boilers [17], due to their better operating costs and carbon emissions compared to fossil-fuel boilers.

6.4 Summary

Different load shifting control strategies for a CAWHP coupled with TES are presented in this chapter. The control strategies were designed to shift the heating electrical demands from peak to off-peak hours following the electricity rates of the Powershift tariff. Three control strategies were developed with the aims to improve the system operation efficiency to obtain minimised running costs and reduced wind power curtailment. TRNSYS simulation software was used to model and simulate the system applied the developed control algorithms. The simulation results indicated that:

- If the cascade heat pump was used for the heating system, the tank size of 1.2 m^3 along with the tank temperature set point of 75 °C could shift wholly the house heat demand to off-peak periods with minimised running costs.
- Strategy C, in which the cascade heat pump was forced to charge the TES at 3.00am (low electricity rate) and 2.00pm (high ambient temperatures),

and the stored energy was then discharged in the morning and afternoon, respectively, was the best load shifting strategy. It could obtain minimised running costs, perfect three-hour peak load shifting, high levels of thermal comfort and high proportions of wind energy integrated into the grid, compared with the other two strategies.

- If the cascade heat pump was not controlled (Base Case scenario), its running costs were highest and it negatively affected on the grid; however, thermal comfort could be achieved well.

- Strategy C could help the cascade heat pump save operating costs (16% - 34%) and carbon emissions (20% - 37%) when it was retrofitted into the houses using oil boilers.

- While the cascade heat pump applied Strategy C could not beat high efficiency gas boilers (70 – 90%) in terms of running costs, it could acquire carbon savings from 3% to 24%.

Chapter 7

Conclusion and Future Work

7.1 Summary of Contributions

In this thesis, the retrofit applications of the variable capacity CAWHP with and without the TES in UK residential buildings using experimentally validated simulations have been presented.

First, the TRNSYS models of an inverter CAWHP, a TES tank, and a whole couple dynamic simulation building, were developed and calibrated/validated against the experimental results. In particular, the variable capacity CAWHP was modelled using the performance map-based approach, which was successfully calibrated and validated against the laboratory and in-situ results. The TES tank and the whole couple dynamic building simulation model were also calibrated utilising the data collected from the field trial experiments.

Second, the annual techno-economic assessment of the CAWHP system (without TES) retrofitted into UK residential buildings was carried out, as explained in Chapter 4. Particularly, the retrofit CAWHP was investigated with different scenarios, including varied property types and ages (nine archetypes), different locations across the UK (four locations), and two control strategies (fixed flow water temperature and weather compensation control). The main outcomes of the simulation results were that the operating costs of the retrofit CAWHP were

higher than those of gas boilers and high efficiency oil boilers (90% efficiency); however, there were cost savings if the 60%, 70% and 80% efficiency oil boilers were replaced by the retrofit CAWHP. In addition to running costs, CO_2 emissions of the retrofit CAWHP were less than those of all gas and oil boilers, ranging from 14% to 58%. Based on these results, it can be concluded that the selected CAWHP is a good candidate for retrofitting the UK domestic built environment in off-gas grid area, where most of the properties are old or high heat losses and running with low efficiency oil boilers (below 80% efficiency). Moreover, while the CAWHP was more expensive to run than the high efficiency oil boilers and all gas boilers, the less carbon emissions of the retrofit CAWHP would be a good sign for the future uptake of this renewable-based technology.

Third, the comparative performance of the retrofit CAWHP coupled with the TES tank in different scenarios was conducted using the validated models in TRNSYS environment, as discussed in Chapter 5. Three operation modes, including direct heating, buffering system, and combined mode, were investigated to compare their energy performance in line with running costs. The direct heating achieved the highest annual efficiency (COP_{sys} of 2.12) followed by the combined (COP_{sys} of 1.88), while the buffering system had the worst performance (COP_{sys} of 1.41). The reasons behind the low efficiencies in the buffering and the combined mode were mainly due to the high outlet water temperatures required to top up the TES tank and its parasitic losses. In terms of running costs, the combined mode was a promising system configuration as its operating cost was lowest thanks to the Economy 7 tariff. However, its operating cost was still higher than those of gas boilers and 90% efficiency oil boilers.

Finally, three load shifting strategies for the CAWHP coupled with the TES in

the hard-to-heat building were studied, as shown in Chapter 6. The load shifting algorithms were designed based on the Powershift tariff to shift the operation of the cascade heat pump to off-peak periods. These control strategies were developed with the aims to improve the system operation efficiency to obtain minimised running costs and reduced wind power curtailment. TRNSYS simulation software was also utilised to simulate the validated models applied the load shifting strategies. The simulation results indicated the tank size of 1.2 m^3 in line with the tank temperature set point of 75 °C could wholly shift the operation of the CAWHP to off-peak periods with minimised running costs. Additionally, the load shifting strategy in which the CAWHP was shifted to charge the TES at 03.00 h (low electricity rate) and 14.00 h (high ambient temperatures) was the best strategy. It could achieve minimised running costs, perfect three-hour peak load shifting, high levels of thermal comfort, and high proportions of wind curtailed prevention. Furthermore, this load shifting strategy could help the CAWHP save operating costs (16 - 34%) and carbon emissions (20 - 37%) when it was retrofitted into the buildings running with oil boilers. While the cascade heat pump applied Strategy C could not beat high efficiency gas boilers (70 – 90%) in terms of running costs, it could acquire carbon savings from 3% to 24%.

7.2 Future Work

This research focussed on: (1) developing and validating the model of a CAWHP model coupled with a TES tank model in a dynamic building simulation model in TRNSYS environment; (2) assessing the annual techno-economic performance of the CAWHP system (without TES) when retrofitted into UK residential buildings; (3) evaluating the system performance of the retrofit CAWHP coupled with TES in different configurations in a residential dwelling; (4) investigating load shifting for the CAWHP coupled with the TES tank with enhanced system

energy efficiency to achieve minimised running costs and reduced wind energy curtailment.

Future work could include:

- In this study, the CAWHP was modelled using the performance map-based approach. Future work could develop and validate this kind of heat pump using physical approaches, which could enable further investigations for the performance of cascade heat pumps at component design level, such as transient states.
- More laboratory tests could be carried out for the inverter CAWHP. Since the data used to model and validate the cascade heat pump model at different part load ratios in this research were obtained from the field trial experiments, future work should test the cascade heat pump at different part load conditions in the lab, where outdoor temperatures can be controlled.
- The annual techno-economic performance of the CAWHP system (without TES) could be conducted for more property types, such as listed buildings which are often in off-gas grid areas along with high heat losses.
- The load shifting strategies for the CAWHP in this research were investigated using parametric study. Therefore, future work could develop the load shifting further using optimisation approaches.
- The designed load shifting strategies were rule-based control which is simple. They were mainly designed and implemented based on the fixed tariffs, the average whole year ambient temperatures and the assumed identical heating demand hours. Therefore, this control approach is inflexible and has some limitations. Model-predictive control which is more

advanced can be used to reduce energy consumption and improve thermal comfort within buildings further. While this advanced control is expensive and requires expertise levels, it can deal with real time dynamic electricity prices, real time ambient temperatures and occupant behaviors. As a result, future work should develop load shifting strategies further using this advanced control approach to optimise energy savings and benefits for grid operations.

- Future avenue for load shifting could study phase change materials for the TES tank, with the aim to reduce the size of the storage while remaining its required heat capacity.

Bibliography

[1] "Energy Consumption in the UK July 2017," tech. rep., Department for Business, Energy and Industrial Strategy. https://www.gov.uk/government/statistics/digest-of-uk-energy-statistics-dukes-2018-main-report [Accessed 13-10-2019].

[2] "Emissions from Heat," tech. rep., Department of Energy and Climate Change. https://www.gov.uk/government/statistics/uk-emissions-from-heat [Accessed 13-10-2019].

[3] L. Zhang, Y. Jiang, J. Dong, and Y. Yao, "Advances in vapor compression air source heat pump system in cold regions: A review," *Renewable and Sustainable Energy Reviews*, vol. 81, pp. 353 – 365, 2018.

[4] N. J. Kelly, P. G. Tuohy, and A. D. Hawkes, "Performance assessment of tariff-based air source heat pump load shifting in a uk detached dwelling featuring phase change-enhanced buffering," *Applied Thermal Engineering*, vol. 71, no. 2, pp. 809 – 820, 2014. Special Issue: MICROGEN III: Promoting the transition to high efficiency distributed energy systems.

[5] "Soni (System Operator for Northern Ireland)," 2019. http://www.soni.ltd.uk/ [Accessed 01-07-2019].

[6] "Northern Ireland electricity tariffs," 2018. https://touch.nihe.gov.uk/latest_tariffs [Accessed 01-07-2019].

[7] "EIRGRID." http://www.eirgridgroup.com/how-the-grid-works/renewables/[Accessed 10-09-2019].

[8] "Energy efficiency best practice in housing - northern Ireland: assessing U-values of existing housing," tech. rep., The Energy Saving Trust.

[9] "EU Directive on the Energy Performance of Buildings (recast) (2010/31/EU)," tech. rep., European Parliament.

[10] "Provisional UK greenhouse gas emissions national statistics 2018," tech. rep., Department for Business, Energy and Industrial Strategy. https://www.gov.uk/government/statistics/provisional-uk-greenhouse-gas-emissions-national-statistics-2018 [Accessed 13-10-2019].

[11] "Carbon Footprint of Heat Generation," tech. rep., Parliamentary Office of Science and Technology. https://researchbriefings.parliament.uk/ResearchBriefing/Summary/POST-PN-0523 [Accessed 13-10-2019].

[12] "Net Zero The UK's contribution to stopping global warming." file:///C:/Users/Khoa/Desktop/Net-Zero-The-UKs-contribution-to-stopping-global-warming.pdf [Accessed 30-10-2019].

[13] N. Kelly and J. Cockroft, "Analysis of retrofit air source heat pump performance: Results from detailed simulations and comparison to field trial data," *Energy and Buildings*, vol. 43, no. 1, pp. 239–245, 2011.

[14] "Greenhouse gas reporting: conversion factors 2018 - GOV.UK," 2018. https://www.gov.uk/government/publications/greenhouse-gas-reporting-conversion-factors-2018[Accessed 5-10-2018].

[15] S. J. Self, B. V. Reddy, and M. A. Rosen, "Geothermal heat pump systems: Status review and comparison with other heating options," *Applied Energy*, vol. 101, pp. 341 – 348, 2013. Sustainable Development of Energy, Water and Environment Systems.

[16] "EN14511: Air conditioners, liquid chilling packages and heat pumps with electrically driven compressors for space heating and cooling (part 1-4), s.l.: BSI," tech. rep., European Committee for Standardization.

[17] "Evidence Gathering – Low Carbon Heating Technologies," tech. rep., Department for Business, Energy and Industrial Strategy. https://assets.publishing.service.gov.uk/government/uploads/system/uploads/attachment_data/file/565248/Heat_Pumps_Combined_Summary_report_-_FINAL.pdf [Accessed 5-10-2018].

[18] "Dwelling stock estimates in england," tech. rep., Ministry of Housing, Communities and Local Government. https://www.gov.uk/government/statistics/dwelling-stock-estimates-in-england-2018 [Accessed 05-03-2020].

[19] "Housing stock statistics," tech. rep., Department of Finance. https://www.finance-ni.gov.uk/topics/statistics-and-research/housing-stock-statistics [Accessed 05-03-2020].

[20] "Detailed analysis from the first phase of the Energy Saving Trust's heat pump field trial 2012," tech. rep., Department of Energy and Climate Change. https://www.gov.uk/government/publications/greenhouse-gas-reporting-conversion-factors-2018 [Accessed 5-10-2018].

[21] "Daikin UK Price List - January 2018," 2018. http://www.oceanairuk.com/wp-content/uploads/2018/01/Daikin_Price_List_2018-19.pdf [Accessed 10-03-2018].

[22] "System Solution Pack Price List - March 2018," 2018. https://siteassets.pagecloud.com/freedomhp/downloads/2018_Hitachi_FHP_price_list-ID-3676ae8d-36d1-4579-d6a9-d41ad9957f3d.pdf [Accessed 10-03-2018].

[23] K. Chua, S. Chou, and W. Yang, "Advances in heat pump systems: A review," *Applied Energy*, vol. 87, no. 12, pp. 3611 – 3624, 2010.

[24] Z. Ma, Z. Yang, Y. Yao, and Y. Yu, "Analysis of using air-source heat pump water chiller-heater units in the cold regions," *Nuantong Kongtiao/HVAC*, vol. 31, no. 3, p. 28, 2001.

[25] J. Wu, Z. Yang, Q. Wu, and Y. Zhu, "Transient behavior and dynamic performance of cascade heat pump water heater with thermal storage system," *Applied Energy*, vol. 91, no. 1, pp. 187 – 196, 2012.

[26] P. J. Luickx, L. M. Helsen, and W. D. D'haeseleer, "Influence of massive heat-pump introduction on the electricity-generation mix and the ghg effect: Comparison between belgium, france, germany and the netherlands," *Renewable and Sustainable Energy Reviews*, vol. 12, no. 8, pp. 2140 – 2158, 2008.

[27] "Annual renewable energy constraint and curtailment - Report 2017." http://www.eirgridgroup.com/Annual-Renewable-Constraint-and-Curtailment-Report-2017-V1.pdf [Accessed 01-07-2019].

[28] N. J. Hewitt, "Heat pumps and energy storage – the challenges of implementation," *Applied Energy*, vol. 89, no. 1, pp. 37 – 44, 2012.

[29] A. Arteconi, N. Hewitt, and F. Polonara, "State of the art of thermal storage for demand-side management," *Applied Energy*, vol. 93, pp. 371 – 389, 2012.

[30] B. Alimohammadisagvand, J. Jokisalo, S. Kilpeläinen, M. Ali, and K. Sirén, "Cost-optimal thermal energy storage system for a residential building with heat pump heating and demand response control," *Applied Energy*, vol. 174, pp. 275 – 287, 2016.

[31] F. Madonna and F. Bazzocchi, "Annual performances of reversible air-to-water heat pumps in small residential buildings," *Energy and Buildings*, vol. 65, pp. 299–309, 2013.

[32] S. Asaee, V. Ugursal, and I. Beausoleil-Morrison, "Techno-economic feasibility evaluation of air to water heat pump retrofit in the canadian housing stock," *Applied Thermal Engineering*, vol. 111, pp. 936–949, 2017.

[33] K. Huchtemann and D. Müller, "Evaluation of a field test with retrofit heat pumps," *Building and Environment*, vol. 53, pp. 100 – 106, 2012.

[34] L. Cabrol and P. Rowley, "Towards low carbon homes - a simulation analysis of building-integrated air-source heat pump systems," *Energy and Buildings*, vol. 48, pp. 127–136, 2012.

[35] J. Palmer and I. Cooper, "United Kingdom Housing Energy Fact File, London, 2013," tech. rep., Department of Energy and Climate Change.

[36] "BS EN 442-2: Radiators and Convectors Part 2: Test Methods and Rating," tech. rep., BSI.

[37] H. W. Jung, H. Kang, W. J. Yoon, and Y. Kim, "Performance comparison between a single-stage and a cascade multi-functional heat pump for both air heating and hot water supply," *International Journal of Refrigeration*, vol. 36, no. 5, pp. 1431 – 1441, 2013.

[38] S. S. Bertsch and E. A. Groll, "Two-stage air-source heat pump for residential heating and cooling applications in northern u.s. climates," *International Journal of Refrigeration*, vol. 31, no. 7, pp. 1282 – 1292, 2008.

[39] H. Willem, Y. Lin, and A. Lekov, "Review of energy efficiency and system performance of residential heat pump water heaters," *Energy and Buildings*, vol. 143, pp. 191–201, 2017.

[40] H. Park, D. H. Kim, and M. S. Kim, "Thermodynamic analysis of optimal intermediate temperatures in r134a–r410a cascade refrigeration systems and its experimental verification," *Applied Thermal Engineering*, vol. 54, no. 1, pp. 319 – 327, 2013.

[41] H. Park, D. Kim, and M. Kim, "Performance investigation of a cascade heat pump water heating system with a quasi-steady state analysis," *Energy*, vol. 63, pp. 283 – 294, 2013.

[42] D. Kim, H. Park, and M. Kim, "Optimal temperature between high and low stage cycles for r134a/r410a cascade heat pump based water heater system," *Experimental Thermal and Fluid Science*, vol. 47, pp. 172 – 179, 2013.

[43] D. H. Kim, H. S. Park, and M. S. Kim, "The effect of the refrigerant charge amount on single and cascade cycle heat pump systems," *International Journal of Refrigeration*, vol. 40, pp. 254 – 268, 2014.

[44] X. Ma, Y. Zhang, L. Fang, X. Yu, X. Li, Y. Sheng, and Y. Zhang, "Performance analysis of a cascade high temperature heat pump using r245fa and by-3 as working fluid," *Applied Thermal Engineering*, vol. 140, pp. 466 – 475, 2018.

[45] W. Wang, Z. Ma, Y. Jiang, Y. Yang, S. Xu, and Z. Yang, "Field test investigation of a double-stage coupled heat pumps heating system for cold regions," *International Journal of Refrigeration*, vol. 28, no. 5, pp. 672 – 679, 2005.

[46] N. N. Shah, C. Wilson, M. J. Huang, and N. J. Hewitt, "Analysis on field trial of high temperature heat pump integrated with thermal energy storage in domestic retrofit installation," *Applied Thermal Engineering*, vol. 143, pp. 650 – 659, 2018.

[47] R. Soltani, I. Dincer, and M. Rosen, "Comparative performance evaluation of cascaded air-source hydronic heat pumps," *Energy Conversion and Management*, vol. 89, pp. 577 – 587, 2015.

[48] D. Fischer and H. Madani, "On heat pumps in smart grids: A review," *Renewable and Sustainable Energy Reviews*, vol. 70, pp. 342 – 357, 2017.

[49] T. Q. Péan, J. Salom, and R. Costa-Castelló, "Review of control strategies for improving the energy flexibility provided by heat pump systems in buildings," *Journal of Process Control*, vol. 74, pp. 35 – 49, 2019. Efficient energy management.

[50] A. Arteconi, N. Hewitt, and F. Polonara, "Domestic demand-side management (dsm): Role of heat pumps and thermal energy storage (tes) systems," *Applied Thermal Engineering*, vol. 51, no. 1, pp. 155 – 165, 2013.

[51] J. Guo, J. Wu, R. Wang, and S. Li, "Experimental research and operation optimization of an air-source heat pump water heater," *Applied Energy*, vol. 88, no. 11, pp. 4128 – 4138, 2011.

[52] O. Ibrahim, F. Fardoun, R. Younes, and H. Louahlia-Gualous, "Air source heat pump water heater: Dynamic modeling, optimal energy management and mini-tubes condensers," *Energy*, vol. 64, pp. 1102 – 1116, 2014.

[53] R. D. Coninck, R. Baetens, B. Verbruggen, J. Driesen, D. Saelens, and L. Helsen, "Modelling and simulation of a grid connected photovoltaic heat pump system with thermal energy storage using modelica," in *8th International Conference on System Simulation in Buildings (SSB2010)*, 2010.

[54] "European Standard EN 14511-3: Air Conditioners, Liquid Chilling Packages and Heat Pumps with Electrically Driven Compressors for Space Heating and Cooling – Part 3 Test Methods, AFNOR, 2004."

[55] "Daikin Altherma HT 11, Daikin UK Limited." `http://www.daikin.co.uk/domestic/needs/heating/air-water-heatpumps-ht/index.jsp` [Accessed 06-10-2017].

[56] J. P. Holman, *Experimental Methods for Engineers*. The McGraw-Hill Companies, Inc., 1221 Avenue of the Americas, New York, NY 10020: Mc-Grall-Hill, 2012.

[57] "TRNSYS 17, a TRaNsient SYstem Simulation program – vol. 3-Component Library Overview." `http://www.trnsys.com/assets/docs/03-ComponentLibraryOverview.pdf` [Accessed 5-10-2018].

[58] "SketchUp." `https://www.sketchup.com/`[Accessed 10-06-2018].

[59] L. B. N. Laboratory, "Genopt." `https://simulationresearch.lbl.gov/GO` [Accessed 06-10-2018].

[60] T. U. of Wisconsin, "Ees." `http://fchartsoftware.com/ees/` [Accessed 14-10-2019].

[61] "Matlab." `https://www.mathworks.com/products/matlab.html` [Accessed 14-10-2019].

[62] "TESS component libraries." `http://www.trnsys.com/tess-libraries` [Accessed 10-06-2018].

[63] C. Underwood, M. Royapoor, and B. Sturm, "Parametric modelling of domestic air-source heat pumps," *Energy and Buildings*, vol. 139, pp. 578 – 589, 2017.

[64] S. Poppi, V. Schubert, C. Bales, and A. Weidinger, "Simulation study of cascade heat pump for solar combisystems," in *EuroSun 2014 / ISES Conference Proceedings (2014)*, 2014.

[65] "Models of Sub-Components and Validation for the IEA SHC Task 44 / HPP Annex 38. Part A: Summary," tech. rep., IEA Solar Heating and Cooling Programme, 2013.

[66] "The R Project for Statistical Computing." `https://www.r-project.org/` [Accessed 08-10-2018].

[67] E. Bettanini, A. Gastaldello, and L. Schibuola, "Simplified models to simulate part load performances of air conditioning equipments," in *Proc. IBPSA 8th Int. Conf. Building Simulation '03*, pp. 107–114, 2003.

[68] D. Fischer, J. Bernhardt, H. Madani, and C. Wittwer, "Comparison of control approaches for variable speed air source heat pumps considering time variable electricity prices and pv," *Applied Energy*, vol. 204, pp. 93 – 105, 2017.

[69] M. E. Baster, "Modelling the performance of air source heat pump systems," Master's thesis, Department of Mechanical Engineering, University of Strathclyde Engineering, 2011.

[70] K. Ogawa, N. Tanaka, and M. Takeshita, "Performance improvement on plate fin-and-tube heat exchangers under frosting conditions," in *ASHRAE Transactions 99 (1993)*, 1993.

[71] W. A. Miller, "Laboratory evaluation of the heating capacity and efficiency of a high-efficiency, air-to-air heat pump with emphasis on frosting/defrosting operation," *NASA STI/Recon Technical Report N*, vol. 83, Oct. 1982.

[72] O. QUEVILLON, L. Lamarche, and S. Kajl, "Couplage d'un Échangeur air-sol pour augmenter la performance en chauffage d'une pompe À chaleur À

air," in *XIIIème Colloque Interuniversitaire Franco-Québécois sur la Thermique des Systèmes 22-24 mai 2017, LUSAC Saint-Lô, France*, 2017.

[73] CIBSE, *CIBSE Guide A: Environmental design*. Page Bros. (Norwich) Ltd., Norwich, Norfolk NR6 6SA: The Chartered Institution of Building Services Engineers London, 2006.

[74] "Ashare guidline 14. measurement of energy and demand savings," tech. rep., American Society of Heating, Refrigerating and Air-Conditioning Engineers, Inc., 2002.

[75] A. Cacabelos, P. Eguía, J. L. Míguez, E. Granada, and M. E. Arce, "Calibrated simulation of a public library hvac system with a ground-source heat pump and a radiant floor using trnsys and genopt," *Energy and Buildings*, vol. 108, pp. 114 – 126, 2015.

[76] C. J. Banister, W. R. Wagar, and M. R. Collins, "Solar-assisted heat pump test apparatus," *Energy Procedia*, vol. 48, pp. 489 – 498, 2014.

[77] P. Raftery, M. Keane, and A. Costa, "Calibrating whole building energy models: Detailed case study using hourly measured data," *Energy and Buildings*, vol. 43, no. 12, pp. 3666 – 3679, 2011.

[78] G. Mustafaraj, D. Marini, A. Costa, and M. Keane, "Model calibration for building energy efficiency simulation," *Applied Energy*, vol. 130, pp. 72 – 85, 2014.

[79] M. Royapoor and T. Roskilly, "Building model calibration using energy and environmental data," *Energy and Buildings*, vol. 94, pp. 109 – 120, 2015.

[80] E. Carlon, M. Schwarz, A. Prada, L. Golicza, V. K. Verma, M. Baratieri, A. Gasparella, W. Haslinger, and C. Schmidl, "On-site monitoring and dynamic simulation of a low energy house heated by a pellet boiler," *Energy and Buildings*, vol. 116, pp. 296 – 306, 2016.

[81] M. Owen, R. American Society of Heating, and A.-C. Engineers, *2009 ASHRAE Handbook: Fundamentals*. 2009 Ashrae Handbook - Fundamentals, American Society of Heating, Refrigeration and Air-Conditioning Engineers, 2009.

[82] I. O. for Standardization, *ISO 7730 2005-11-15 Ergonomics of the Thermal Environment: Analytical Determination and Interpretation of Thermal Comfort Using Calculation of the PMV and PPD Indices and Local Thermal Comfort Criteria*. International standards, ISO, 2005.

[83] A. Safa, A. Fung, and R. Kumar, "Performance of two-stage variable capacity air source heat pump: Field performance results and trnsys simulation," *Energy and Buildings*, vol. 94, pp. 80–90, 2015.

[84] A. Safa, A. Fung, and R. Kumar, "Comparative thermal performances of a ground source heat pump and a variable capacity air source heat pump systems for sustainable houses," *Applied Thermal Engineering*, vol. 81, pp. 279–287, 2015.

[85] P. C. da Silva, V. Leal, and M. Andersen, "Influence of shading control patterns on the energy assessment of office spaces," *Energy and Buildings*, vol. 50, pp. 35 – 48, 2012.

[86] *Fuel Efficiency Degree Days*. 1993.

[87] Ofgem, "Domestic Renewable Heat Incentive (RHI)." `https://www.ofgem.gov.uk/environmental-programmes/domestic-rhi` [Accessed 06-10-2018].

[88] "Electricity price comparison table - The Consumer Council." `http://www.consumercouncil.org.uk/sites/default/files/2018-11/Electricity_Price_Comparison_Table_8_November_2018.pdf`. [Accessed 11-01-2019].

[89] "Home Heating Oil." http://www.consumercouncil.org.uk/consumers/save-money/energy/home-heating-oil [Accessed 08-10-2018].

[90] "Gas price comparison for Greater Belfast and Larne area 2018." http://www.consumercouncil.org.uk/search?search_api_fulltext=filestore+documents+Gas+Price+Comparison+Table+April+2018+pdf [Accessed 08-10-2018].

[91] "Greenhouse gas reporting: conversion factors 2017 - GOV.UK," tech. rep., Department for Business, Energy and Industrial Strategy. https://www.gov.uk/government/publications/greenhouse-gas-reporting-conversion-factors-2017 [Accessed 03-02-2018].

[92] N. Kelly, P. Tuohy, and A. Hawkes, "Performance assessment of tariff-based air source heat pump load shifting in a uk detached dwelling featuring phase change-enhanced buffering," *Applied Thermal Engineering*, vol. 71, no. 2, pp. 809–820, 2014.

[93] "Economy 7 - The Consumer Council." http://www.consumercouncil.org.uk/sites/default/files/2018-11/Economy%207%20Price%20Comparison%20Table%2029%20November%202018.pdf [Accessed 11-01-2019].

[94] "The Northern Ireland Housing Statistics 2017-18." https://www.communities-ni.gov.uk/publications/northern-ireland-housing-statistics-2017-18 [Accessed 09-10-2019].